ENVIRONMENTAL IMPACTS OF ACID ROCK DRAINAGE REMEDIATION IN A COAL WASTE PILE: AN EXPERIMENTAL AND HYDRO-GEOCHEMICAL MODELING APPROACH

by

Fernando J. Plaza Vera

Civil Engineer, Catholic University of Guayaquil-Ecuador, 2001

Master of Engineering, National Autonomous University of Mexico, 2010

Submitted to the Graduate Faculty of

Swanson School of Engineering in partial fulfillment

of the requirements for the degree of

Doctor of Philosophy

University of Pittsburgh

2018

UNIVERSITY OF PITTSBURGH

SWANSON SCHOOL OF ENGINEERING

This dissertation was presented

by

Fernando J. Plaza Vera

It was defended on

July 3, 2018

and approved by

Carla Ng, Ph.D., Assistant Professor, Department of Civil and Environmental Engineering

Rosemary Capo, Ph.D., Associate Professor, Department of Geology and Environmental Science

Jeen-Shang Lin, Ph.D., Associate Professor, Department of Civil and Environmental Engineering

Dissertation Director: Xu Liang, Ph.D., Professor, Department of Civil and Environmental Engineering

ENVIRONMENTAL IMPACTS OF ACID ROCK DRAINAGE REMEDIATION IN A COAL WASTE PILE: AN EXPERIMENTAL AND HYDRO-GEOCHEMICAL MODELING APPROACH

Fernando J. Plaza Vera, Ph.D.

University of Pittsburgh, 2018

The mining-related acid rock drainage (ARD) constitutes a serious type of pollution that causes widespread degradation of water resources in regions with mining activity. Despite of a large number of research activities carried out on this topic, studies about ARD passive remediation have shown various existing issues that require further investigation. For instance, what long-term impacts will the remediation techniques have? Is there an optimal content of the reactive material that should be applied in the field? What impacts will the hydrological processes have on the ARD remediation techniques at the watershed scale?

To investigate these issues, a comprehensive and systematic approach is developed through this dissertation research work in which laboratory experiments (> 3 years), complemented with field measurements (> 5 years), and hydro-geochemical modeling have been combined to explore the effectiveness and long-term impacts of a remediation technique -- alkaline clay (AC), an industrial waste, used as the remediation material in coal refuse (CR) waste piles. Our study yielded the following main findings: 1) AC is an effective and environmentally sustainable material for passive ARD remediation, maintaining a neutral pH and immobilizing metals/metalloids; 2) There is a range for the mixing ratio between the amount of AC and CR to

achieve an optimal or close to optimal remediation effectiveness; 3) The appropriate depth for the amended layer was determined and it was found to be mostly constrained by the root zone depth; 4) Complementary strategies such as a vegetated cover and a saturated sand layer are highly beneficial; 5) The utilization of a sophisticated hydro-geochemical model allowed to investigate the remediation effectiveness and its long-term performance at a watershed scale, making possible the assessment inside and outside the coal waste pile ; and 6) Both the laboratory experiments and modeling results show that the proposed remediation design can lead to the total alkalinity in the system exceeding the total acidity over a long time period.

In summary, this study provides valuable new insights through three defined stages (i.e., laboratory experiments, field measurements and modeling) to demonstrate the effectiveness and sustainability of the proposed remediation approach.

TABLE OF CONTENTS

LIST OF TABLES

LIST OF FIGURES

ACKNOWLEDGEMENTS

First of all, I would like to show my deepest appreciation and admiration to my advisor and committee chair, Dr. Xu Liang, who has guided me with wisdom and patience throughout this entire process. It has been a true honor having the opportunity of working under her direction. She will always be a great example to me.

I would like to deeply thank the committee members: Dr. Carla Ng., Dr. Rosemary Capo and Dr. Jeen-Shang Lin. Their honest commitment with my research has allowed me to significantly improve the quality of this dissertation. It's been a privilege to have had such a high-level committee.

I am also grateful for the important collaboration that I received from other faculty, staff and students, especially Dr. Daniel Bain, David Malehorn, Yipei Wen, Yi Xu, Hannah Perone, William Clavijo and Thomas Slater.

I would also like to thank the most important person in my life, my wife Gloria, who has been my main support to achieve this milestone in my career. I also thank my daughter Amelia, for giving me so much joy and for teaching me so much in so little time. Of course, I also thank the other member of my family, my dog Fidi, who has been a source of happiness for all of us.

I thank my parents, Maria Rosa and Alberto, for their support, for always encouraging me to achieve my goals. They are also artifices of my success.

Finally, I would like to thank the University of Pittsburgh and its community. It has been an honor to be a part of this great institution.

To Glorita and Amelia

1.0 INTRODUCTION

1.1 BACKGROUND AND JUSTIFICATION

The acid rock drainage (ARD) process associated with the mining industry constitutes one of the most serious types of water pollution in regions such as the Northern Appalachian Coalfield in the USA, where the mining activity has caused widespread degradation of water resources *[Herlihy et al., 1990; Cravotta, 2008]*. Surface and groundwater affected by this pollution are characterized by their acidity and high content of sulfates and metals/metalloids. The ARD process initiates when sulfide minerals, highly contained in mining wastes, oxidize through complex chemical reactions involving the combined action of oxygen (e.g. the oxidant) and water (e.g. the solvent). As pyrite is usually the sulfide mineral involved, this process is often referred as pyrite oxidation.

Three main stoichiometric chemical reactions *[Garrels and Thompson, 1960; Singer and Stumm, 1970]* are often used to describe aqueous pyrite (FeS_2) oxidation: 1) pyrite (e.g. the sulfide mineral) oxidizes and produces dissolved iron (Fe^{2+}), sulfate (SO_4^{2-}) and hydrogen (H^+), that leads to the increase in the total dissolved solids and the acidity of the water, resulting in the decrease in pH, 2) in the presence of adequate oxygen (O_2) and hydrogen (H^+) concentrations, ferrous iron (Fe^{2+}) will oxidize into ferric iron (Fe^{3+}) and, 3) ferric iron may also oxidize pyrite into ferrous iron, sulfate and hydrogen. In addition, at low pH levels (< 3.5), ferric iron precipitates into iron

oxide hydroxide ($Fe(OH)_{3\ solid}$) and, simultaneously, produces hydrogen ions, thus resulting in lowering the pH.

Due to the severity of this environmental problem, several strategies have been developed to neutralize ARD generation. The most common approach is to divide the treatment into active and passive remediation processes *[Johnson and Hallberg, 2005]*. Both strategies use biological and abiotic treatment.

Passive abiotic treatment emerges as a low-cost and effective strategy for ARD remediation. It does not require continuous operation and, moreover, it may harness non-conventional materials as neutralization agents (e.g. alkaline wastes). In other words, this treatment can operate in a more sustainable way *[Younger et al., 2002]*. It has been found that, to some extent, passive treatment could have lower overall environmental impacts compared to active treatment technologies *[Hengen et al., 2014]*. Hence, this study will focus on passive abiotic ARD remediation.

Despite several previous studies of passive ARD remediation, there are still issues requiring improvement. For instance, the majority of the experimental strategies use complex systems for water addition (e.g. pumping), which sometimes generate artificial conditions that are difficult to replicate in-situ (e.g. limiting oxygen and water diffusion). Moreover, in most cases there is not a sufficient focus on the long-term impacts of the remediation technique nor is there an analysis of the optimal content of the reactive material to be applied in the field. On the modeling side, there are several conceptual and physically-based models that have been widely used to simulate ARD processes *[Kimball et al., 1994, Wunderly et al., 1996, Gerke et al., 1998, Webster et al., 1998, Amos et al., 2004, Molson et al., 2005, Runkel et al., 2011, Petrilakova et al., 2014, Masindi et al., 2015]*. However, these models are usually limited to small scales (e.g. soil

column, point discharges or a river reach) and they often overlook the hydrological processes and the parameters involved in the generation of ARD (e.g. spatial scale, infiltration, evapotranspiration, surface and subsurface runoff, terrain characteristics, etc.). Due to the necessity of having a more sophisticatedd model, *Xu [2014]* developed the Hydro-Thermal-Geochemical Model (HTGCM), in which the hydrological model DHSVM *[Wigmosta et al.,1994]* was coupled with the geochemical model PHREEQC *[Parkhurst, and Appelo, 1999]* and, in addition, adversion-dispersion, thermal transport and shrinking- core *[Davis and Ritchie, 1986]* modules were also coupled. This model was implemented for a remediation plot in a mine waste site in Southwestern Pennsylvania. However, HTGCM can be significantly improve to have a more complete geochemical characterization and a larger spatial scale.

1.2 SCIENTIFIC QUESTIONS

In this study, alkaline clay (AC), a highly basic nonhazardous industrial waste (according to the Resource Conservation and Recovery Act or RCRA) from the alumina refining process, is used as the remediation material to inhibit pyrite oxidation in waste coal piles. Through a series of static (i.e. batch and acid base accounting) and kinetic (i.e. flow through columns) experiments, complemented with field measurements and hydro-geochemical modeling (*see Figure 1.1*), the proposed research addresses at the following scientific questions:

- Is alkaline clay (AC) an adequate material for ARD remediation in a waste coal pile?
- What is the optimal AC/CR mixing ratio to be applied in the amended layer?
- What is an appropriate depth for the amended layer in the study site?

- What effects do complementary measures such as vegetation and saturated sand barrier might have in the amended layer?
- What is the feasibility of modeling the acid rock drainage remediation processes in a watershed scale, utilizing a physically-based hydro-geochemical model? Can this model be extrapolated to another study site?
- What are the implications of the long-term performance of the proposed remediation in the site (e.g. the trends of the main parameters involved in this process such as pH, concentrations of sulfate, ferrous iron and other metals)?

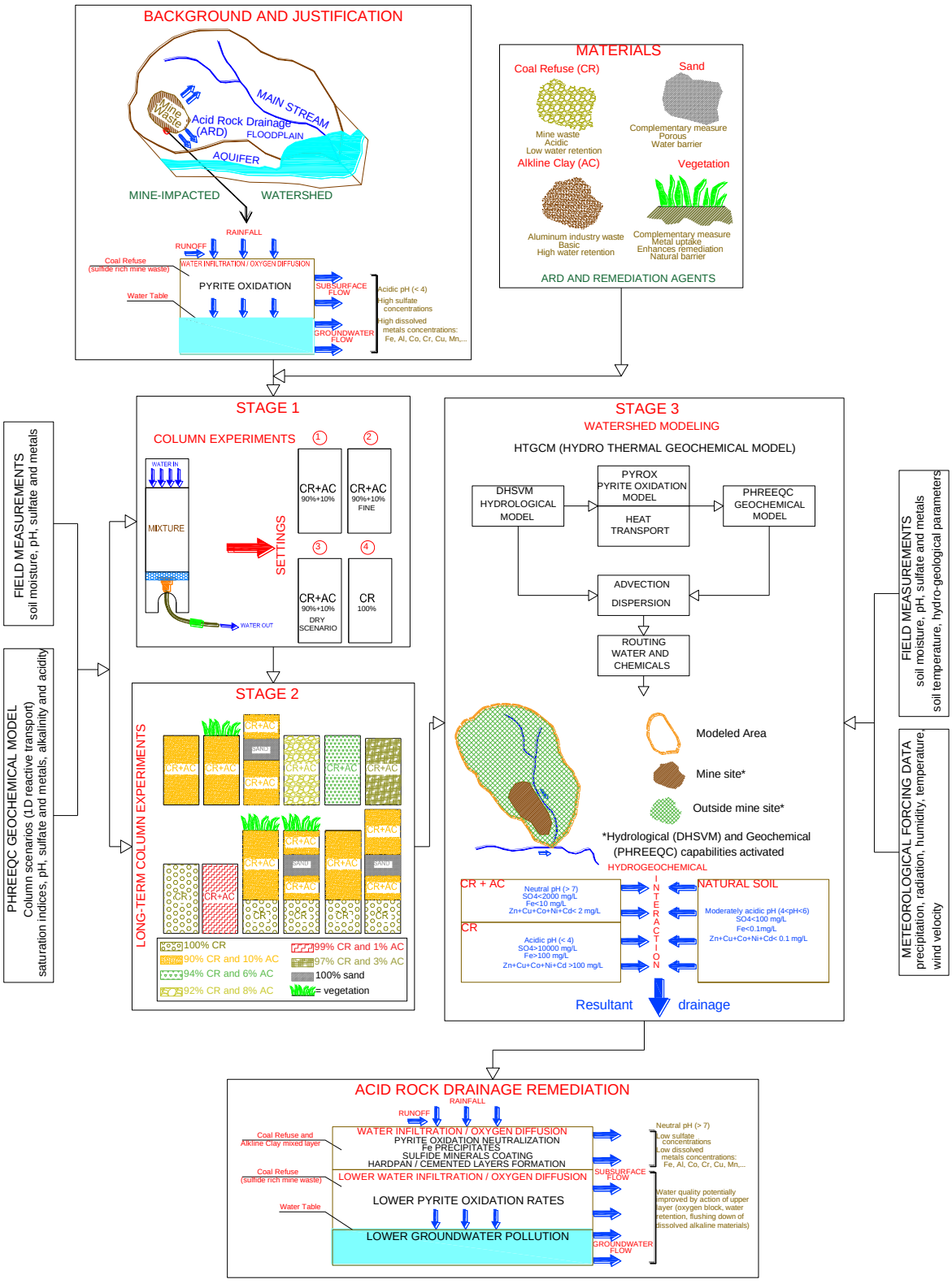

Figure 1.1. Research design

1.3 STATE OF THE ART

Several ARD passive treatment approaches have been developed in recent years, where the main concern is the search for an adequate alkaline remediation material. The choice of the alkaline material depends on many factors such as: neutralization potential, cost, production distance from the site, and supply according to the treatment demand *[Pérez-López et al., 2011]*. For instance, an added value regarding passive remediation is the utilization of waste alkaline materials, thereby resulting in an environmentally friendly and sustainable solution.

Jurjovec et al. [2002] investigated the mechanisms of acid mine neutralization, including the release of metals from mine tailings, through a complex column experiment setup where water was pumped at the bottom of the column and collected at the top. This study focused in the relationship between pH and metal concentration. It has been found that metal mobility in the effluent water is controlled by the pH. Non-oxidized fresh tailings with low content of Fe(III)-(oxy)hydroxide were utilized, therefore, it would be expected that, for oxidized tailing, metal concentration in the leachate could be higher.

Kannan et al. [2003] studied the potential use of fluidized-bed combustion (FBC) ash, a waste by-product of advanced coal combustion, in an underground coal mine for ARD control. This remediation mechanism consisted in mixing the FBC with other elements to form a grout that could be injected through boreholes in the mine tailings, thus restricting water and oxygen flow into pyrite and decreasing acid production. The key point of this approach was to optimize the number of boreholes needed per area of tailings.

Gibert et al. [2003] explored a permeable reactive barrier (PRB) as a passive, in-situ treatment for ARD. PRB are trenches in the mine tailings where drainage water flows through.

These trenches are filled with an appropriate reactive material able to induce physicochemical and/or biological processes that remediate contaminated groundwater. Experimental columns were built, using limestone and compost as the main components of the PRB. Low oxygen conditions were maintained by pumping nitrogen into the columns. After 120 days, results indicated pH neutralization and metal depletion. However, no significant sulfate removal was observed.

Another PRB approach was studied by *Lapointe et al. [2006]*. They ran, during around 90 days, column experiments using Bauxsol, a chemically and physically treated bauxite refinery residue, as the ARD remediation material. Bauxsol is produced when red mud (a residue from alumina production) is treated with another material (e.g. seawater or other magnesium/calcium rich brines) in order to produce a near-neutral material that can be used to treat ARD *[McConchie et al. 2003]*.Five columns, containing from 20 to 25% of Bauxsol, were tested. Acidic water (pH = 2) was pumped at the bottom and collected a top of each column. According to the results, on a short term basis, Bauxsol proved to be a valid ARD treatment, concerning metal removal from the leachate. pH showed a decreasing trend and, at the end of the experiments, pH had a range from 4 to 7, depending on the column design.

Paradis et al. [2006] conducted a study to neutralize ARD through batch and column leaching tests using red mud bauxite as the reactive material. After around 120 days, a stable and above the neutral level pH was obtained in all columns containing red mud bauxite (from 10 to 20%). Metals and sulfate depletion was also observed. In this study, the hardpan formation at the surface of the mine tailings was analyzed. Hardpan is a low permeability thin layer that is formed due to the presence of alkaline materials in the mine waste piles, acting as a natural barrier that limits oxygen and water diffusion *[Blowes et al., 1991]*.

The potential main benefits of the cemented layer–hardpan in sulfide-bearing mine tailings are a probable attenuation of some toxic compounds (e.g. Pb), a restriction of the downward movement of the oxidation front, and a protection of the surface of the tailings against erosion (e.g. by wind or water) *[Graupner et al., 2007]*. These potential benefits are increased with a heterogeneous distribution of grain sizes and low permeability surface layers. Cemented layers have a significant influence on natural attenuation of the toxic As and Pb species owing to their capacity of water retention *[Kohfahl et al., 2010]*. Furthermore, the grain size distribution was proved to have a major effect on oxygen diffusivity due to its control on the water saturation.

Daubert et al. [2007] worked with crab shell chitin to design a passive remediation system for ARD. The experiments, conducted during only for 9 days, consisted in collecting ARD water and soil samples from a stream near Altoona, Pennsylvania, a few miles downstream of the nearest coal mine. These samples were treated before tested (e.g. degassed with nitrogen to obtain low dissolved oxygen) and then, mixed with crab shell chitin. Results showed pH increase (without reaching neutral level), acidity decrease and alkalinity increase. However, no long term impacts could be established due to the short duration of the experiments.

Perez Lopez et al. [2007] investigated the iron-coating role on the oxidation kinetics of a pyritic sludge doped with fly ash. The iron-coating or "pyrite microencapsulation" *[Evangelou, 1995]* is a process by which pyrite grains are coated by Fe precipitates, thus reducing grain surface subject to oxidation by its contact with oxidizing agents (i.e. water and oxygen). Non-stirred and stirred flow-through experiments with a controlled environment in terms of water addition (i.e. pumping) and oxygen content (i.e. low dissolved oxygen) were designed and carried out during 40 days. Only for non-stirred conditions, there was a coating of the pyrite grains by Fe precipitates as ferric oxyhydroxide. The main finding of this kinetic approach was that fly ash is an ideal

remediation material to neutralize pyrite oxidation by inducing pyrite microencapsulation in a relatively short term. On the downside, fly-ash utilization might release some toxic elements in solution during the leaching *[Querol et al., 2001]*. Due to the fact that the coating of pyrite grains is enhanced in high alkalinity environments, this entails an additional benefit of ARD passive remediation, as this will implicate the decrease in the alkalinity demand in the mine tailings (i.e. in the long term) *[Huminicki et al., 2009]*.

Yeheyis et al. [2009] carried on another ARD remediation study using coal fly ash (collected from a power plant), mixed with mine tailings, and tested in columns. The duration of the experiments (i.e. 80 weeks) enabled to observe the long term behavior of the system. This study also tested various columns with different coal fly ash content. However, it is not certain the effectiveness of this approach in highly oxidized mine tailings, as results show that, in the case of the control column (i.e. without fly ash), pH values are mostly above the neutral level. Moreover, sulfate concentrations in the control column are relatively low (i.e. around 2000 mg/l).

Ouangrawa et al. [2010] analyzed ARD prevention with the elevated water table (ETW) technique. Results obtained through column experiments conducted for approximately 500 days, showed pH neutralization, iron and sulfate removal. However, some complications are faced with this strategy (e.g. controlling oxygen diffusion and water table elevation), making it a relatively expensive in-situ remediation.

Toro et al. [2012] proposed pyrite oxidation inhibition by using limestone (i.e. inhibition by pH increase) and olive pomace (i.e. inhibition by organic compounds). They conducted a series of batch experiments during approximately one month to analyze the potential use of these remediation materials, acting together. They mainly focused in pH and Fe. This remediation

strategy was identified as potentially economical and environmentally friendly. No long term impacts were analyzed.

Sahoo et al. [2013] studied ARD remediation through the potential use of two industrial wastes: coal fly ash and clinker dust. Three column experiments were conducted during around 40 days. In general, results indicate that pyrite oxidation neutralization occurs, as pH values are around the neutral level (pH=7). There is also a removal of some metals and sulfate from the leachates, a clear indication of solid precipitates.

In recent years, PHREEQC *[Parkhurst and Appelo, 1995, 1999, 2013]* has become a valuable tool for simulating geochemical processes in a variety of environmental conditions. *Sahoo et al. [2013]* utilized PHREEQC to calculate the saturation indices (SI) of various Fe-oxyhydroxides (HFO) and calcium carbonates phases from the leachates of columns experiments. *Appelo et al. [1998]* modeled in PHREEQC the chemical composition of a column effluent. *Motalebi et al. [2012]* explored the effect that some input parameters of PHREEQC (e.g. flowrate, initial pH, grain size distribution) have on the transport of dissolved metals such as Mn, Ni and Cd in a mine tailing. MINTEQ2 *[Jacques et al., 2008]* is another model for geochemical modeling as it is able to calculate the equilibrium reaction in aqueous systems.

Regarding hydro-geochemical modeling, the framework of the model HYDRUS *[Šimůnek et al., 1998; Šimůnek et al., 1999]* has been widely used for simulating pyrite oxidation based on hydrological processes and solute transport. Moreover, several models include the pyrite shrinking-core concept *[Davis and Ritchie, 1986]*. For example, the model POLYMIN *[Molson et al., 2005]* was developed based on HYDRUS with 2D transport. The model MINTEQA2 *[Allison et al., 1991]* was developed for hydro-geochemical simulations in a waste coal pile profile. The

model THERMOX *[da Silva et al., 2009]* was developed coupling the HYDRUS-2D with an early version of PHREEQC *[Parkhurst et al., 1995]*. The model HP1 *[Jacques et al., 2006; Šimůnek et al., 2008]* is a 1D hydro-geochemical model which was developed based on HYDRUS-1D and PHREEQC v2.0 *[Parkhurst and Appelo, 1999]*.

The TOUGH AMD model *[Lefebvre, 1994]* was developed based on TOUGH2 *[Pruess, 1991]*, which emphasized the flow movement in porous media, does not use the HYDRUS framework. The idea of the shrinking core model was also applied into TOUGH AMD to include the physical process of pyrite oxidation. Likewise, the MIN3P model *[Mayer et al., 2002]* also includes the shrinking core model and its own hydrological processes. The SWAT model *[Neitsch et al., 2002 and 2005]* is another tool that have been used for assessment of water quality through a hydrological processes.

HTGCM *[Xu, 2014]* is a hydro-thermal-geochemical model based on the framework of DHSVM *[Wigmosta et al., 1994]* model. It is able to deal with the processes of hydrology, thermal transport and geochemical transport at field scale and watershed scale. The shrinking core model, the heat generation modules, the different runoff mechanisms e.g. saturated runoff and infiltration excess runoff in DHSVM and the infiltration in the hilly region are all included. This model has been successfully calibrated and validated in four experimental plots in the Mather mine, located in Pennsylvania, USA, where AC has been used as a remediation material. However, there are improvements that can be made to this model to achieve a better performance in characterizing the ARD and ARD neutralization processes. Moreover, there is a great availability of geographical, meteorological and hydrological data from the model's study site. Therefore, an improved HTGCM model will be utilized in this study.

1.4 RESEARCH DESIGN

1.4.1 Study sites for sample collection, material characterization, field monitoring, calibration and validation

1.4.1.1 Mather mine The coal refuse (CR) samples were collected from a former coal mine in operation from 1925 to 1965, located in Mather, Greene County, Pennsylvania, USA *[Figure 1.2]*. In 2009, a reclamation plan was started through the construction of four experimental plots, covering an approximate area of 1 ha. Two of the test plots were constructed according to the following specifications:

- Plot 1: 100% CR (control plot).
- Plot 2: 90% CR with 10% AC mixed layer with a depth of 61 cm.

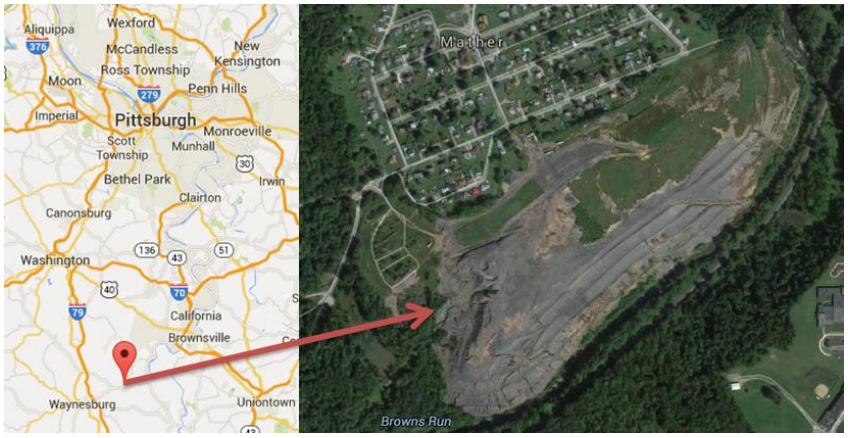

Figure 1.2. Location of the Mather mine

a)

b)

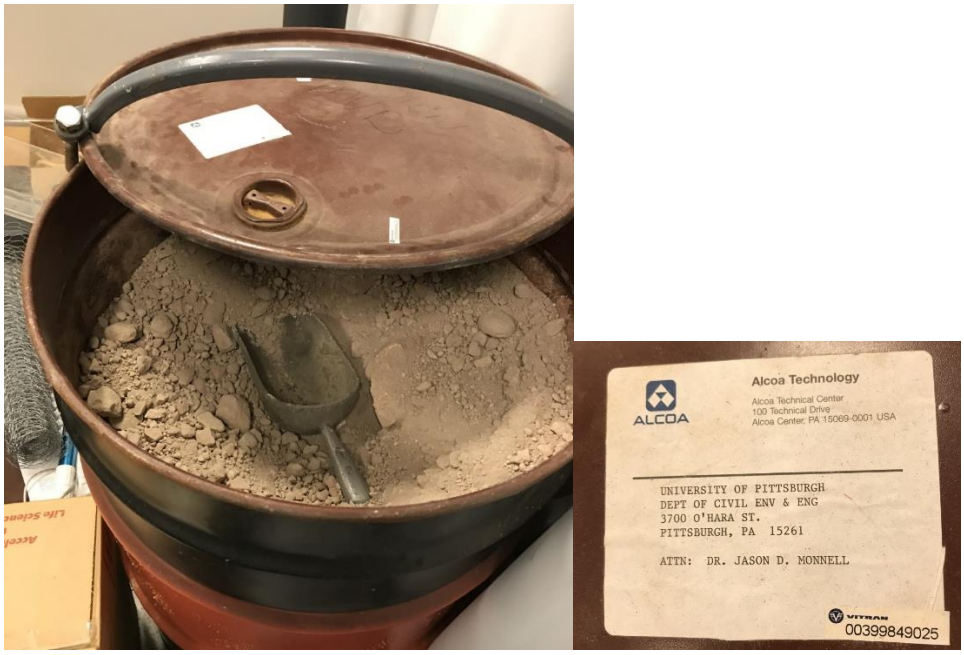

Figure 1.3. a) Field work in Mather: data logger data download and coal refuse samples collection. b) Alkaline clay provided by Alcoa

At various points along the plots, instrumentation was installed to monitor the environmental impacts of the remediation, including lysimeters for collecting drainage water samples (at 61 cm and 91 cm) that were later tested in the laboratory for pH, sulfate, and metals/metalloids. Data loggers were also installed along the plots *[Figure 1.3a]*. These instruments were connected to sensors that measured soil moisture, soil water potential and soil temperature at various depths, from 5 cm to 91 cm. In addition, an X-Ray Diffraction (XRD) test was used to obtain the mineral composition for both coal refuse and alkaline clay *[Table 1.1]*.

Table 1.1. Solid compositions of Coal Refuse (CR) and Alkaline Clay (AC) (Source: ALCOA)

Coal refuse composition	Percentage (%)
Quartz: SiO_2	55.6
K-mica: $KAl_2(AlSi_3O_{10}(OH)_2)$	24.0
Jarosite-K: $KFe_3(OH)_6(SO_4)_2$	9.9
Kaolinite: $Al_2O_32SiO_22H_2O$	8.3
Calcite: $CaCO_3$	1.0
Gypsum: $CaSO_4 \cdot 2H_2O$	0.9
Pyrite: FeS_2	0.3

Alkaline clay composition	Percentage (%)
Dicalcium silicate: $2CaO(SiO)_2$	57
Sodalite: $Na_8(Al_6Si_6O_{24})Cl_2$	12
Gehlenite: $Ca_2Al(AlSiO_7)$	10
Hematite: Fe_2O_3	8
Calcium aluminum sulfate: $Ca_6Al_2(SO_4)_3(OH)_{12} \cdot 26H_2O$	2
Calcium titanium oxide: $CaTiO_3$	2
Quartz: SiO_2	3
Titanium dioxide: TiO_2	2
Calcium carbonate: $CaCO_3$	3
Gibbsite: $Al(OH)_3$	1

Mather was the study site for the development of HTGCM. However, the model was only tested at a plot scale (< 1 ha). In the proposed study, among other changes detailed in the subsequent sections, the model will be tested at a watershed scale.

1.4.1.2 Ernest Mine The Ernest Mine operation is located in White and Rayne Townships, Indiana County, Pennsylvania, USA *[Figure 1.4]*. The operation is utilizing waste coal ash for alkaline addition to treat ARD. The refuse material is taken out, transported to the Cambria CoGeneration power plant, and FBC coal ash produced from burning the refuse is returned and placed on the site. Ash placement commenced in October 1996 and has continued to the present. However, results have shown the coal ash addition haven't significantly improve the water quality at the mine discharge *[Pennsylvania Minefill Study, 2007]*.

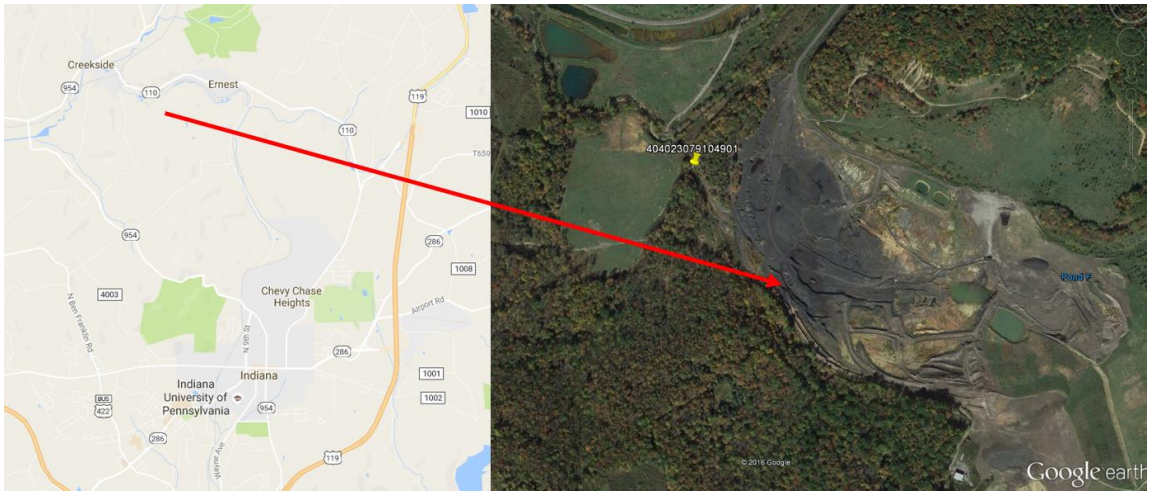

Figure 1.4. Location of the Ernest Coal Mine.

This mine have been continuously monitored for over a decade. Moreover, the majority of the sampling sites are located at the mine's drainage discharge, which makes possible the implementation of the HTGCM model in this watershed *[Figure 1.5]*.

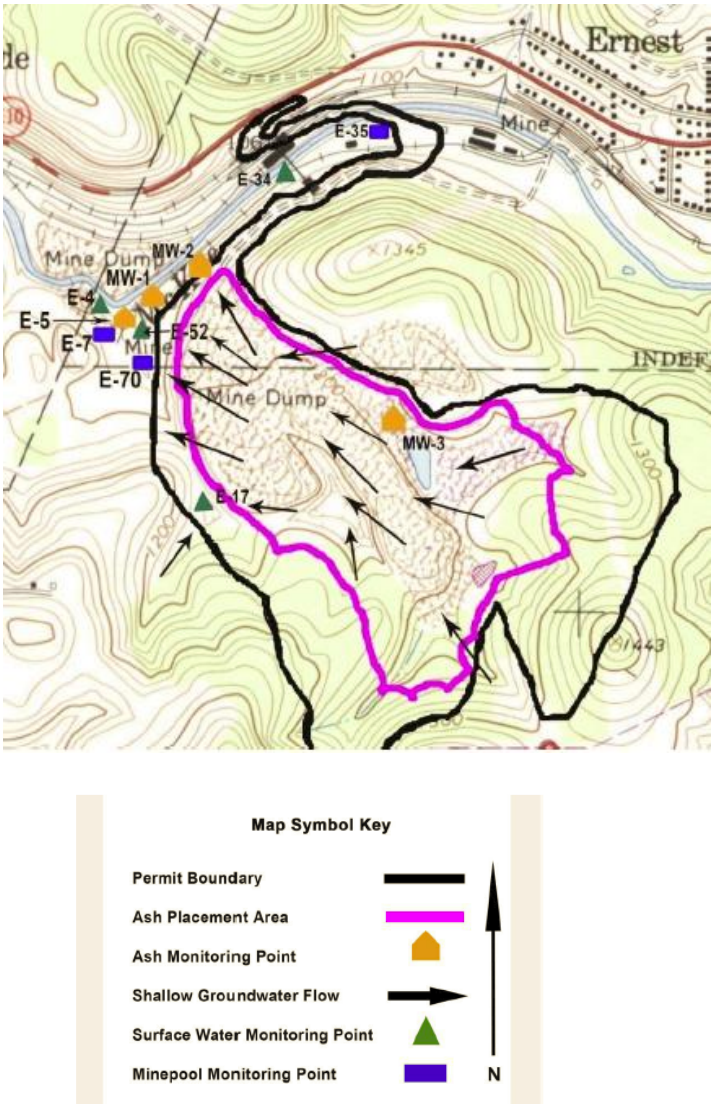

Figure 1.5. Location of the sampling sites at the Ernest Coal Mine *[Pennsylvania Minefill Study, 2007]*.

1.4.2 Laboratory Experiments

1.4.2.1 Static tests: batch and acid base accounting For the batch experiments, dry CR (samples were collected since 2012, in a different location than the experimental plots, inside the Mather site) and AC samples were passed through a #16 sieve. A 30 g sample was packed into a 50 mL beaker *[Figure 1.6]*. Samples were moistened using deionized water and kept at room temperature

(25℃) for 0-7 days. The focus of the batch experiments was aimed at investigating the effect of the following factors:

- AC content or mixing ratio with respect to coal refuse (from 0%/100% to 60% / 40%)
- Water content, in order to reflect the effect of soil moisture in the column experiment. The chosen water amounts were 0, 5, 10 and 15 mL
- Reaction time, in order to reflect the effect of water flushing frequency in the subsequent column experiment. The chosen reaction times were 1, 3 and 7 days

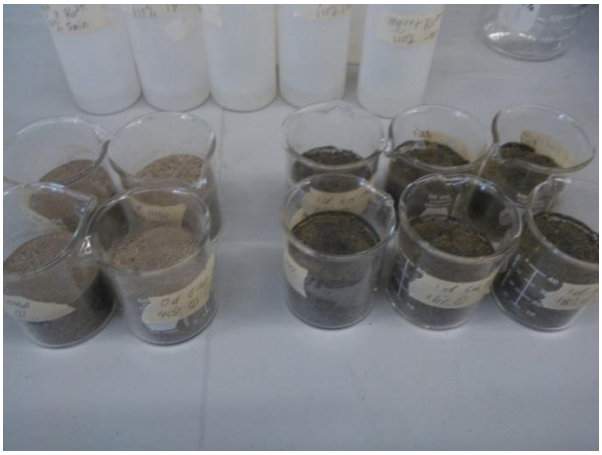

Figure 1.6. Batch reaction experiments

Once the intended reaction time was reached, 90 mL of deionized water was mixed with the sample and stirred for 15 minutes. Then, the supernatant was extracted and filtered with a 0.45 μm membrane. The pH of the filtered liquid was measured immediately. As a control, 30 g samples with 0 day reaction time and no water addition were prepared. The remaining treatment procedure for the control batch is the same as the one described above.

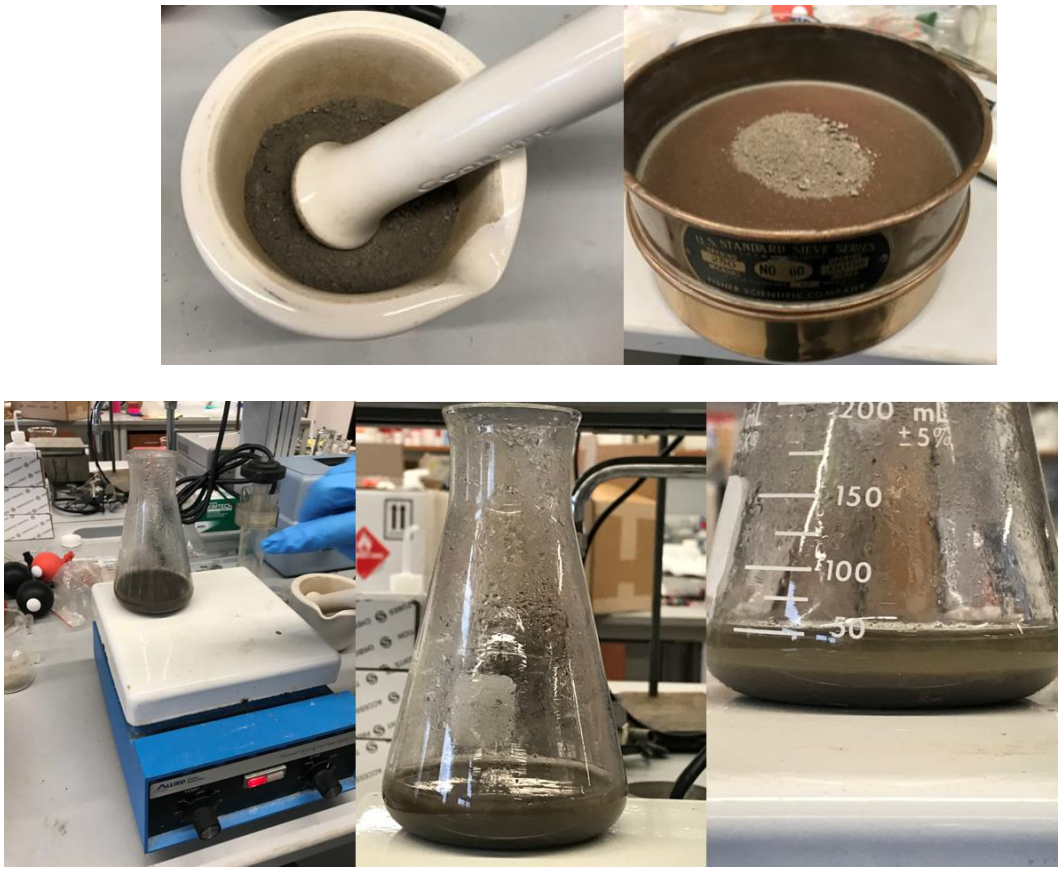

Figure 1.7. Acid base accounting experiments

The acid base accounting test *[Figure 1.7]*, based on the methodology developed by *Sobek et al. [1978]*, was performed to establish a balance between the acid-producing and acid-consuming components in the mixture. The main assumptions of this method are: a) pyrite is oxidized by oxygen, b) the acid production potential is based on the total sulfur content (%S), c) 1 mole of S produces 2 moles of acid (H^+), which is neutralized by 1 mole of calcium carbonate ($CaCO_3$), thus requiring 31.25 kg of $CaCO_3$ per ton of material to neutralize 1% S. The %S was calculated from the XRD analysis and the acid potential (AP) was calculated using the above-mentioned relationship.

Samples of AC and CR were acidified with hydrochloric acid (HCl) and then titrated with sodium hydroxide (NaOH) in order to determine the acid consumption. Later, the acid neutralization potential (NP) in terms of Kg $CaCO_3$/ton was calculated for both AC and CR.

For both static tests, the sample analysis was triplicated and the results presented in this study correspond to the average value of each described case.

1.4.2.2 Kinetic tests: flow-through columns Two sets of column experiments were designed to evaluate ARD remediation. The columns were built using polycarbonate tubes with an internal diameter of 10 cm. The columns were filled with uncompacted CR (samples were collected from 2013) and AC, passing through a #4 sieve, to a height of 15 cm. A net containing 4 mm diameter glass beads was installed to prevent clogging at the bottom outlet of each column.

The column sides were covered to prevent light from reaching the mixture *[Figure 1.8a]*. Deionized water (pH = 7) was added periodically (i.e. slowly to avoid water accumulation at the surface) at the top of the columns to simulate rainfall. The water was allowed to drain freely through the column. At the bottom, water was collected through a rubber hose. An acceptable amount of fine particles were lost through the beads at the outlet. For all of the columns, except one, 200 mL of water were added per week (equivalent to approximately 1,300 mm per year), which is similar to the average annual precipitation in southwestern Pennsylvania *[www.usclimatedata.com]*. Saturated conditions were maintained at the bottom of the columns, which inhibited oxygen diffusion through the outlet. *Figure 1.8b* shows a schematic column design. The conditions of some columns were duplicated to provide a comparative analysis of the kinetic tests for the amended and non-amended scenarios.

After the leachate was collected at the bottom of the columns, the sample was filtered using a 0.45 µm MF-Type (mixed cellulose esters) filter membrane and the pH was measured immediately. The sample was then subject to chemical composition analysis using an ICP-MS:Perkin Elmer NeXION 300X inductively coupled plasma mass spectrometer (EPA Method 200.8) *[Figure 1.9a]* and an IC:DIONEX ICS-1100 (EPA Method 300.0) *[Figure 1.9b]* to measure the concentration of dissolved metals/metalloids and sulfate, respectively.

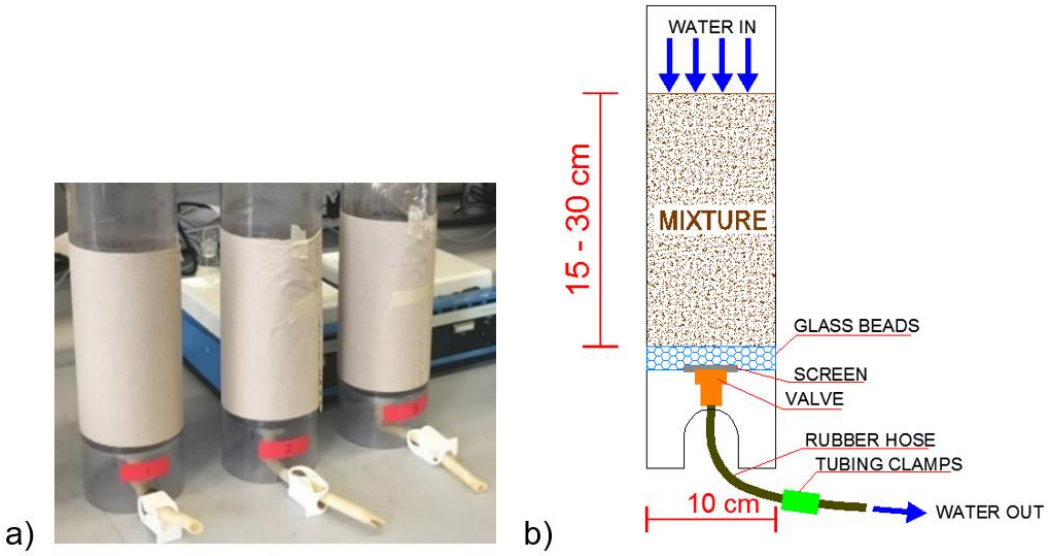

Figure 1.8. Column experiments: a) image of the columns, showing the covered sides b) schematic design of the columns

a)

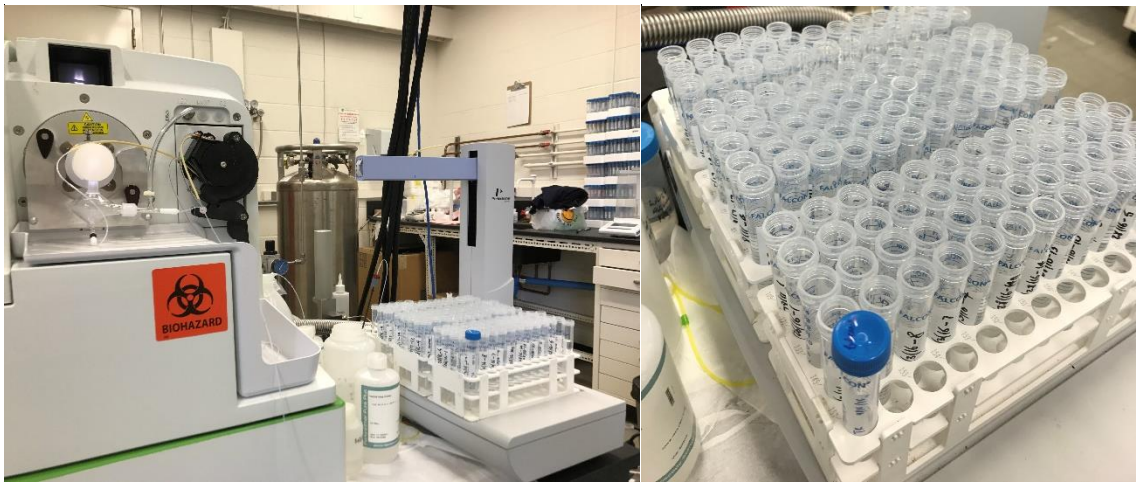

b)

Figure 1.9. a) ICP-MS. b) IC

1.4.2.3 Acidity and alkalinity in the leachate To determine the balance between acidity and alkalinity (expressed as mg/L of $CaCO_3$) in the leachate over time, a measured and calculated alkalinity was compared to a theoretical acidity for several collected water samples from the columns. This approach has been demonstrated to correctly reflect the amount of alkalinity

required to successfully neutralize the acidity *[Kirby and Cravotta, 2005a,b]*. The alkalinity was measured by a titration method *[APHA, 1998a,b]* and was also computed using the PHREEQC model. The acidity, assumed to be mostly due to metals, was calculated using *Eq. (1-1) [Kirby and Cravotta, 2005a,b, Watzlaf et al., 2004 and Hedin et al., 1994]*:

$$Acidity\ (mg/L\ CaCO_3) = 50(10^{(3-pH)} + 2C_{Fe}/55.8 + 2C_{Mn}/54.9 + 3C_{Al}/27.0) \quad (1\text{-}1)$$

Where C_{Fe}, C_{Mn} and C_{Al} are the concentrations in mg/L of Fe, Mn and Al, respectively. These concentrations were obtained from the procedure described in *Section1.4.2.2*. Later, the net alkalinity was computed according to *Eq. (1-2)*:

$$Net\ alkalinity\ (mg/L\ CaCO_3) = Alkalinity - Acidity \quad (1\text{-}2)$$

1.4.2.4 Metals/metalloids measurements in grass To help assess the impact of vegetation in the ARD remediation process and explore the possible metal toxicity suffered by plants, metals were measured from vegetation (grass) samples, growing in mixed soil with CR and AC. As a control, the measurements were also done for grass grown in regular soil. The grown grass (various pots were used), excluding the roots, was washed with DI water, then oven-dried at 70°C, powdered, acidified (9 mL of concentrated nitric acid) and digested (0.5 and 0.25 g of the dry matter) at 180 ± 5°C during 9.5 minutes inside a microwave digester (EPA Method 3052) *[Figure 1.10]*. After digestion, the resultant solution was completely extracted from the microwave vessel and filtered using a 0.45 µm MF-Type (mixed cellulose esters) filter membrane. Finally, metals/metalloids will be measured using the same methodology detailed in *Section 1.4.2.2*.

Grass grown in CR soil (failed attempt): grass unable to grow due to the high acidity of the environment

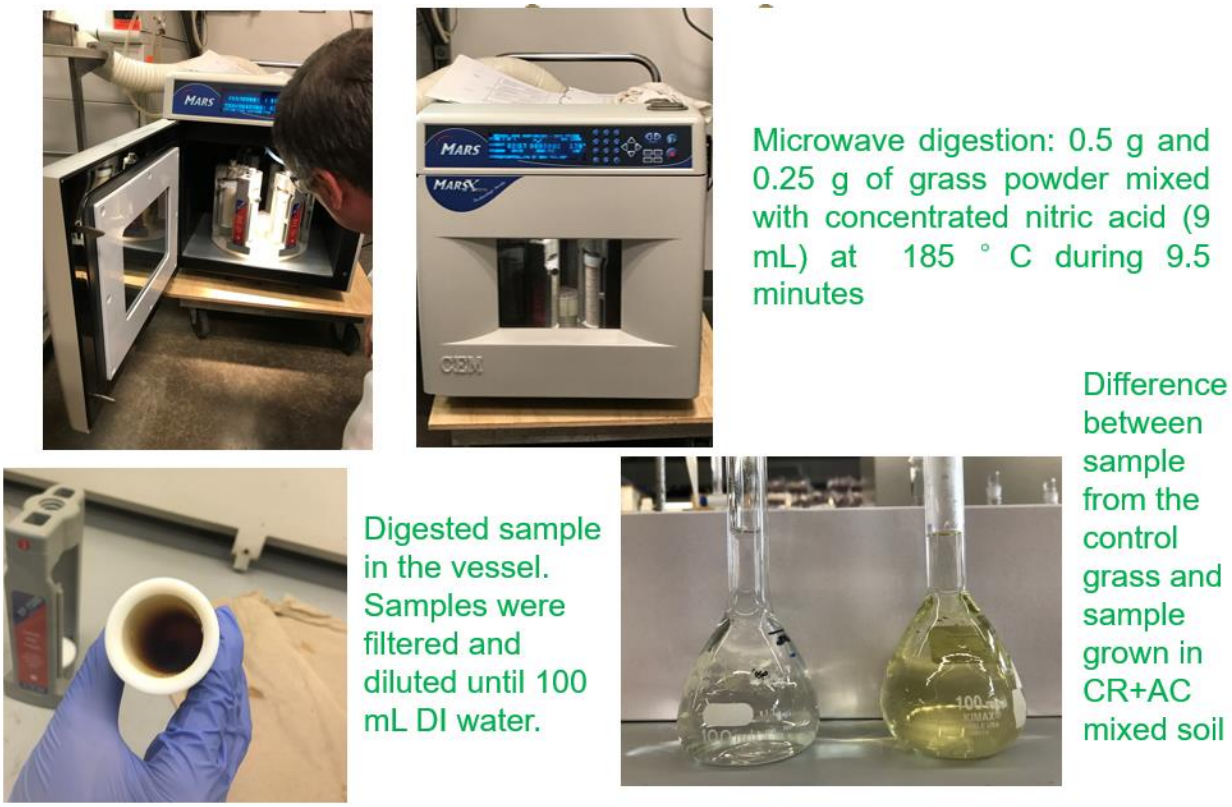

Figure 1.10. The process of grass acid digestion

1.4.3 ARD Modeling

1.4.3.1 Geochemical modeling: PHREEQC In the first stage of the modeling framework, described in Chapters 2 and 3, PHREEQC simulations, assuming the column scenarios of the experiments, will provide an important input about the dissolution/precipitation processes through the interactions between the aqueous and minerals phases. In addition, PHREEQC will be utilized to predict the long-term behavior of the system, beyond the experimental time (i.e. ≈ 900 days).

ARD simulations (for amended and non-amended scenarios) using the PHREEQC model were made under the following main assumptions:

1. Pyrite oxidation was only produced by dissolved oxygen (DO) or by ferrous iron (Fe^{3+}) as the oxidants. This assumption was based on the theoretical principle developed by *Williamson and Rimstidt [1994]*. For pH < 3.5 (i.e. non-amended scenario in column 4), Fe^{3+} is the oxidant *[Eq. (1-3)]*, while for pH > 3.5 (i.e. amended scenario in column 1), DO is the oxidant *[Eq. (1-4)]*.

$$r = 10^{-6.07} \frac{m_{Fe^{3+}}^{0.93}}{m_{Fe^{2+}}^{0.4}} \quad (1\text{-}3)$$

$$r = 10^{-8.19} \frac{m_{DO}^{0.5}}{m_{H^+}^{0.11}} \quad (1\text{-}4)$$

2. The initial dissolved oxygen saturation index was assumed to be -0.7 *[Parkhurst et al., 1999 and 2013]*. The saturation index indicates the saturation with respect to the phase. In this case is the saturation of DO with respect to the aqueous phase. For gases, this number is the log of the partial pressure. A positive saturation index means an oversaturation and a negative saturation index means that the phase is not saturated.
3. The mineral content, besides pyrite (e.g. quartz, gypsum, calcite, jarosite, etc.), identified in the XRD test, was initially assumed to be in equilibrium in the aqueous phase (saturation index = 0), which means that the minerals could either dissolve or precipitate. These minerals are compounds of Fe, S, Ca, Mn, Al, Mg, C, etc.
4. The initial moles in the PHREEQC equilibrium and kinetic models were calculated based on *Eq. (1-5)*, where: $Moles_{mineral}$ is the initial content of the mineral phase (moles),

$\%XRD$ is the percentage of the mineral detected in the XRD analysis, SRM is the saturated rock mass (6.3 kg) considering a soil dry density and porosity of 2700 kg/m^3 and 30%, respectively, $Mol\ mass$ is the mineral molar mass (g/mol) and, The number "1000" means that the calculation refers to 1 liter (1000 g) of water. For instance, the initial pyrite content was calculated as 0.15 mol, from the initial pyrite content in the mixture (1.2 wt%), detected in the XRD test. The usual pyrite content range in the technical literature is from 0.1 wt% to 5 wt%.

$$Moles_{mineral} = \frac{\%XRD}{100}\ x\ SRM\ x\ \frac{1000}{Mol\ mass} \quad (1\text{-}5)$$

5. The initial solutions (i.e. dissolved metals and non-metals, sulfate, pH) were approximately equal to the characterized solutions for column 1 (i.e. the amended scenario) and column 4 (i.e. the non-amended scenario). These parameters were obtained from the pH meter, ICP-MS and IC.

1.4.3.2 Hydro-Thermal-Geochemical Model (HTGCM) improvement and implementation

The final stage of the modeling framework will be performed using a modified version of the Hydro-Thermal-Geochemical Model (HTGC), originally developed by *Xu [2014]* to simulate the acid rock drainage and alkaline neutralization processes in an amended and non-amended plots in the Mather mine site. Among the main objectives in this final modeling stage is to expand the modeling scale to a watershed scale, a more complete characterization of the output water quality

and the improvement of the physically-base component of the model. Several changes and improvements were made to the original model, aiming at the following particular issues:

1. Setup to run the model in a watershed scale. Create a new mask file to represent the coal mine and outside-coal mine areas within the watershed. Currently, the model has been only tested in a plot scale. Since the model will be tested in a larger scale, a 10m resolution will be utilized, instead of the 3m resolution of the experimental plots in Mather.
2. Add more dissolved metals to be calculated in the model: *Zn, Cu, Cr, Ni* and *Co*. These metals have been detected in the ICP-MS testing, for both the amended and non-amended columns. Accordingly, include these new chemicals in the PHREEQC input file (initial concentrations). Metals such as *As, Pb* and *Cd*, detected in other bituminous mine discharges, can be included in the model as well.
3. Include new reactions in the PHREEQC database that involve all the new metals that are going to be included. Moreover, some buffer reactions such as the dissolution of calcite (CaCO3) can also be included into the model. Calcite combines with pyrite, water and oxygen to release iron precipitates, Ca and sulfate. Later, both Ca and sulfate can precipitate as gypsum ($CaSO_4\,2H_2O$). In other words, the dissolution of calcite neutralizes acid and can help to increase the pH and alkalinity of the mine wáter.
4. Include the "real" chemicals proportion (i.e. solid phase) within the soil (kg chemical / kg soil), based on the mineral composition obtained in the XRD test.
5. In the pyrite oxidation – shrinking core module, include de effect of the pyrite grain coating by iron precipitates. Currently, this module assumes a constant oxygen diffusion coefficient over the entire simulation. However, in fact, the oxygen diffusion decreases over time due to the pyrite coating. Thus, introducing a variable oxygen diffusion as a function of time

will make the model take into account the effect of the pyrite coating. The continuous calculation of the diffusion coefficient will be a function of the amount of Fe released, the amount of Fe precipitated into the pyrite surface, the pyrite surface area per mass unit and the coating porosity. At the end, the pyrite dissolution, pyrite grain shrinking and the pyrite grain coating will be the factors that control pyrite oxidation.

6. Modify the amended layer depths and/or the amended layers setup or the remediation design (e.g. two amended layers with different %AC), according to the outcomes of the research (i.e. laboratory experiments) and the model testing.

All these changes will be first tested in the Mather mine watershed (Case Study 1) and then in the Ernest mine watershed (Case Study 2).

2.0 ACID ROCK DRAINAGE PASSIVE REMEDIATION: POTENTIAL USE OF ALKALINE CLAY, OPTIMAL MIXING RATIO AND LONG TERM IMPACTS

2.1 INTRODUCTION

Acid rock drainage (ARD) is one of the most adverse environmental problems of the mine industry. Surface water and ground water affected by this pollution are characterized by their acidity and the high content of sulfates and heavy metals. ARD loads may also cause high concentration of toxic elements at the bottom sediments of a reservoir *[Sarmiento et al, 2009]*. Damage associated with ARD might result in the total disappearance of the aquatic fauna in the affected ecosystem, as well as the impossibility of water resources to become suitable for human, agricultural or industrial consumption.

The acid mine drainage process initiates when sulfide minerals, highly contained in mining wastes, oxidize through complex chemical reactions, involving the combined action of oxygen (e.g. the oxidant) and water (e.g. the solvent). Coal deposits might contain between 1 to 20% amounts of pyritic sulfur, which is a generic term that includes other iron sulfide minerals *[Johnson et al, 2005]*. As pyrite is usually the sulfide mineral involved, this process is often referred as pyrite oxidation, which results in the production of sulfate and ferrous iron, and other byproducts such as elemental sulfur, polysulfide, hydrogen sulfide, ferric hydroxide, iron oxide or iron oxyhydroxide *[Chandra et al., 2010]*. Acid mine drainage is mostly formed in the underground

water of deep mines and it is characterized by low pH and high concentrations of heavy metals and other toxic elements. It can severely contaminate surface and groundwater, as well as the soil *[Peppas et al., 2000]*.

Three main stoichiometric chemical reactions *[Garrels et al., 1960 and Singer et al., 1970]* are often used to describe aqueous pyrite (FeS_2) oxidation.

$$FeS_2 + 7/2\ O_{2\ (aq)} + H_2O \rightarrow Fe^{2+} + 2SO_4^{2-} + 2H^+ \quad (2\text{-}1)$$

$$Fe^{2+} + 1/4\ O_{2\ (aq)} + H^+ \rightarrow Fe^{3+} + 1/2\ H_2O \quad (2\text{-}2)$$

$$FeS_2 + 14Fe^{3+} + 8H_2O \rightarrow 15Fe^{2+} + 2SO_4^{2-} + 16H^+ \quad (2\text{-}3)$$

Eq. (2-1) represents the oxidation of the pyrite (e.g. the sulfide mineral) into dissolved iron (Fe^{2+}), sulfate (SO_4^{2-}) and hydrogen (H^+), that leads to the increase in the total dissolved solids and the acidity of the water, resulting in the decrease in pH. In the presence of adequate oxygen (O_2) and hydrogen (H^+) concentrations, ferrous iron (Fe^{2+}) will oxidize into ferric iron (Fe^{3+}), according to the reaction described in *Eq. (2-2)*. Finally, ferric iron may also oxidize pyrite into ferrous iron, sulfate and hydrogen *[Eq. (2-3)]*. In addition, at low pH levels (< 3.5), ferric iron precipitates into iron oxide hydroxide ($Fe(OH)_{3\ solid}$) and, simultaneously, oxidizes into hydrogen, thus resulting in lowering of the pH *[Eq. (2-4)]*.

$$Fe^{3+} + 3H_2O \rightarrow Fe(OH)_{3\ solid} + 3H^+ \quad (2\text{-}4)$$

These main reactions show that oxygen and ferric iron are the two most important oxidants in the pyrite oxidation process.

Despite several previous studies of passive ARD remediation, there are still issues requiring improvement. For instance, the majority of the experimental strategies use complex systems for water addition (e.g. pumping), which sometimes generate artificial conditions that are difficult to replicate in-situ (e.g. limiting oxygen and water diffusion). Moreover, in most cases there is not a sufficient focus on the long-term impacts of the remediation technique nor is there an analysis of the optimal content of the reactive material to be applied in the field.

In this chapter, alkaline clay (AC), a highly basic nonhazardous industrial waste (according to the Resource Conservation and Recovery Act or RCRA) from the alumina refining process, was analyzed as a remediation material to inhibit pyrite oxidation in waste coal piles. The utilization of waste materials and by-products from other industries (e.g., AC) aims at the remediation sustainability. Through a series of static (i.e. batch and acid base accounting) and kinetic (i.e. flow-through columns) experiments, complemented with field measurements and geochemical modeling, three important issues associated with this passive and sustainable ARD remediation method were investigated: 1) the potential use of AC as an ARD remediation material, 2) the adequate alkaline clay / coal refuse mixing ratio (AC/CR) to ensure pH values close to neutral conditions, and, 3) the implications for long-term performance, in terms of the trends of the main parameters involved in this process such as pH, concentrations of sulfate, ferrous iron and other metals.

2.2 FIELD MEASUREMENTS

Figure 2.1 shows data retrieved from the Mather samples over a five-year period (i.e. 2009 – 2014) for the non-amended plot 1 (i.e. 100% CR) and plot 2 with a 61 cm amended layer (i.e. 90% CR +

10% AC). Due to permanent damage suffered by the sensors in the control plot, it was covered with the same amended layer as plot 2 in the spring of 2011.

Regarding pH levels, results showed a significant increase in pH in plot 2. At 61 cm, the pH varied approximately from 3 to 7. In the same plot, but underneath the amended layer (i.e. 91 cm) the pH was acidic during the first two years, ranging from 2 to 3. However, near the end of the five-year period, the pH was almost neutral (i.e. 6.37). As expected, the pH in the non-amended plot 1 is acidic during the entire study period. However, after the amendment of plot 1 in early 2011, the pH increases to nearly 4. As a direct consequence of the amendment of plot 1, in the long term, its pH is expected to have a similar behavior as the pH in the amended plot 2, but obviously, with a 2-year lag time, approximately.

Sulfate (SO4) concentrations in Mather were mostly within the expected range. Sulfate is a major contaminant produced by the pyrite oxidation. Field measurements were made in 2010 and 2011. In the amended plot 2, at 61 cm and 91 cm, sulfate ranged approximately from 1,700 to 2,200 mg/L. In the non-amended plot 1, sulfate varied from around 4,000 to 6,000 mg/L. However, following the amendment of plot 1 in 2011, there was some reduction in sulfate concentrations to 1,800 mg/L within the amended zone (i.e. 61 cm) and to 2,400 mg/L below the amended zone (i.e. 91 cm), respectively.

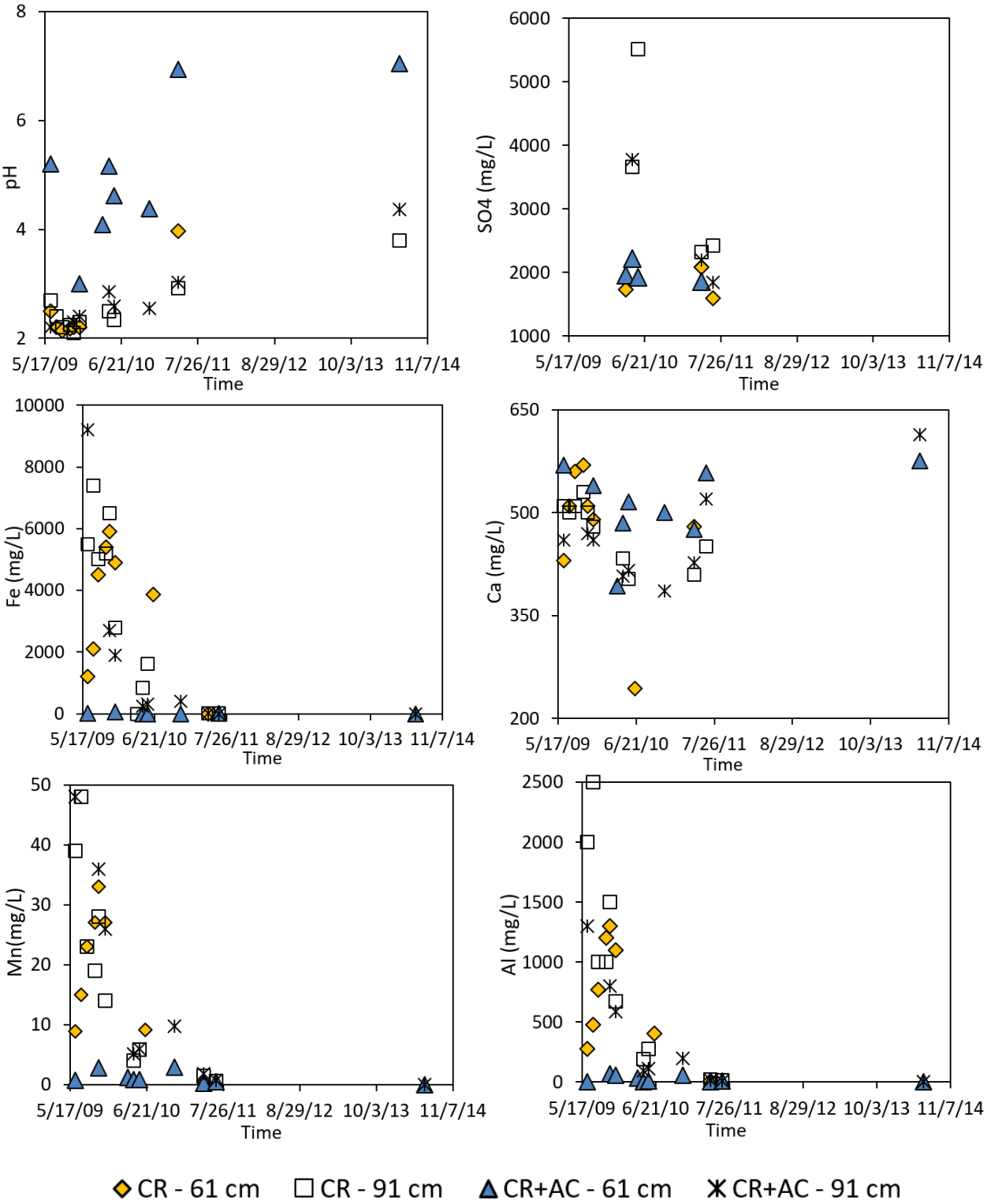

Figure 2.1. Field measurements for plots 1 (100% CR) and 2 (90% CR + 10% AC). Plot 1 was replaced by the materials of plot 2 in spring of 2011.

A general decreasing trend in Iron (Fe) concentrations can be seen in *Figure 2.1*, even in the non-amended plot 1. One of the possible reasons for the decreasing concentration was that Fe tends to precipitate, therefore, its concentration is limited in aqueous solution. In the non-amended plot 1, the initial Fe data in 2009 had a wide range, from 500 to 7,000 mg/L. Fe was usually higher at 91cm than at 61 cm depth. Data from 2011, following the amendment of plot 1, yielded much lower Fe concentrations, from around 10 to 20 mg/L. In the case of the amended plot 2, the initial results at 61cm showed concentrations less than 60 mg/L and the results from June 2014 showed concentrations less than 1 mg/L. In the amended plot 2, at 91 cm (i.e. beneath the amended layer), the results showed a high influence of the amended layer (i.e. Fe concentrations reduced to 1.41 mg/L by the end of the study period), which is likely due to the infiltration of high pH water from the overlying amended layer.

Calcium (Ca) is likely to be produced by the dissolution of carbonates during the neutralization of acidity produced by the pyrite oxidation. Therefore, Ca has two main characteristics: it tends to be conservative and, it has similar concentration in the amended and non-amended zone. In both plots 1 and 2, Ca concentrations varied from about 400 to 550 mg/L.

Manganese (Mn) also showed a clear decreasing trend in plots 1 and 2, but the orders of magnitude were different: in the amended plot, from 2009 to 2011, Mn decreased from 8 to 0.2 mg/L and, in the non-amended plot, it decreased from 36 to 10 mg/L. In 2014, when the non-amended plot had changed its settings, Mn concentration was around 2 mg/L.

Figure 2.1 shows Aluminum (Al) following a similar decreasing trend as Fe. The amended layer in plot 2 had initial concentrations of Al of around 150 mg/L and, by 2014, they were less than 0.1 mg/L. Below the amended layer in plot 2 (i.e. at 91 cm), Al decreased from approximately

800 to 0.07 mg/L, in the same period of time. In the non-amended plot 1, Al concentrations were higher, ranging from around 1,500 to 200 mg/L, from 2009 to 2010.

In general, results showed that the chemical concentrations in the Mather plots were highly representative of coal pile mine drainage. It was also shown that the use of AC was beneficial to remediate the acid drainage in the coal waste at least during the five years of measurements. In the amended plot 2, there was a clear indication of dissolved metal immobilization (e.g., Fe) that led to lower rates of H^+ *[Eq. (2-1) to Eq. (2-4)]* and the consequent pH increase towards neutral levels. Moreover, it was shown that despite plot 2 only having a 61 cm amended layer, there was evidence that this amended layer was beneficial to the non-amended layer below at the depth of 91 cm (i.e. lower levels of dissolved metals and sulfate than in the non-amended plot 1). Finally, it is worth mentioning that the data gap observed in *Figure 2.1* from 2011 to 2014 was due to access issues (i.e., getting permission enter the site) that didn't allowed us to retrieve samples.

2.3 STATIC TESTS

2.3.1. Batch Reactions

The pH values in the batch experiments are influenced by the AC/CR ratio and moisture content *[Figure 2.2a]*. It was noticeable that higher moisture content produced higher pH values. One possible reason could be lower oxygen diffusion rates due to higher saturated soil conditions. Another possibility may be due to a weathering effect (e.g. neutralization reactions), which would produce more alkaline substances available to react *[Dold, 2014]*. Alternatively, due to the fact that the AC content is several times lower than the CR and allowing the possibility that AC

particles are not homogeneously distributed throughout the mix, additional water is likely responsible for increasing reaction between the AC particles and the CR, which would explain the increase in the alkalinity during the short duration of the batch experiments. An experiment was designed to test the reaction time for various AC contents and, to initiate the reaction, 5 mL water were added.

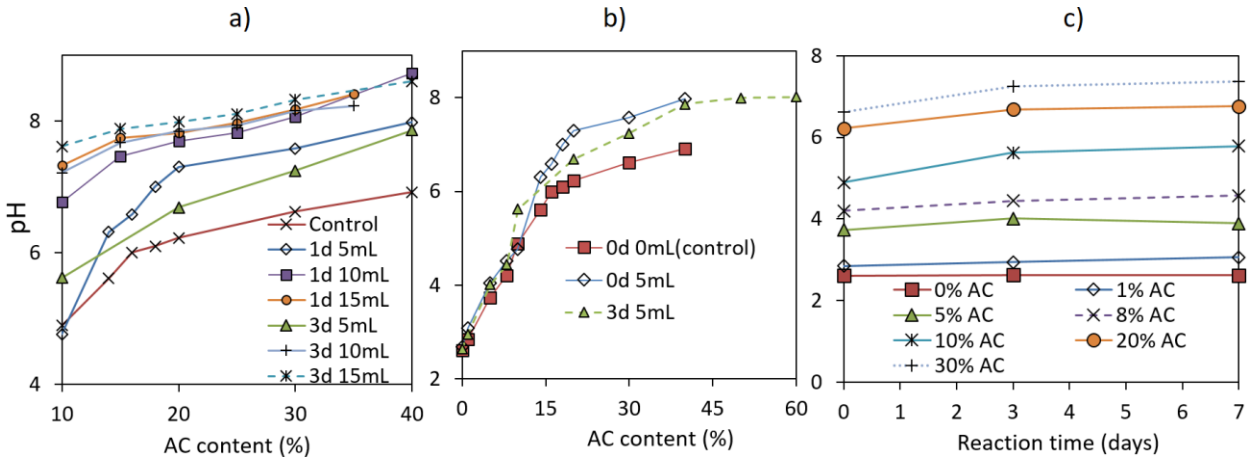

Figure 2.2. Results of batch experiments: a) pH versus percentage of AC with different reaction days and water addition amounts. b) pH versus percentage of AC with 5 mL water addition for 0 and 3 reaction days. c) pH versus reaction time with different percentage of AC. In a) and b), the control group corresponds to 0 day reaction time and no water addition.

It was observed that the pH for the batch reaction experiments for the control group was lower than almost every other sample tested *[Figure 2.2b]*. This was expected because the absence of initial soil moisture resulted in less dissolved alkalinity. Regarding the AC content, in all three cases the trend was similar. It was also noticed in *Figure 2.2b* that for 5% or less AC content, the pH was 4 or lower, which suggests that the pH in the leachate was primarily controlled by pyrite oxidation, both by oxygen and ferrous iron. For 8% AC, the pH was around 4 - 4.5, which is still close to the threshold where ferrous iron can oxidize pyrite. Therefore, it would appear that, in order to have a substantial positive impact, AC content should be higher than 8%. On the other

hand, at 16% AC, the pH was higher than 6, which is within the range of un-affected natural waters around the study area *[Chaplin et al., 2007, Sams et al., 2000 and Williams et al., 1990]*.

It is necessary to emphasize that these batch experiments were intended to replicate the initial conditions of the remediation, at the time of the first rainfall, right after the AC is mixed with the CR in the field. Therefore, these initial pH measurements were expected to be less than subsequent values, as the pyrite oxidation rates are initially faster than the generation of alkalinity *[Huminicki et al., 2009]*.

In order to have a narrower range from where to choose an optimal mixing ratio, *Figure 2.2c* provides more clarification. This figure shows the pH results for various AC contents for three reaction times: 0, 3 and 7 days. It is clear that, for 5% AC or less, the pH did not seem to be influenced by the reaction time. In this case, it is probable that the AC content was not enough to rapidly increase the neutralization capacity. At 8% AC, the reaction time seemed to have some influence; however, the pH remained lower than 5. Although the pH can eventually reach neutral levels at 8% AC, there is some uncertainty regarding the long-term stability of this mixing ratio. In other words, for 8%AC, it is uncertain if the pH is going to be on the neutral side and how long it will remain this way until the alkalinity is consumed.

The pH for the 10% AC mixture showed a more significant influence regarding the reaction time, increasing from 4.9 to 5.8. Similarly, the pH in the 20% AC and 30% AC mixtures also was influenced by the reaction time. In these two cases the AC content was relatively high; therefore, it took time for the alkalinity to reach a stable dissolving rate (i.e. a longer “activation” time). It is noticeable that, in the case of the 7-day reaction time, increasing the AC from 8% to 10%, increased the magnitude of the pH by 1.3. However, increasing the AC from 10% to 20%, only increased the magnitude of the pH by 1. This suggests that there might be an AC content within the range of

10%-20% whereby increasing the AC content does not necessarily improve the remediation in terms of the pH value.

In summary, at the lower limit, it is clear that the optimal AC content should be higher than 8%. The upper limit is slightly more complex to define. Our analysis might indicate that the optimal AC content should be less than 14%. In addition, considering that it is our intent to determine the least AC content possible that has an effective performance (i.e., having a neutral or near neutral pH and high metal immobilization), 10% AC seems to be a reasonable assumption to be close to optimal conditions.

2.3.2. Acid Base Accounting

Figure 2.3 shows the results from the acid base accounting test and its interpretation. It is necessary to be aware of the limitations of this methodology in order to have a proper interpretation of the results, as under real field conditions, not all S will produce acid, neither will all the alkaline material be available to react and neutralize the acidity.

There are two main criteria to interpret the results. The first criterion is based on the Net Neutralization Potential (NNP), which is the difference between the Neutralization Potential (NP) and the Acid Potential (AP) (i.e. NNP = NP – AP) *[Brady et al., 1992]*. NNP values in the range of -20 to 20 g $CaCO_3$ / kg are generally considered to be uncertain. NNP values less than -20 are typically taken to indicate acid producing potential while NNP values greater than 20 are usually identified with little potential to produce net acidity. Based on these criteria, *Figure 2.3a* shows that a minimum of 6% AC is required to be in the range of limited potential to produce net acidity

(i.e. NPP ≥ 20 g $CaCo_3$ / kg). Mixed samples of AC between 1% and 6% are assumed to be in the uncertainty range. Samples with less than 1% AC have acid producing potential.

The second criterion is based on the Neutralization Potential Ratio (NPR = NP/AP) *[Price et al., 1997]*. The results in *Figure 2.3b* show that samples with AC between 0% and 3.5% are likely to generate ARD. Samples with AC between 3.5% and 9.5% are less likely to produce ARD. With 9.5% and 20% of AC content, there is no potential for ARD generation, while for samples with more than 20% AC, it is assumed with more certainty that there will be no ARD.

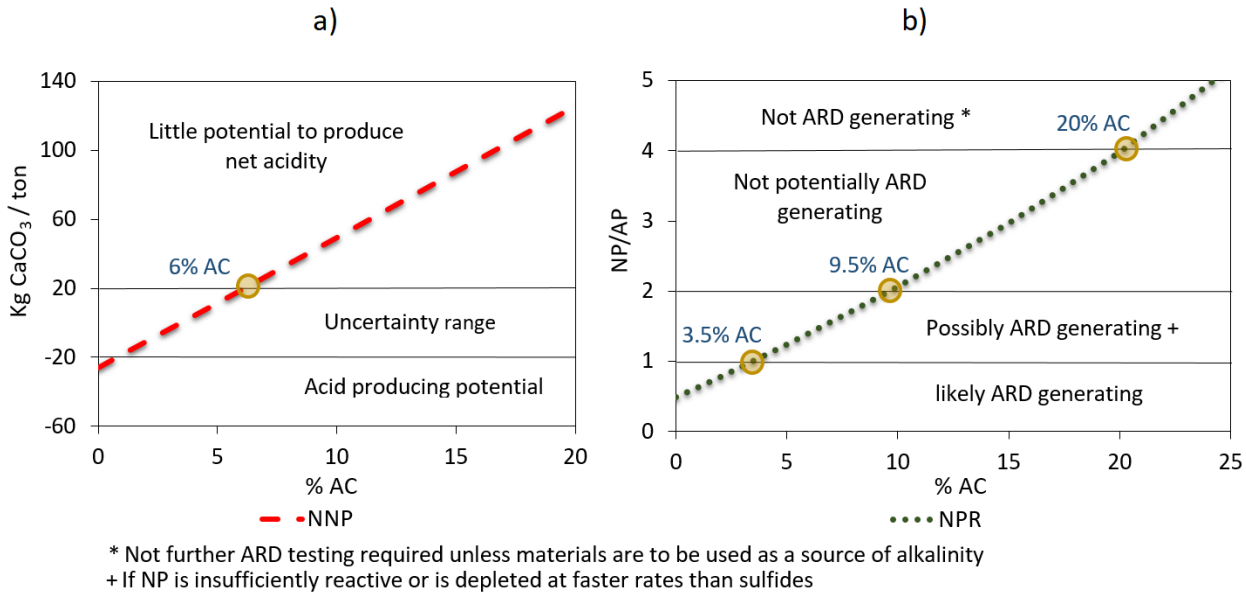

Figure 2.3. Acid base accounting test results interpretation, based on the sample's %AC. a) Net Neutralization Potential (NNP) criterion. b) Neutralization Potential Ratio (NPR) criterion. NP=Neutralization Potential, AP= Acid Production Potential, NNP= Net Neutralization Potential, NPR= Neutralization Potential Ratio.

Based on these results, our assumption is strengthened that a minimum of 10% AC is required for long-term remediation purposes. Specifically, 10% AC is assumed to be the minimum amount of remediation material that could guarantee that sufficient alkalinity is provided to neutralize the acidity in the long term, even beyond the duration of the field measurements and the

kinetic experiments (i.e. > 5 years). Therefore, a 10% AC mixture will be adopted for the amended scenario of the kinetic tests (i.e., flow-through columns).

2.4 KINETIC TESTS

In the first stage of the kinetic experiments, four columns were started to explore the generation and remediation of ARD. The layer depth of all columns was 15 cm. The mixture in column 1 consisted of 10% AC and 90% CR. Column 2 used the same mixture as column 1 except that the solid sample used to pack it was ground and, therefore, featured a smaller grain size in general. This column was designed for testing the effect of the particle size. Column 3 also used the same mixture as column 1 but varied the amount of water added. Only 100 mL of water was added to column 3 to simulate drier environmental conditions. Column 4 served as the control column (100% CR). At the beginning of the experiments, the water retention time varied from around 1 to 3 h. *Table 2.1* shows the columns specifications.

Table 2.1. Settings of the first set of columns

COLUMN ID	CR(%)	AC(%)	WATER ADDED (ml/week)
Column 1	90	10	200
Column 2	90	10	200
Column 3	90	10	100
Column 4	100	0	200

2.4.1 pH

Figure 2.4a shows the leachate pH from the columns previously described. The average pH for columns 1 and 2, during the experiment was 7.59 and 7.83, respectively. After a 600-day period, there was no indication of a pH decrease. It was noticeable that the pH in column 2 was slightly higher than in column 1. This is likely due to the fact that column 2 had smaller particles (i.e., samples were ground before sieved), which made the mixture more homogeneous, and also, there is a higher surface contact between the water and the AC particles. However, the smaller particle size in column 2 did not produce a significant difference compared to column 1.

As previously mentioned, water addition frequency was 100 mL/week in column 3, which was assumed to be close to the moisture conditions in the field during the dry season. The leachate from column 3 took around two weeks to reach a neutral pH, after which the pH values remained mostly above 7.5. This column was neglected after approximately 200 days, as enough data were collected to note that reducing the water by half did not significantly change the pH compared to columns 1 and 2.

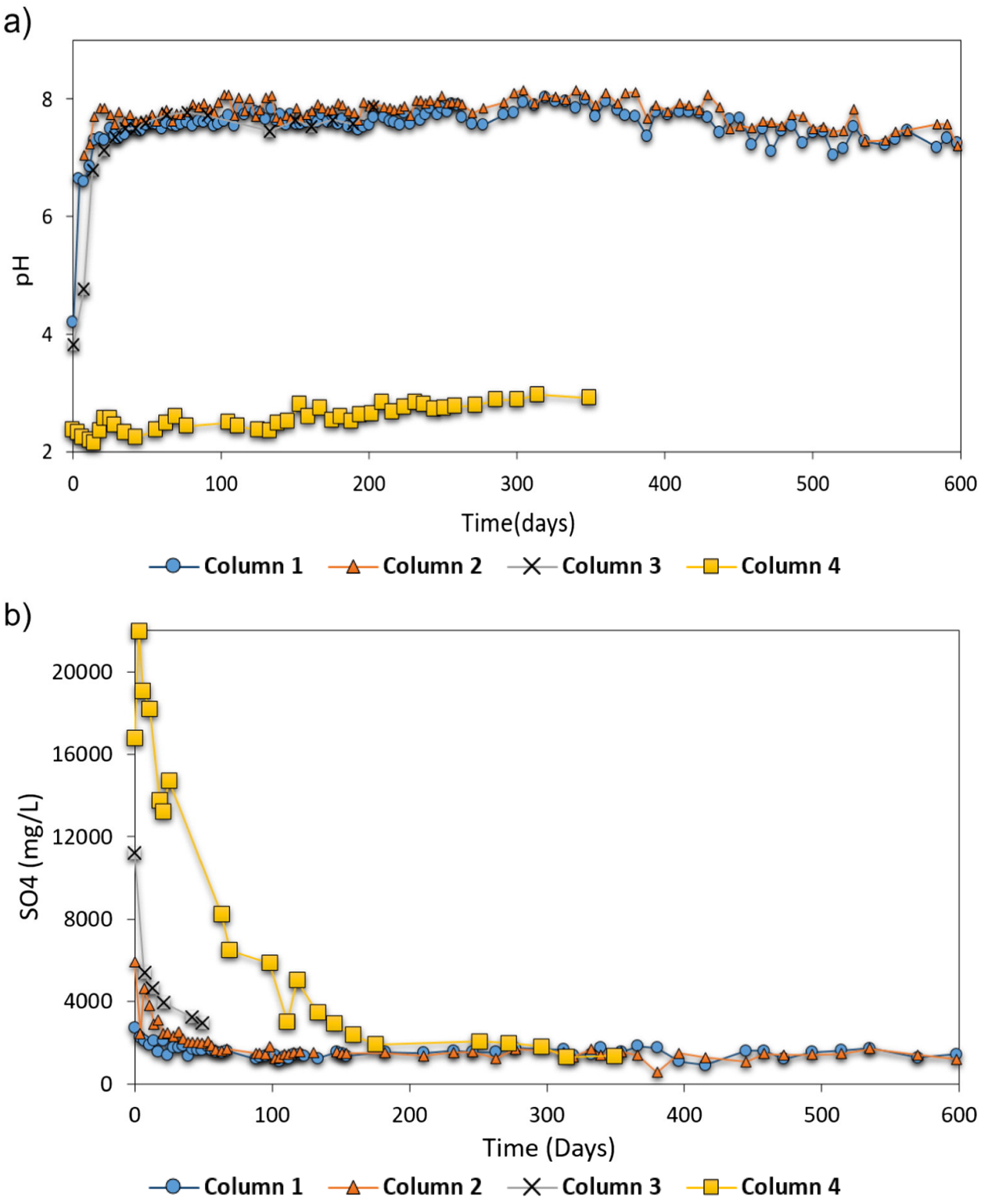

Figure 2.4. a) pH and b) sulfate results from the column leaching experiments. Column 1: 10%AC + 90%CR. Column 2: 10%AC + 90%CR (ground particles). Column 3: 10%AC + 90%CR (less mount of water added). Column 4: 100%CR.

In all these three columns it was evident that the increase in pH conditions was due to the addition of the alkaline material (i.e., AC). As a consequence, these conditions should reduce the proliferation of bacteria (i.e., thiobacillus ferroxidans), increase the metal adsorption and enhance the precipitation of HFO *[Doye and Duchesne et al., 2003]*. These hydrous oxides of Fe (III) are fundamental in the transport and attenuation of trace metals via adsorption *[Webster et al., 1998]*. In addition, due to the low solubility of these Fe-oxide phases under alkaline conditions, they can eventually encapsulate the sulfide mineral grain (e.g. pyrite), and lower the amount of mineral surface in contact with the oxidants, thus inhibiting the oxidation process until a state is reached, where the coating's effectiveness causes the acid generation to be less than the alkalinity of the ground water *[Huminicki et al., 2009]*. Additionally, higher water retention in column 2 (i.e. fine particles) could play an important role for the coating of pyrite, as hydrodynamic conditions are important in the early stages of the coating development, where higher flow rates might remove Fe (II) and HFO before they can react and attach to the pyrite surface *[Huminicki et al., 2009]*.

After 350 days, the pH in column 4 (i.e., control column) is within the range of 2.5 - 3. At pH < 3.5, the solubility of HFO increases and pyrite oxidation by Fe (III) is faster than oxidation by dissolved oxygen *[Williamson et al., 2006]*. Moreover, low pH conditions favor the growth of acidophilic bacteria (i.e., thiobacillus ferroxidans) that oxidize aqueous Fe(II) to Fe(III) *[Doye and Duchesne et al., 2003]*. Finally, low pH inhibits precipitation and sorption reactions. Consequently, metals such as Al, Cu, Mn and Zn are likely to experience a conservative transport *[Runkel et al., 2012]*.

2.4.2 Sulfate

In ARD chemistry, sulfate is usually seen as an indicator of sulfide mineral oxidation. *E*ven without the contribution of dissolved oxygen, pyrite oxidation by Fe(III) produces sulfate *[Doye and Duchesne et al., 2003]*. Moreover, sulfate is also controlled by mineral solubility, as it is associated with several mineral phases that are present in mine tailings, among which are jarosite ($KFe_3(OH)_6(SO_4)_2$) and gypsum ($CaSO_42H_2O$). Secondary sulfate minerals associated with ARD include Fe and Al-hydroxysulfate minerals *[Hammarstrom et al., 2005]*.

Figure 2.4b shows sulfate (SO_4) concentrations obtained from the columns' leachates. It is noticeable that, while the orders of magnitude are different, a similar trend is present in the sulfate concentrations for all four columns, characterized by an early steep decrease followed by an apparent plateau.

Column 1 had an average sulfate concentration of 1,872 mg/L during the first 100 days, after which the average plateaued around 1,481 mg/L. Column 2 had an average sulfate concentration of 2,865 mg/L during the first 100 days, after which the average plateaued 1,490 mg/L. Once again the particle size has no significant impact (i.e. column 2 results compared to column 1) .It appears that the neutralization potential of the AC has a higher control compared to the other possible factors that might enhance the remediation process (e.g., higher water retention, less oxygen diffusion and more AC surface contact due to finer particles).

In column 4, the non-amended scenario, sulfate experienced a very steep decrease during the first 100 days, dropping from an initial 22,000 mg/L to approximately 6,000 mg/L. This might indicate an initial high dissolution of sulfate minerals. After that, the sulfate continued to drop for

another 50 days (i.e., from 6,000 to 2,000 mg/L). From that point onward, the sulfate concentration stabilized at around 2,000 mg/L (i.e., at about day 200) for approximately 100 days and, then continued to gradually decrease until around 1,800 mg/L at day 350.

2.4.3 Dissolved metals/metalloids

Drainage water quality in reactive and remediated mine tailings is highly influenced by factors like water saturation level, particle size distribution and soil permeability, but may also be influenced by the mineral composition of the soil, which in turn controls the distribution of metals.

Figure 2.5 shows concentrations for the most important metals dissolved in the leachate for the amended and non-amended scenarios (columns 1 and 4, respectively). There is approximately 450 days of measurements for column 1 and 200 days for column 4. The reason for this difference is that column 4 was started later than column 1. Average Fe concentration in column 1 was 2.85 mg/L (range 2.13 to 3.77 mg/L). Under alkaline pH conditions when pyrite is being oxidized, the released Fe rapidly precipitates as HFO phases such as ferrihydrite and goethite *[Yee et al., 2006]*. Considering the data length (i.e. 450 days), it seemed that the Fe concentrations in column 1 were controlled by the Fe mineral solubility. Eventually, it is expected that the Fe concentrations would decrease. As an evidence, actual field measurements from the Mather site show a decrease in Fe concentration *Figure 2.1*.

Ca concentrations in the amended scenario showed two clear trends. The first was characterized by a relatively stable increase during the first 180 days, where the concentration of Ca is generally within the range of 300 - 600 mg/L. The second trend is where the Ca concentration increases from 500 to 700 mg/L. This relatively high concentration of Ca could be an indication

of ARD neutralization by the dissolution of Ca carbonates, such as calcite ($CaCO_3$), due to the alkaline additive, thus releasing Ca. Usually, calcite is identified with acidic neutralization, enabling various metal removal mechanisms *[Sun et al., 2013]*. However, high dissolution rates of Ca minerals could also occur in active mine tailings (e.g., CR).

Mn showed a decreasing trend in the amended scenario. In mine tailings, Mn is usually produced by the dissolution of ankeritic dolomite contained in rocks *[Banks, 2006]*. In column 1, Mn dropped from around 0.9 to 0.4 mg/L during the first 230 days, after that, it stabilized around 0.2 mg/L, being 0.16 the lowest value. At neutral pH values, precipitation of Mn phases occurs via bacterial mediation *[PlumLee et al., 1999]*.

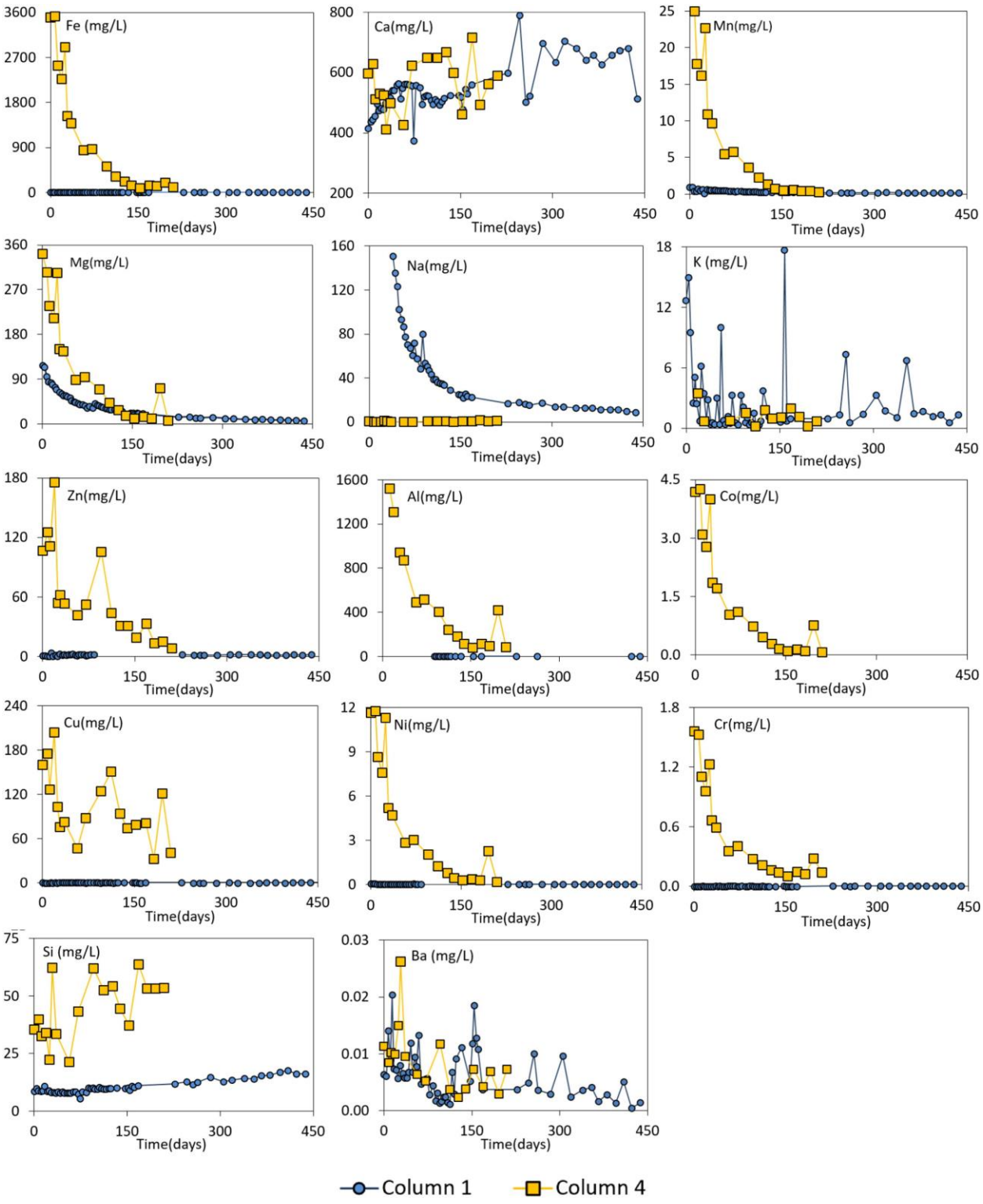

Figure 2.5. ICP-MS results for the column experiments (columns 1 and 4).

The Mg concentrations also showed a decreasing trend in the amended scenario, from the range 300 – 100 mg/L to 8 - 6 mg/L, a relatively low concentration, which might indicate the precipitation of Mg carbonates. Likewise, Na concentrations showed a dramatic decreasing trend, from 160 to approximately 10 mg/L, which might be an indication of flushing out of brines and Na minerals initially present at the CR waste piles and/or the alkaline remediation material (e.g., sodalite ($Na_8(Al_6Si_6O_{24})Cl_{12}$)). Decreasing concentrations of K (i.e. from 12 to 2 mg/L, approximately) might also be related to the flushing of brines. In the amended column, Zn had a very stable trend within the range of 0.5 – 2.5 mg/L, with an average concentration of 1.42. Zn is absorbed on Fe (II) oxides and hydroxides at moderately acidic and neutral pH conditions *[Sracek et al., 2009]*.

Other important metals that characterize ARD such as Al and Co, were mostly below the detection limits in the amended scenario. When detected, Al varied from 0.001 to 0.07 mg/L. One of the main reasons for the low Al concentrations in the amended columns is that, at a close to neutral pH, Al is limited by the precipitation of Al hydroxides *[Nordstrom and Alpers, 1999]*. Cu showed an oscillatory behavior within the range of 0.02 to 0.10 mg/L, with an approximate average of 0.04 mg/L. This low Cu concentration might be due to the fact that Cu hydroxide precipitates at pH > 5.3 Cu is strongly adsorbed onto HFO and other oxide phases *[Britton, 1955]*. Other important dissolved metals detected at relatively low concentrations were Ni and Cr, with average concentrations of 0.036 and 0.039 mg/L, respectively. Finally, Si concentrations had an increasing trend during the whole experiments from around 9 to 17 mg/L in column 1. It is clear that Si concentrations are controlled by Si minerals solubility (e.g., neo-formed silicates).

In contrast, Fe concentrations in the non-amended scenario (column 4) went from an initial 3,500 mg/L to a final 107 mg/L. Fe concentrations in the reactive tailings are controlled by a

complex set of minerals including pyrite, chalcopyrite, HFO, Fe oxides, and jarosite *[Doye and Duchesne et al., 2003]*. In fact, pyrite and jarosite were the main Fe minerals detected in the XRD analysis. The initial high concentrations of Fe might indicate high pyrite oxidation rates and high dissolution rates of Fe minerals. After that, it seemed that the rate of Fe precipitation was higher than the rate of oxidation and the coating of reactive grains, thus causing the concentration to drop.

Ca had similar concentrations in the amended and non-amended scenarios. Many reactive tailings can have a high content of Ca minerals and still generate acidic pH. Calcite ($CaCO_3$) and gypsum ($CaSO_4H_2O$) were the Ca minerals detected in the XRD analysis *[Table 1.1]*.

Mn is a very common metal that can be found in acidic mine waters. At near neutral level of pH, its removal is enhanced. However, in low pH conditions, formation of HMO is kinetically slow compared to HFO formation. For the non-amended scenario, Mn showed a decreasing trend from 25 to 0.3 mg/L, implicating precipitation of secondary Mn minerals.

Al concentrations went from more than 1,500 mg/L to about 82 mg/L. Al might be controlled by the dissolution of gibbsite *[Cravotta III et al., 2015]*. A discontinuity of the Al curve is noticeable in the case of column 1, meaning that Al was not always detected in the amended scenario. Low and stable Na (i.e. average of 0.5 mg/L) and K (i.e. average of 1.2 mg/L) concentrations in column 4 indicate low brine content in the reactive tailings.

Other potentially toxic metals, such a Cu, Co, Zn, Ni and Cr, had high concentrations in column 4. Since no minerals of these metals were detected in the XRD, they might be controlled by the dissolution / precipitation of secondary phases. Cu was within the range of 40 – 200 mg/L. Co was below the detection limits in column 1, but in the case of column 4, it had a decreasing

trend from 4 to 0.06 mg/L. Zn, Ni and Cr were within the ranges of 175 - 8 mg/L, 12 – 0.2 mg/L and 1.6 – 0.14 mg/L, respectively.

In summary, the non-amended scenario (i.e., column 4) showed high concentrations of dissolved metals, while the amended scenario (i.e., column 1) showed high immobilization of dissolved metals. *Table 2.2* shows the estimated removal efficiency, in percentage, for the most important metals based on their initial concentrations (i.e., comparing the amended and the non-amended columns). This analysis, based on the initial concentrations (i.e., "day 0" in *Figure 2.5*) for both the amended and non-amended scenarios, shows the significance of having the remediation treatment in a mine tailing. For example, the proposed remediation design ensures that approximately 99.93% of the high Fe loads are neutralized and are not dissolved in water. Other metals, such as Al and Co are also unlikely to dissolve and be transported in the leachate of the amended environment.

Table 2.2. Metal removal efficiency

Description	Initial Concentration Column 4 (mg/L)	Initial Concentration Column 1 (mg/L)	Removal (%)
Fe	3496	2.33	99.93
Mn	24.9	0.90	96.39
Cu	160	0.04	99.98
Cr	1.6	0.003	99.84
Zn	106.5	0.50	99.53
Ni	11.7	0.07	99.40
Al	1518	0.01	100.00
Co	4.2	0.00	100.00

2.4.4 Controls of pH on sulfate and dissolved metals/metalloids. Water quality analysis

Based on the results presented in this study and those from previous studies *[Nordstrom and Balls, 1986, Nordstrom and Alpers, 1999 and PlumLee et al., 1999]*, it has been sufficiently demonstrated that low pH levels accelerate the release of heavy / toxic metals, which, in turn, can negatively affect the survival of aquatic life and have other harmful impacts on the environment.

For the purpose of interpreting the variations of the mine drainage water chemistry, a Ficklin diagram can be utilized *[PlumLee et al., 1992 and PlumLee et al., 1999]*. The usual Ficklin diagram is a scattergram, in which the sum of the base metals Zn, Cu, Pb, Cd, Co, Ni is plotted against the pH. In addition, the Ficklin diagram can be adapted to create similar plots using parameters other than the above mentioned base metals.

Figure 2.6a shows a Ficklin diagram based on the results presented in the previous sections, including the amended (columns 1 and 2) and non-amended (column 4) scenarios. For the non-amended scenario, the diagram shows that the quality of the leachate is categorized near the threshold of the *high acid-extreme metal* and *high acid-high metal* groups. As shown in the results, the non-amended scenario had initial high metal concentrations followed by a decreasing trend in metal concentrations with a pH within the range of 2 - 3 the entire time. Evidently, there was a dissolved metal reduction in column 4, but as the pH remained low, the metals concentrations were still high. For the amended scenario, the leachate quality is characterized by the *near neutral-high metal* and the *near neutral-low metal* groups. Similar to column 4, columns 1 and 2 also showed a decreasing trend in the metal concentrations, but obviously the initial concentrations in the amended scenarios were much lower. As the pH remained on the neutral level (i.e. 7 – 8) the entire time, the immobilization of dissolved metals was enhanced.

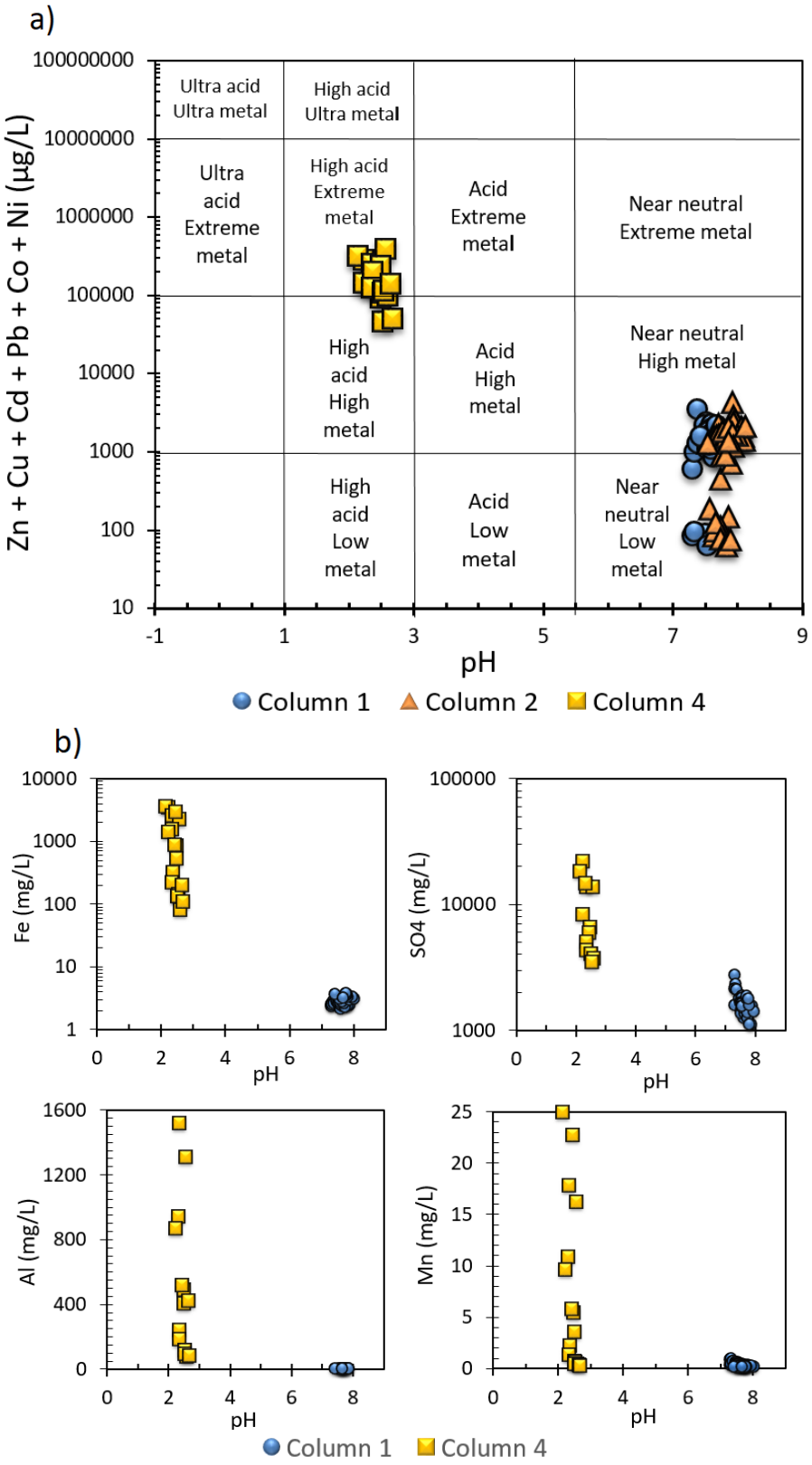

Figure 2.6. Ficklin diagrams for the column leaching experiments (columns 1, 2 and 4).

In addition, *Figure 2.6b* shows adapted Ficklin diagrams for other important parameters like Fe, SO_4, Al and Mn, for columns 1 and 4. For column 1, where all the samples have a pH above 7, the range of concentrations in sulfate and in other metals (i.e., Fe, Al, and Mn) is relatively narrow, thus it is evident that it has an effective ARD neutralization process. On the other hand, in column 4 there is a wide range in sulfate and metal concentrations with a very narrow pH range, indicating the release of metals due to the high acidity.

For the implications of the outcome regarding water quality standards, U.S. Federal Regulations *[EPA, 2002]* provide general guidelines about effluent discharges related to coal mining. The only parameters that are regulated are Fe, Mn, pH and total suspended solids (TSS). The effluent in the amended scenario fully complies with these regulations, while for the case of the non-amended scenario, such standards are not met on both the instantaneous and average values as they are always higher than the maximum admissible. Moreover, the leachate in the amended scenarios complies, for many parameters (e.g., Ba, Cu, Pb, Ni, Zn), even with the higher quality standards *[EPA, 1994]* such as those related to drinking water.

2.5 GEOCHEMICAL MODELING: PHREEQC

Geochemical simulations were mainly focused in the amended scenario (i.e., column 1). However, some investigations for the non-amended scenario (i.e., column 4.) were also explored. *Table 2.3* shows the initial aqueous solutions for the amended and non-amended scenarios, which are the main inputs to the model.

Figure 2.7a shows the most important parameters (i.e. pH, SO_4, Fe, Ca, Al, Mn) modeled by PHREEQC against the respective measurements from the leachate of column1 (i.e., amended scenario). In terms of pH and sulfate, the results from the simulation (shown in red) are close to the experiments (shown in blue).

The simulation curves for these parameters had a decreasing trend, most clearly visible in the case of sulfate. In the case of pH, the model simulation began with a pH above 9, and was not able to replicate the initial behavior of the system for the first 120 days, approximately. A slow saturation process within the column may explain the discrepancy between the model and experimental results during this time. As the amount of particles reacting slowly increases, it takes some time until the introduced alkalinity in the mixture reaches higher dissolution rates. This is why the pH from the leachate of column 1 is acidic at the beginning (see *Figure 2.4a*) but after a few days it reaches the neutral level. Another important conclusion is that the model was not very sensitive to the initial pH value given to the solution *[Table 2.3]*. On the other hand, sulfate simulations showed a better adjustment to the experimental data during the entire time, indicating more sensitivity to the initial input sulfate concentration.

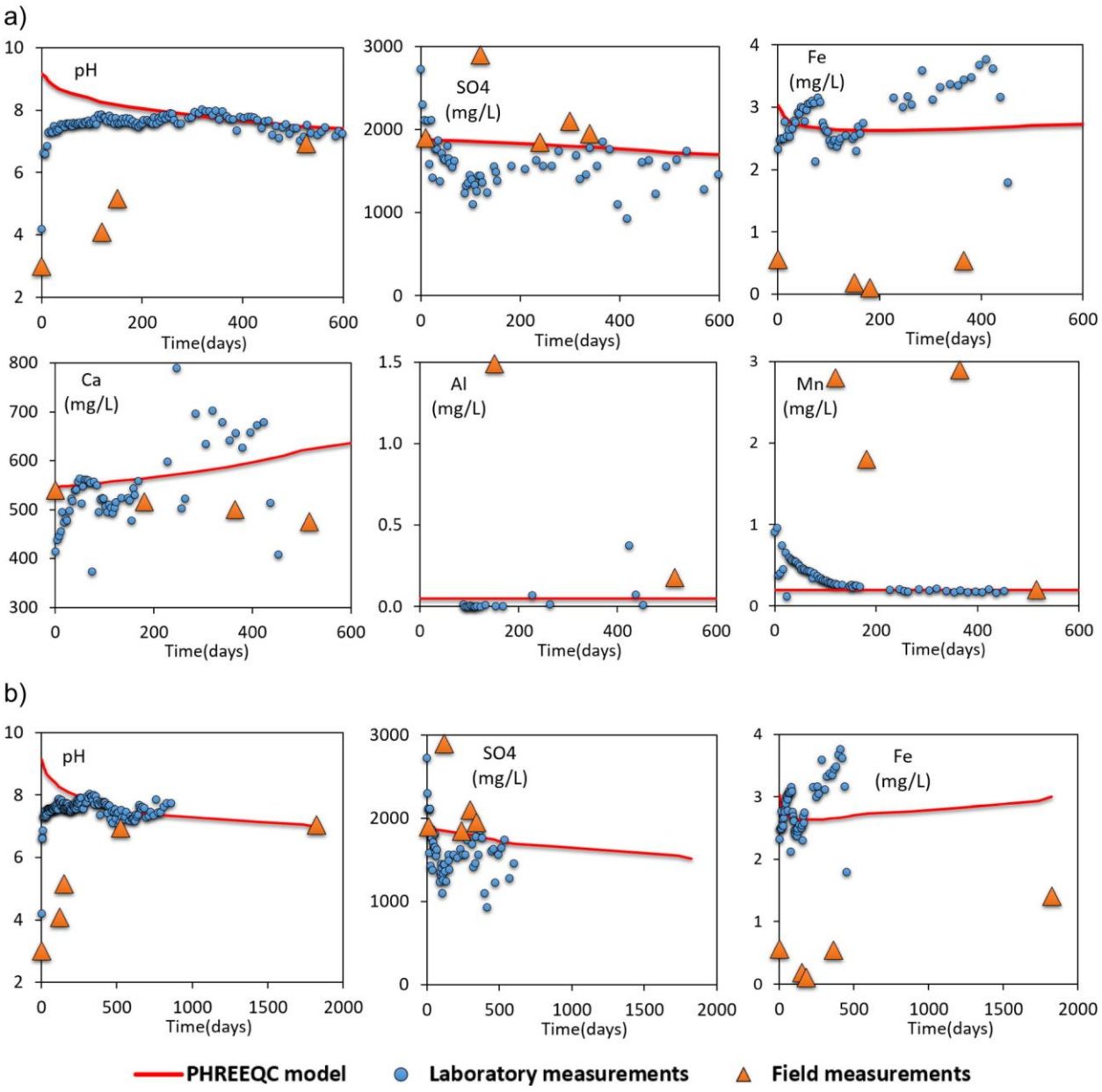

Figure 2.7. a) PHREEQC modeling results for the amended scenario (column 1). The small circles represent the laboratory measurements (column 1). The large triangles represent the field measurements at 61 cm depth (amended plot 2). b) PHREEQC 5-year simulation for the amended scenario (column 1).

Table 2.3. PHREEQC initial solutions (amended and non-amended scenarios)

	Amended Scenario	Non-amended Scenario
Description	Concentration (mg/L)	Concentration (mg/L)
Al	0.05	200
Ba	0.01	0.01
Ca	500	550
Cu	0.04	100
Fe	2.50	200
K	4.00	0.50
Mg	100	150
Mn	0.20	5.00
Na	120	0.40
SO_4	1800	8000
Si	9.00	40
Zn	0.80	100
pH	7.00	2.50

Dissolved metal concentrations were also modeled. Fe and Ca are typically the most important dissolved metals to be analyzed in ARD, since they are related to the pyrite oxidation and alkaline neutralization, respectively. Fe had an initial oscillatory behavior within the range of 2.5 – 3 mg/L and then experienced a small increase to 3 – 3.5 mg/L. Although the Fe simulation curve also had an increasing trend after 200 days, it stayed around 0.5 mg/L lower than the experimental data. Al and Mn simulations were highly influenced by the initial input concentrations and their curves did not show major changes from the initial values. This might be due to various factors such as the magnitude of the concentrations (e.g., Al was below the detection limits in the majority of the samples) and the mineral solubility control (i.e., precipitation of Al and Mn minerals). In the specific case of Mn, other factors such as bacterial activity might play an important role in its significant depletion. Microorganisms including heterotrophic bacteria

Pseudomonas, Clostridium and Desulfovibrio can directly reduce Mn *[Kuyukak, 2002]*. In other words, PHREEQC fails to replicate the initial behavior of metals such as Mn, where additional factors such as bacterial activity may have some control on Mn mobility.

In addition, saturation indices (SI) were calculated to establish the probable mineral phases that might be controlling the aqueous composition of the leachates. *Table 2.4* shows the SI calculations of the most important primary and secondary mineral phases in columns 1 and 4. In general, the leachate in this amended scenario showed supersaturation with respect to HFO phases, which led to low metal concentrations, especially Fe, because of the high sorption capacity of these phases that might also lead to the removal of SO_4, for what the precipitation of jarosite could also contribute significantly *[Jones et al., 2006]*. The geochemical model showed equilibrium with respect to gypsum, (e.g. SO_4 usually decreases due to precipitation of gypsum) which was reasonable as there is an obvious acid neutralization process in this scenario; however, sulfate showed a conservative behavior within the range 1000 – 1500 mg/L. Therefore sulfate concentrations were controlled by the dissolution of another sulfate mineral such as anhydrite. Despite an initial neutral pH, the sulfate concentrations were relatively high (> 2000 mg/L) which could be controlled by the dissolution of jarosite, which was undersaturated with respect to the solution composition.

Low Al concentrations in the amended scenario were controlled by the precipitation of gibbsite, k-mica and kaolinite. Mn concentrations were controlled by the precipitation of manganite and rhodrochrosite. Moreover, bacterial activity could also contribute to precipitation of Mn phases at a near neutral pH.

Table 2.4. PHREEQC Saturation Indices (amended and non-amended scenarios)

Amended Scenario

Description	Chemical Formula	Initial SI	Final SI
Anhydrite	$CaSO_4$	-0.36	-0.36
Aragonite	$CaCO_3$	1.85	1.85
Dolomite	$CaMg(CO_3)_2$	3.52	3.11
Iron(III) oxide-hydroxide	$Fe(OH)_3$	2.79	2.79
Gibbsite	$Al(OH)_3$	-0.92	1.66
Gypsum	$CaSO_4.2H_2O$	0.00	0.00
Jarosite-K	$KFe_3(SO_4)_2(OH)_6$	-6.28	0.76
K-mica	$KAl_3Si_3O_{10}(OH)_2$	2.28	8.41
Kaolinite	$Al_2Si_2O_5(OH)_4$	-1.25	4.59
Manganite	MnO(OH)	9.03	3.79
Quartz	SiO_2	-0.11	0.24
Rhodochrosite	$MnCO_3$	0.60	0.19

Non-amended Scenario

Description	Chemical Formula	Initial SI	Final SI
Anhydrite	$CaSO_4$	0.13	0.13
Iron(III) oxide-hydroxide	$Fe(OH)_3$	-1.83	-1.90
Gibbsite	$Al(OH)_3$	-4.25	-4.43
Gypsum	$CaSO_4.2H_2O$	0.43	0.43
Jarosite-K	$KFe_3(SO_4)_2(OH)_6$	1.71	1.68
K-mica	$KAl_3Si_3O_{10}(OH)_2$	-12.98	-13.59
Kaolinite	$Al_2Si_2O_5(OH)_4$	-6.02	-6.39
Manganite	MnO(OH)	-4.10	-4.22
Quartz	SiO_2	0.82	0.82
Geothite	FeO(OH)	4.06	3.99
K-feldspar	$KAlSi_3O_8$	-10.09	-10.34
Chlorite	$Mg_5Al_2Si_3O_{10}(OH)_8$	-58.42	-59.40

Typically, the leachates from non-amended tailings are highly reactive, thus facilitating the dissolution of most of the primary minerals and the formation of the secondary phases. The leachate in this non-amended scenario showed undersaturation with respect to HFO phases, which led to higher metal concentrations, especially Fe. Moreover, decreasing sulfate concentrations were controlled by the precipitation of sulfate minerals such as gypsum, anhydrite and jarosite. In

acid mine waters, Fe can reach saturation with respect to jarosite *[Nordstrom and Balls, 1986]*. Unlike the amended scenario, in this case the Al concentrations were relatively high, similar to most reactive tailings. Al was controlled by the dissolution of several minerals such as gibbsite, k-mica, kaolinite, k-feldspar and chlorite. Al minerals like gibbsite are highly soluble with low pH *[Nordstrom and Alpers, 1999]*. Mn concentrations were controlled by the dissolution of manganite.

Finally, an extended 5-year simulation was performed for the amended scenario (see *Figure 2.7b*). Although these results should not be taken as definitive, the fact that they were supported by a calibration process that replicated the initial 600 days of the system behavior made this exercise a valuable planning and decision making tool, especially in terms of the long-term effectiveness of the remediation approach described in this study. Obviously, these simulations are highly linked to the experimental data (e.g., calibration process). Upon retrieving more experimental data, another model validation should be performed.

The three most important ARD parameters (i.e., pH, SO_4 and Fe) were analyzed in the long-term simulations. The pH showed an expected decreasing trend until it reached around 6.8 after 5 years of simulation. Sulfate data showed an initial decreasing trend, where simulations were adjusted to the experimental data, after that and until the end of the simulation time, it showed a more conservative behavior, only decreasing from approximately 1700 to 1500 mg/L. According to the SI calculations for the amended scenario, the main sulfate mineral, gypsum, was at equilibrium (SI ~ 0) at all times. This might indicate that gypsum formation occurs quickly enough on pyrite grain surfaces that it remains close to saturation in the bulk phase *[Dold, 2014 and Hammarstrom et al., 2003]*. Therefore, the factor controlling sulfate was the dissolution of secondary phases such as aragonite. This led to relatively low and conservative sulfate

concentrations. Fe simulations showed an increasing trend, until it reached a concentration of 3.3 mg/L after 5 years. This low Fe concentration was controlled directly by the neutral pH, which favored the precipitation of Fe phases.

In general, the model could fairly replicate most of the experimental results; however, several uncertainties related to the geochemical modeling remain. These uncertainties are related to the nonlinearity of the system *[Amos et al., 2004]*. Some of the main sources of error in the model could be the identification of the appropriate solid phases and the associated equilibrium constants for the precipitation reactions.

2.6 IMPLICATIONS FOR LONG-TERM PERFORMANCE OF THE REMEDIATION

Field measurements, laboratory experiments and geochemical modeling have been analyzed jointly to determine the possible long-term behavior of the remediation proposed in this study. The determination of the necessary alkalinity supply is an important initial strategy for long-term ARD remediation *[Huminicki et al., 2009]*. The static tests allowed to determine the minimum AC/CR mixing ratio that provides the amount of alkalinity that, potentially, will make the system not ARD-generating. Furthermore, the performed kinetic tests and the field measurements validated the adoption of a 10%AC/90%CR mixing ratio in terms of pH, sulfate and metals/metalloids. At the end of the experiments, there was no indication of alkalinity exhaustion.

It was observed that, for the amended scenario, the pH remained over 7 after 600 days. Moreover, there is a clear indication of metals/metalloids immobilization, as opposed to the non-

amended scenario. However, even in the non-amended scenario, the concentrations of the majority of the metals (e.g. Fe, Mn, Cr, Cu, Ni, Zn, Al) and sulfate showed a decreasing behavior, hence suggesting a decreasing alkalinity demand. Based on the results of the kinetic tests and field measurements retrieved over a period of 5 years, a geochemical simulation was performed (i.e. 600 days and 5 years) which indicated HFO formation in the amended scenario. This HFO formation can accelerate the consumption of sulfide minerals *[Huminicki et al., 2009]*.

The longer the leachate remains on the alkaline side, the more enhanced the generation of iron precipitates that could produce the pyrite grain coating becomes. In addition, the pyrite grains and other sulfide minerals will dissolve in time (alkaline minerals will also dissolve), which means that, in the long term, once the majority of the AC is dissolved, the alkalinity demand in the mine tailing will be relatively small due to the combined processes of dissolution and coating of pyrite and other sulfide minerals. Furthermore, the precipitation of some minerals will make the amended layer less porous, thus increasing water retention and reducing oxygen diffusion. In summary, the combined processes have shown that the pH value can be kept around 7 for at least 600 days based on the column experiments (see *Figure 2.4*) and for five years, based on the field measurements (see *Figure 2.1*) and numerical simulations (see *Figure 2.7*). Such results strongly suggest that the utilization of AC is beneficial for ARD long-term remediation.

2.7 CONCLUSIONS

This first stage of the research investigated the potential use of AC as a passive remediation material for waste coal mining that has the potential to generate ARD. Based on this study, AC is

shown to be an effective remediation material. Results indicated that a 10% AC/90% CR mixing ratio provides near-optimal remediation conditions. This mixing ratio is only considered as an upper remediation layer for the waste piles. Moreover, results suggested that this remediation approach has long-term stability (i.e., neutralization rate is equal to or higher than pyrite oxidation rate). Immobilization of contaminants, such as Fe, Mn or SO_4, and an increase in calcium carbonates implicated a strong pyrite ARD oxidation neutralization capability. Concentrations of other major contaminants, such as As and Al, were below the detection limits in the amended scenario.

Field measurements have also proved that the use of AC is beneficial to remediate the acid drainage in the coal waste. During the period of time in which these measurements were made, pH showed an increase in the amended plots; at the same time, sulfate and dissolved metals showed a decreasing behavior in these plots. However, there are some future improvements that could be made to this field remediation approach in order to increase its effectiveness. These might include soil compaction in the amended layer and the utilization of ground particles of AC to increase the surface area of the neutralizer and decrease the porosity of the medium. However, further study is required to evaluate the potential benefits of these strategies. Long term and continuous data would also be crucial for this characterization.

3.0 ACID ROCK DRAINAGE PASSIVE REMEDIATION USING ALKALINE CLAY: HYDRO-GEOCHEMICAL STUDY AND IMPACTS OF VEGETATION AND SAND ON REMEDIATION

3.1 INTRODUCTION

In mining regions such as the Northern Appalachian Coalfield in the USA, the abundance of coal refuse deposits enables the generation of acid rock drainage (ARD), a serious type of water pollution (i.e. water with acidic pH and high concentrations of sulfate and metals/metalloids) that has caused a widespread degradation of water resources throughout the region *[Herlihy et al., 1990 and Cravotta, 2008a, 2008b]*.

Due to the severity of this environmental problem, over the past decades many states with coal mining activity, such as Pennsylvania, have been developing several reclamation projects to prevent or remediate ARD *[Toffey et al., 1998]*. Among the remediation approaches, passive abiotic treatment possesses many advantages such as low cost and the harnessing of non-conventional materials as neutralization agents (e.g. alkaline wastes), thus operating in a more sustainable way *[Younger et al., 2002]* as well as having lower overall environmental impacts compared to active treatment technologies *[Hengen et al., 2014 and Jia et al., 2016]*. Usually, the main concern regarding passive remediation is the selection of an adequate remediation material,

which could depend on factors such as neutralization potential, cost, production distance from the site, and supply according to the treatment demand *[Perez-Lopez et al., 2011]*.

In addition, other approaches and complementary measures are also addressed in passive ARD remediation, such as the use of acid and metal-tolerant vegetation *[Saalting et al., 2016, Ma et al., 2015, Adams et al., 2013, Padmavathiamma and Li, 2007, Batty et al., 2006]* or saturated barriers to cover the tailings *[Pabst et al., 2014, Ouangrawa et al., 2010, Ouangrawa et al., 2009, Waybrant et al., 2002]*.

In Chapter 2, it was established the beneficial use of alkaline clay (AC), a highly basic nonhazardous industrial waste (according to the Resource Conservation and Recovery Act or RCRA) from the alumina refining process, for ARD passive remediation. Moreover, it was suggested that this passive remediation approach has long-term stability. This chapter aims to complement the research done in the previous chapter and published in *Plaza et al., [2017]* by focusing on the following particular issues: 1) the hydrogeochemical study of the mixture in terms of the percentages of AC and CR, and, 2) the implementation of complementary measures to enhance the remediation process such as use of a vegetation cover and a saturated sand barrier. To achieve this, a series of static (i.e. acid base accounting) and kinetic (i.e. flow-through columns) experiments, complemented with geochemical modeling were carried out. Additional field data from Mather will be presented in this chapter to complement what is presented in the Chapter 2.

The major focus in this stage is the setup of 12 columns, which characteristics are summarized and illustrated in *Table 3.1* and *Figure 3.1*. For clarity purposes, the columns were divided into two groups based on the acidity or alkalinity of their leachate: neutral / near neutral pH (group A) and acidic pH (group B). These kinetic tests were designed to cover a wide range of

scenarios in terms of the AC/CR mixing ratio, vegetation and sand layer. It is worth mentioning that columns A1 and B1 constitute, respectively, the continuation of columns 1 (90% CR + 10% AC) and 4 (100% CR) from Chapter 2 and *Plaza et al. [2017]*.

Table 3.1. Columns design

	Layer 1				Layer 2		Layer 3			Layer 4		
Column ID	Height (cm)	CR (%)	AC (%)	S (%)	Height (cm)	S (%)	Height (cm)	CR (%)	AC (%)	Height (cm)	CR (%)	Vegetation?
A1	15	90	10	0								NO
A2	15	90	10	0								YES
A3	5	90	10	0	5	100	10	90	10			NO
A4	15	92	8	0								NO
A5	15	94	6	0								NO
A6	15	97	3	0								NO
B1	15	100	0	0								NO
B2	15	99	1	0								NO
B3	15	90	10	0						10	100	YES
B4	5	90	10	0	5	100	5	90	10	10	100	YES
B5	15	90	10	0						10	100	NO
B6	10	90	10	0	5	100	5	90	10	10	100	NO

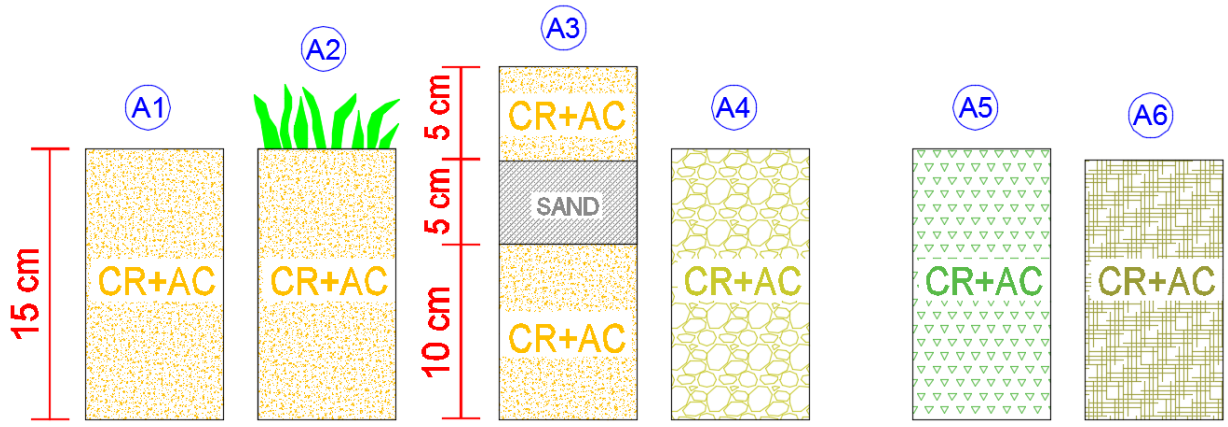

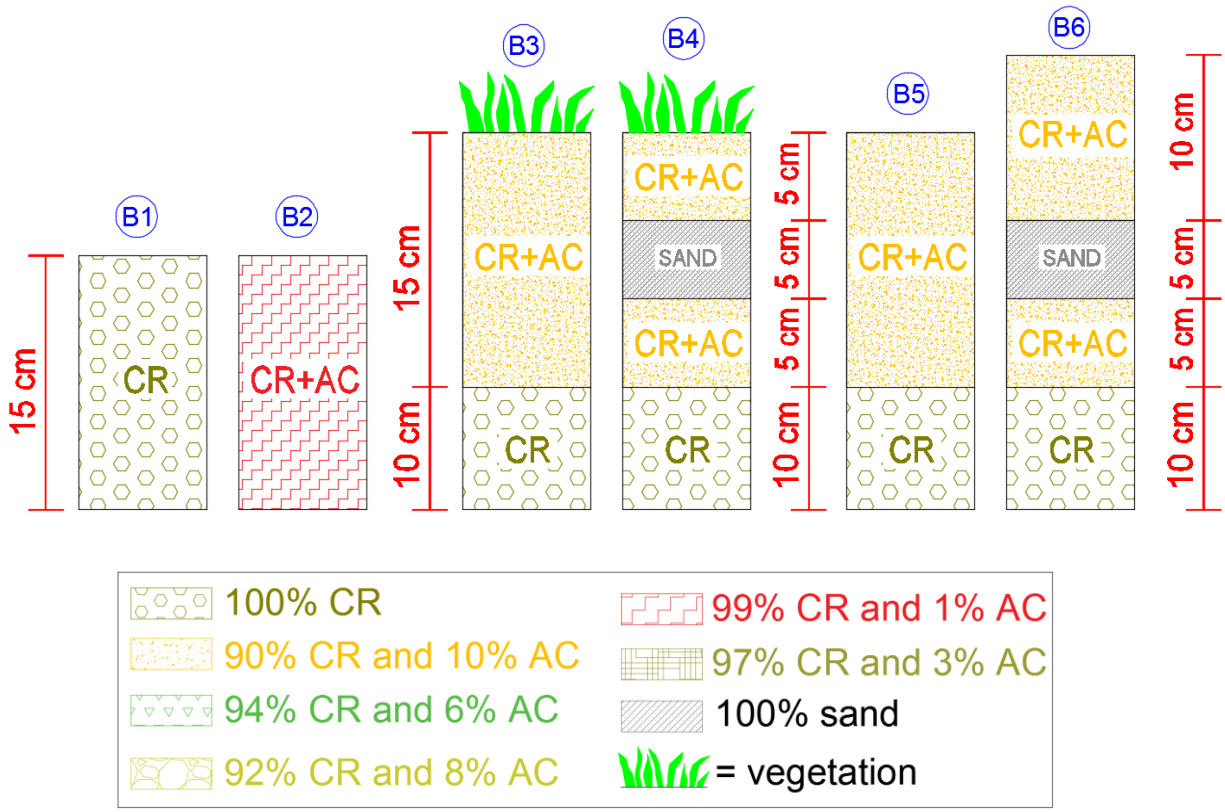

Figure 3.1. Column experiments: Specific design of the columns

3.2 SAMPLE COLLECTION, MATERIAL CHARACTERIZATION AND PRELIMINARY LABORATORY TESTS

Figure 3.2a shows a particle size distribution test (sieve analysis) for both AC and CR. The acid base accounting test considers that both CR and AC have a similar particle size distribution ($D \leq 0.25$ mm). However, CR and AC have different particle size distribution. For fresh samples, and considering the size used in the columns ($D \leq 4.76$mm), it is observed that AC features smaller particles than CR. Assuming the D_{50} as the mean diameter and assuming that the particles have spherical form, the estimated surface area (e.g. m^2) per unit volume (e.g. m^3) for AC is

approximately 48% greater than for CR. This high surface area difference could produce that the alkalinity, mainly contained in AC, would be released at faster rates than the acidity, mainly contained in CR.

a)

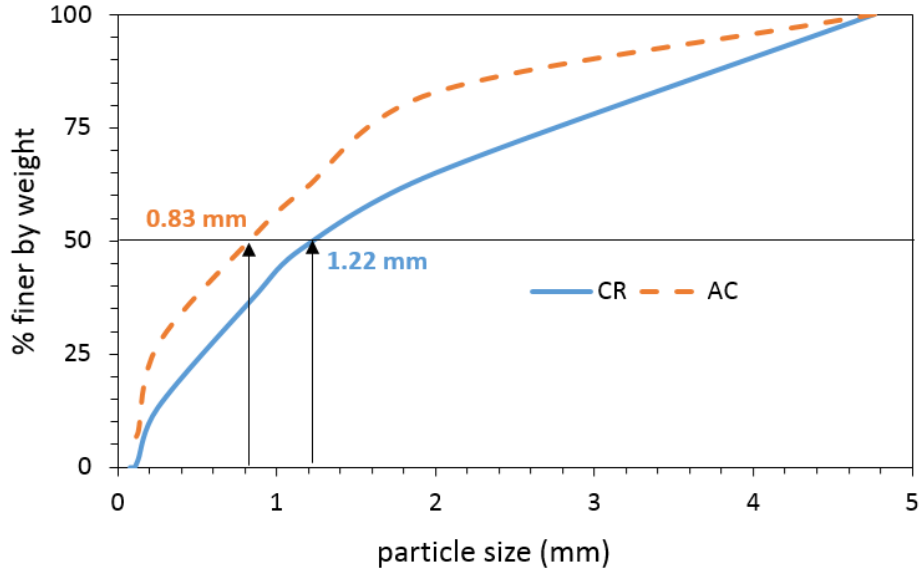

b1)

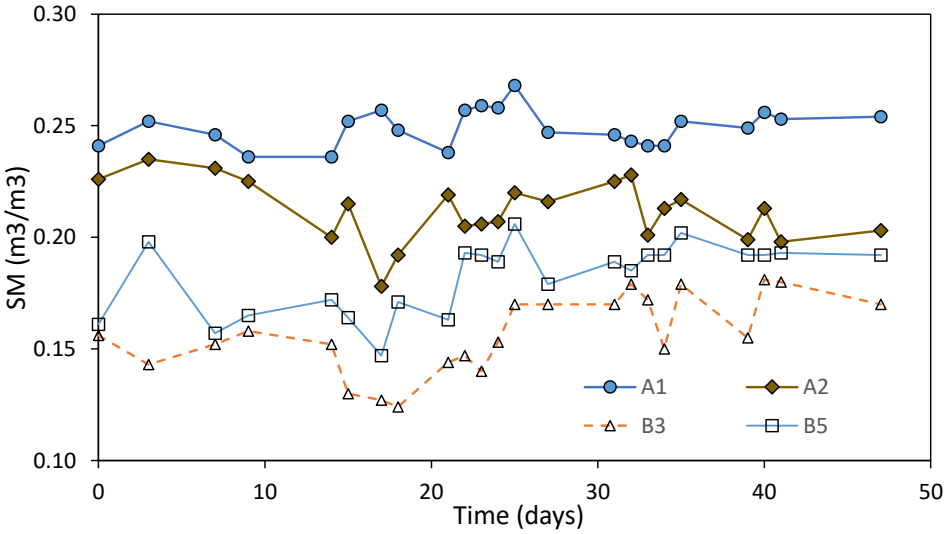

b2)

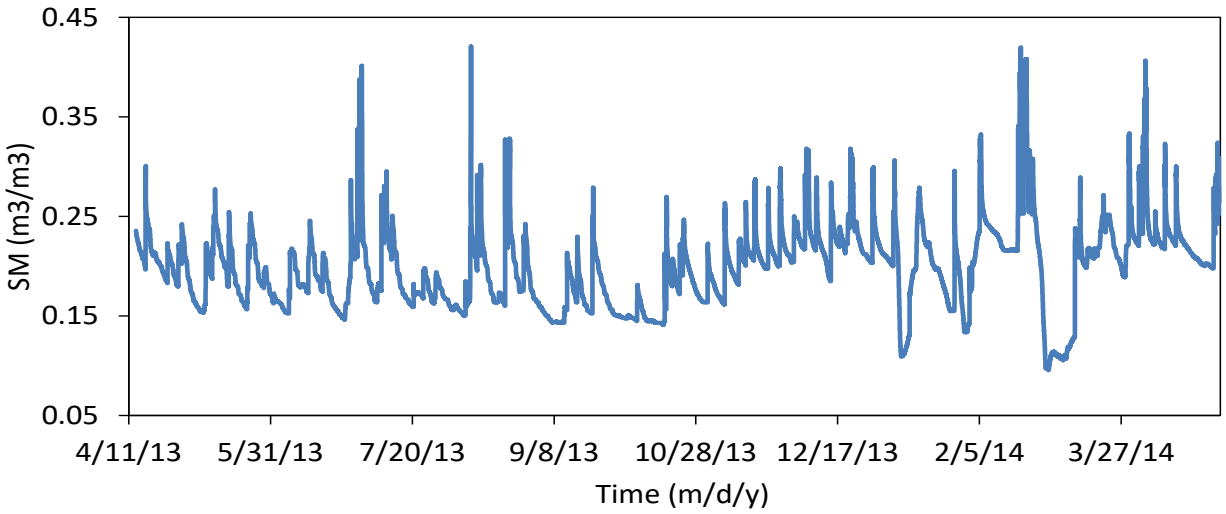

Figure 3.2. a) CR and AC particle size distribution and b) soil moisture (m^3/m^3) measured in the columns (b1) and in amended plot at Mather (b2).

Fig 3.2b shows soil moisture (SM) measurements (m3/m3) retrieved at 5 cm from four of the columns, compared to the SM retrieved at the same depth from the amended plot in Mather. Since the columns were located in a controlled environment where some parameters are different from the field conditions (e.g., temperature, wind, humidity, sun light exposure), it is expected that the soil moisture from the column experiments and the field is not the same. However, the general range of the soil moisture and its relevant behaviors may be comparable since water dynamics and physical/chemical properties are the main players affecting the ARD generation and remediation processes. *Fig 3.2b1* shows the SM retrieved from the columns A1, A2, B3 and B5 during approximately 50 days. SM in the columns ranges from 0.12 to 0.27. The peaks represent the days when water was added (i.e., "rainfall"). It is worth mentioning that columns A1 and A2 have 15 cm depth and columns B3 and B5 have 25 cm depth. As a consequence, the A columns had higher water content due to the lower soil volume. Moreover, the columns that had vegetation on the top (i.e., A2 and B3) had less SM than their "counterpart" columns but without vegetation (i.e., A1 and B5, respectively), which was expected due to water uptake by the roots and the higher porosity

of the soil. However, it is noticed that the SM in the columns had similar magnitude to that in the field, as seen from the SM measured in the amended plot in Mather for approximately one year *[Figure 3.2b2]*.

Initially, it was taken into consideration the idea of "correcting" the soil moisture factor (i.e., less soil moisture in the larger columns) by adding more water into the bigger columns, but this was later discarded for two main reasons:

1) It is desirable to keep similar input parameters in all the columns, just like as it happens in natural conditions (i.e. water addition based on the column surface and not based on the soil depth).

2) The water sample collected for all columns is the same (50 – 60 mL). In other words, once the columns are saturated at the beginning of the experiments, afterwards the change in storage is the same for all of them. It is needed to take notice that the measured moisture conditions are at 5 cm for all the columns, while the sample collection occurs at different depths, from 15 to 30 cm, depending on the column's depth, a location where the exact magnitude of soil moisture is unknown, so the difference in soil moisture at 5 cm was not considered a sufficiently strong factor to modify the water addition amount for some columns.

3.3 ACID BASE ACCOUNTING TEST FOR ALREADY-REACTED SAMPLES

In Chapter 2 (*Section 2.3.2*), it was measured that, based on the Net Neutralization Potential criterion (i.e. NNP = NP – AP) *[Brady et al., 1992]*, a mixed sample with an AC content >6% has little potential to produce net acidity. Mixed sample with AC between 1% and 6% are assumed to

be in the uncertainty range *[e.g., Brady et al., 1992; Skousen et al., 2002]*. Samples with <1% AC have acid producing potential. On the other hand, based on Neutralization Potential Ratio criterion (NPR = NP/AP) *[Price et al., 1997]*, mixed samples with AC between 0% and 3.5% are likely to generate AMD. Samples with AC between 3.5% and 9.5% are less likely to produce AMD. With 9.5% and 20% of AC content, there is no potential for AMD generation, while for samples with <20% AC, it is assumed with more certainty that there will be no AMD at all.

Figure 3.3 shows results from the new acid base accounting test for CR and AC samples already-reacted up to around 1000 days inside the columns. Some of the samples have illustrated that the alkalinity contained in the samples has been gradually consuming over time. For example, in column A1 (10%AC + 90%CR), the NP has decreased from 96 (day 0) to 63 (day 948) Kg $CaCO_3$/ton, yielding an approximate alkalinity consumption rate of 0.035 Kg $CaCO_3$/ton/day. If this rate is assumed to be constant over time, all the alkalinity would be exhausted in around 7.5 years.

Initially, AP was calculated based on the sulfur content (%S) given by the XRD analysis *[Table 1.1]*. Accordingly, it is also expected that certain amount of acidity has been consumed over the time the columns have been reacting. Therefore, it would not be adequate to assume that the AP remains the same. To make this adjustment, the results from a more recent XRD (Philips X'pert diffractometer) analysis were used. CR and AC samples that had been reacting over a year were tested. This analysis yielded that gypsum ($CaSO_4 \cdot 2H_2O$) has increased its composition in the mineral phase (from 1% to around 25%). The presence of gypsum is an indication of mineral precipitation by the reaction of SO_4 with Ca *[Hammarstrom et al., 2005, Nordstrom and Balls, 1986, Nordstrom and Alpers, 1999 and PlumLee et al., 1999]*, in both AC and CR. Moreover,

gypsum has the particularity that it is little or none reactive and is therefore considered not acid producing *[Nordstrom and Balls, 1986 and Nordstrom and Alpers, 1999]*.

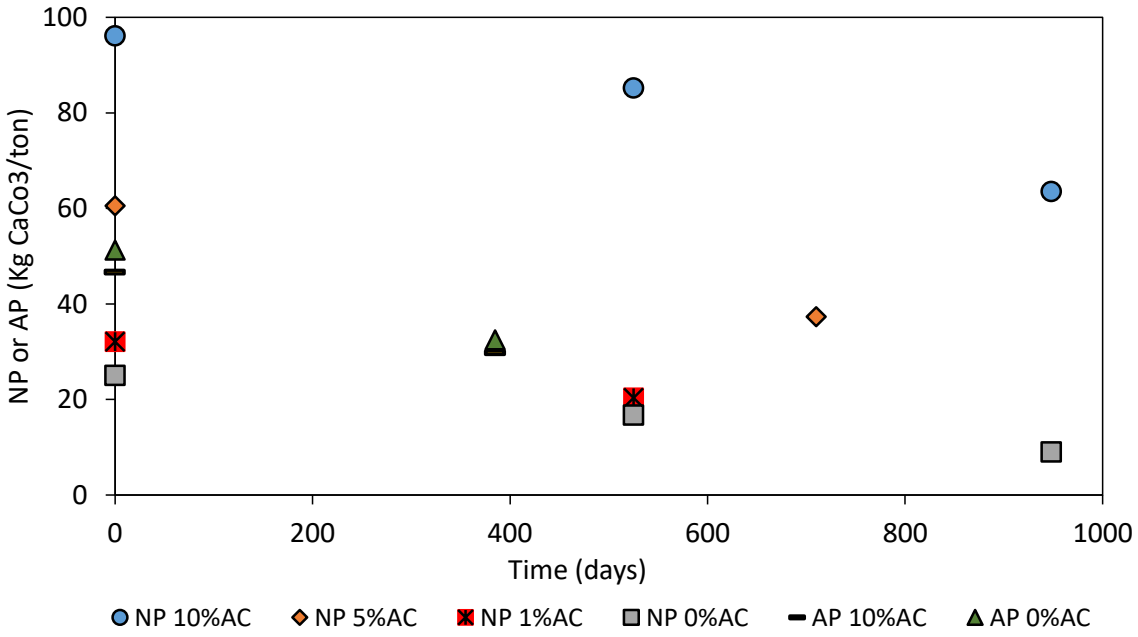

Figure 3.3. Acid base accounting test results for AC and CR samples, in terms of Acid potential (AP) and neutralization potential (NP), in order to reflect acidity and alkalinity consumption over time. The time in the horizontal axis represents how long the samples have been reacting in the columns.

Consequently, it was possible to calculate the approximate AP after a year, considering sulfur content (%S) in the last XRD test, but excluding the %S in gypsum. With this assumption, the AP also decreases and is consistent with the NP decrease *[Figure 3.3]*. For example, in column A1, the AP has decreased from 47 (day 0) to 30 (day 385) Kg $CaCO_3$/ton, yielding an approximate acidity consumption rate of 0.044 Kg $CaCO_3$/ton/day. If this rate is assumed to be constant over time, all the acidity would be exhausted in around 3 years.

It is worth to emphasize that the estimations of the alkalinity and acidity consumption time should be taken more as a qualitative reference than a quantitative one, since they were based on the assumption that the system behaves linearly. However, these results provided us a clear

indication and important insights that AC is an effective material for ARD passive long-term remediation. This is because the alkalinity demand will not likely exceed the total alkalinity over an extensive period of time. Thus, the use of the AC material would make the remediation sustainable.

3.4 COLUMN EXPERIMENTS

3.4.1 pH

The pH in the mine water environment, whether there is a remediation process or not, is indicative of the balance between acid and neutralization production by the minerals in the tailings, and it might also influence the dissolution, precipitation or adsorption reactions in the tailings *[Heikkinen et al., 2009]*. Overall, the rise in pH is inversely proportional to the rise in several metal concentrations. Moreover, the addition of alkaline material increases the metal adsorption and enhances the precipitation of HFO *[Doye and Duchesne, 2003, Webster et al., 1998]*.

Figure 3.4a shows the pH measurements from all the columns described in *Section 3.1*. On the alkaline side, column A1 shows a relatively stable trend around 7.5 after 3.7 years. This illustrates the effectiveness of the remediation designs in terms of keeping a neutral pH in the long term. Column A2, which is similar to A1 but with vegetation on the surface, has shown a similar behavior over around 800 days, indicating that, despite making the soil more porous and allowing more oxygen diffusing through it, vegetation does not affect the amended layer's neutralization capability (i.e. keeping the pH at neutral levels). Such results from column A2 imply that, on the one hand, the increase of the porosity in the soil by vegetation roots facilitates the pyrite oxidation

by allowing more oxygen to diffuse into the CR over the drier period; and on the other hand, the more porous soil holds more water and keeps the soil wetter for a longer period of time, which in turn blocks the oxygen diffusion process. But overall, due to transpiration from the vegetation, the soil moisture is lower with vegetation than without, i.e., columns A1 vs. A2 and columns B5 vs. B3, as shown in *Figure 3.2b1*.

Altogether, these results indicate that the overall impact of vegetation on the pH is insignificant. Moreover, previous studies *[Conesa and Faz, 2010, Lupton et al., 2013 and Rufaut et al., 2015]* show that vegetation exerts more influence in metal immobilization (i.e., metal uptake by roots) than in pH variation. Actually, pH is considered to be a key conditioning factor in plant growth and development in waste mine sites *[Borden and Black, 2005]*. Nevertheless, it is important to emphasize that the role played by vegetation in the ARD remediation proposed in this study will be secondary, since the main neutralization agent will be AC; so it is fair to assume that, under our remediation design, the vegetation will grow in a neutral or near-neutral environment.

Other noticeable fact is that column A3 (similar to A1 but with a middle sand layer) shows the highest pH levels, after > 2 years. This result is consistent with previous studies with shorter durations *[Pabst et al., 2014, Ouangrawa et al., 2010, Ouangrawa et al., 2009, Waybrant et al., 2002]*. For instance, this behavior was observed in *Pabst et al. [2014]* over 18 months and in *Ouangrawa et al. [2010]* over 500 days. In all of these studies, it was found that the sand layer acts like a saturated barrier that blocks oxygen diffusion and also decreases the amount of water draining downwards, enhancing the acid neutralization below and keeping the pH in higher levels for longer periods of time.

The hydro-geological principle behind the sand layer saturation (more permeable layer alternating with less permeable layers such as AC+CR layers) can be explained by the fact that

water flows more easily through sand than through AC+CR, thus the less permeable layer (i.e., the sand layer) forms a type of semi-barrier to flow. In other words, when rainfall infiltrates and reaches the sand layer between the two AC+CR layers, the water in the sand layer will build up pressure (or head) because more water is coming in than can be pushed out downwards *[Raffensperger et al., 2017 and Srinilta, 1967]*.

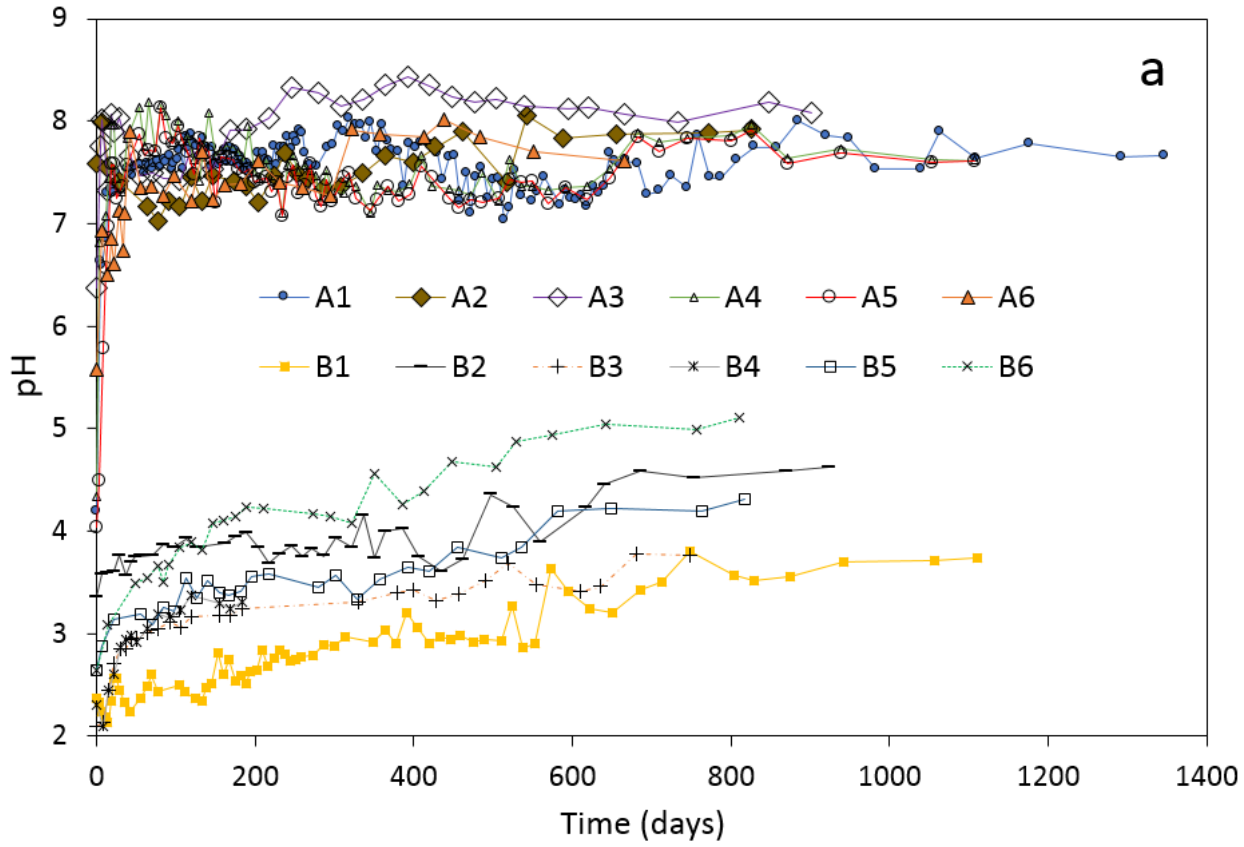

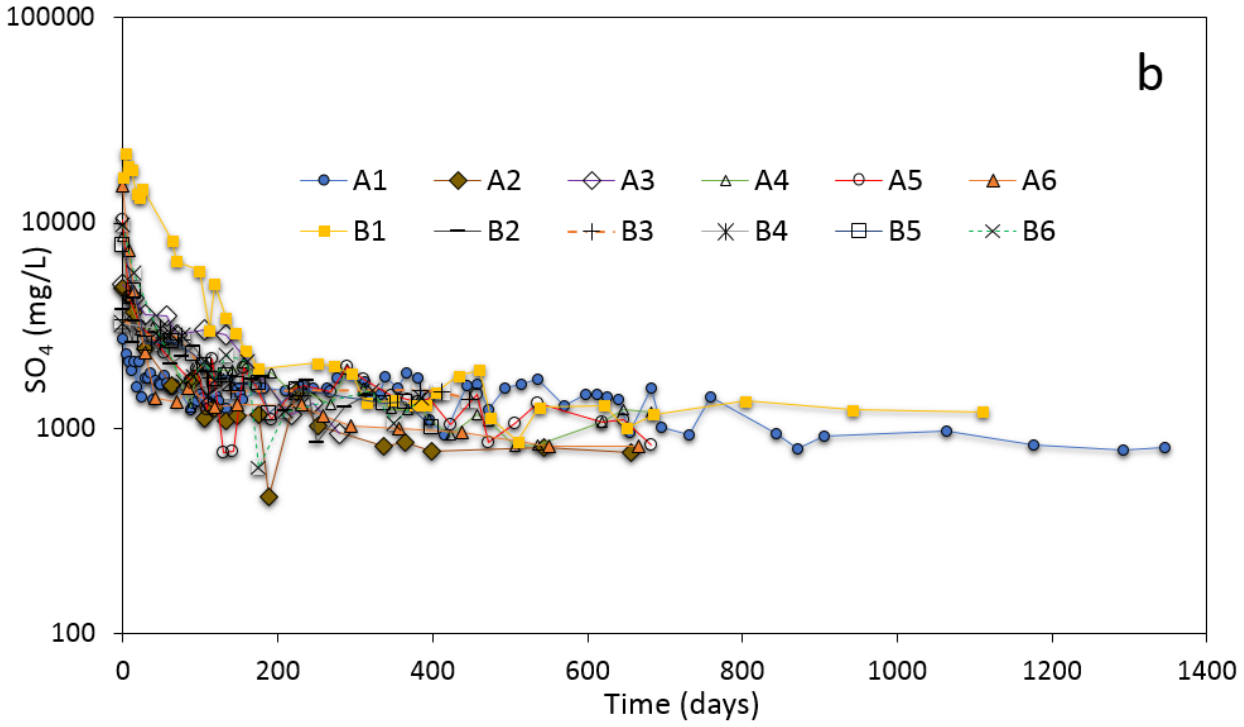

Figure 3.4. a) pH and b) sulfate results from the column leaching experiments.

To explore for an optimal content of the alkaline material for the CR remediation, different fractions of the AC material were added to the CR material. *Figure 3.4a* shows the impacts of these different AC fractions on the pH values over time: Columns A4 (8%AC), A5 (6%AC) and A6 (3%AC). As can be seen, the pH in these columns showed the same behavior as in column A1 (10%AC), despite having lower AC contents. This can be explained based on the acid base accounting results and analysis (*Section 2.3.2*). For instance, column A6 has approximately the minimum %AC where the total amount of alkalinity is equal to the total amount of acidity, therefore the mixture is within an uncertainty level, in which ARD could or could not be produced. However, in the case of column A6, after > 600 days, the pH is still higher than 7 and there is no indication of a decreasing trend. The acid base accounting test and the leachate pH implied that as long as a sufficient amount of AC is provided in the mixture (i.e., alkalinity ≥ acidity), ARD is not

likely to be produced, since AC proved to be sufficiently reactive and it depletes at lower rates than the sulfide minerals in the mixture.

On the acidic side, column B1 (i.e. non-amended scenario) has experienced a slight pH increase since it was started >1100 days ago. The pH in this column has increased from 2.2 to 3.8. This is a clear indication of a decreasing alkalinity demand over time, as reported in previous studies as well *[Huminicki and Rimstidt, J. D., 2009]*. This is mainly a consequence of iron and sulfur precipitates that will not generate acidity anymore. Column B2 (1%AC and pH~4.6 after > 900 days), along with column A6 (3% and pH~7.6 after >650 days) show the complexity of the system in determining kinetically the exact threshold where the amount of alkalinity and acidity should be the same *[Brady et al., 1992 and Price et al., 1997]*. Column B6 (i.e., the only acidic column with a sand layer whose experiment is still carried on) shows the strong influence of the saturated layer on the pH levels, even in the acidic environment. This column is currently above the threshold (pH > 4.5) where the leachate has an alkalinity higher than zero. In addition, column B4 had to be stopped after around 200 days because the vegetation root zone reached the saturated sand layer, creating pathways that caused water to drain more easily downwards, rendering the sand layer ineffective for the purpose of preventing the water and oxygen diffusion downward towards the non-amended layer. In general, columns B3 to B6 were designed to investigate the influence of the upper amended layer on the lower non-amended layer. Moreover, the vegetation in B3, which reached the lower CR layer, showed signs of metals intoxication. At least in terms of pH, it was showed that even with an alkaline drainage produced above, the drainage underneath the amended layer is still acidic as expected. This fact, along with the root zone depth, could be important constraints to consider when we decide for an appropriate depth for the amended layer.

3.4.2 Sulfate

In acid mine drainage chemistry, sulfate is usually seen as an indicator of sulfide mineral oxidation *[Plaza et al., 2017]*. However, even in highly acidic environments there can be sulfate reduction due, for example, to mineral solubility, as it is associated with several mineral phases that are present in mine tailings, among which are jarosite ($KFe_3(OH)_6(SO_4)_2$) and gypsum ($CaSO_4 2H_2O$). Moreover, mine water chemistry can be affected by bacterial sulfate reduction, where organic compounds use sulfate and release hydrogen sulfide and bicarbonate *[Hammarstrom et al., 2005 and Watzlaf et al., 2004]*. In the case of the columns in this study, all of them showed a similar behavior in the long term (even though their initial values have different magnitudes), which might be an indication of sulfate reduction.

Fig 3.4b shows sulfate (SO_4) concentrations retrieved from the columns' leachates. It is noticeable that, while the orders of magnitude are different at the beginning, sulfate concentrations show similar trends for all columns (i.e., amended and non-amended scenarios), with a very steep decreasing trend during the first few days and an apparent plateau of the sulfate curve with all columns approaching to similar level of the sulfate concentrations for the rest of the experiment time so far.

In the case of the control column B1, it started with a sulfate concentration over 20,000 mg/L, but that concentration decreased immediately and dramatically, and by the last 700 days it was close to the sulfate concentrations in the columns that contain AC. This might be an indication that at the beginning of the process there is some mineral solubility control that influences the relatively high sulfate concentrations in the control column (100%CR). The highly acidic pH in the control column eases the release of sulfate and heavy metals. Afterwards, the production of

sulfate is similar in the columns in which the main oxidant is either oxygen (CR + AC columns) or ferrous iron (CR column), as a probable consequence of sulfate mineral precipitation (e.g. gypsum), which was detected on a recent XRD analysis. Moreover, PHREEQC model calculations from Chapter 2 and *[Plaza et al., 2017]* showed the dissolution/precipitation of mineral phases that controlled sulfate concentrations. Other observed fact was that neither vegetation nor saturated sand barrier played a role in sulfate concentrations, as observed from columns A2, A3, B3, B4 and B6.

3.4.3 Dissolved metals

In this section, an adapted Ficklin diagram *[Ficklin et al., 1992, PlumLee et al., 1992 and PlumLee et al., 1999]* was utilized to analyze base dissolved metals in the columns' leachate. *Figure 3.5* shows an adaptation of the Flicklin diagram to present the results of the neutral (group A) and acidic (group B) columns. Compared to the original diagram, the only difference is that, in *Figure 3.5*, the metal concentrations are a function of time and not a function of the pH. Therefore, the pH is considered neutral/near neutral if it is >5.5 (A columns). The pH is highly acidic if it falls within the 1 – 3 range (initially, all B columns except B2). Finally, the pH is acidic if it falls within the 3 – 5.5 range (the present status of all B columns). In general, this analysis allows one to identify geologic controls in the water composition, since not all acidic mine waters would transport significant quantities of some dissolved metals *[PlumLee et al., 1999]*. The concentrations of major ions (i.e. Fe, Al and Mn) and their relation with pH are addressed in *Section 3.4.4*.

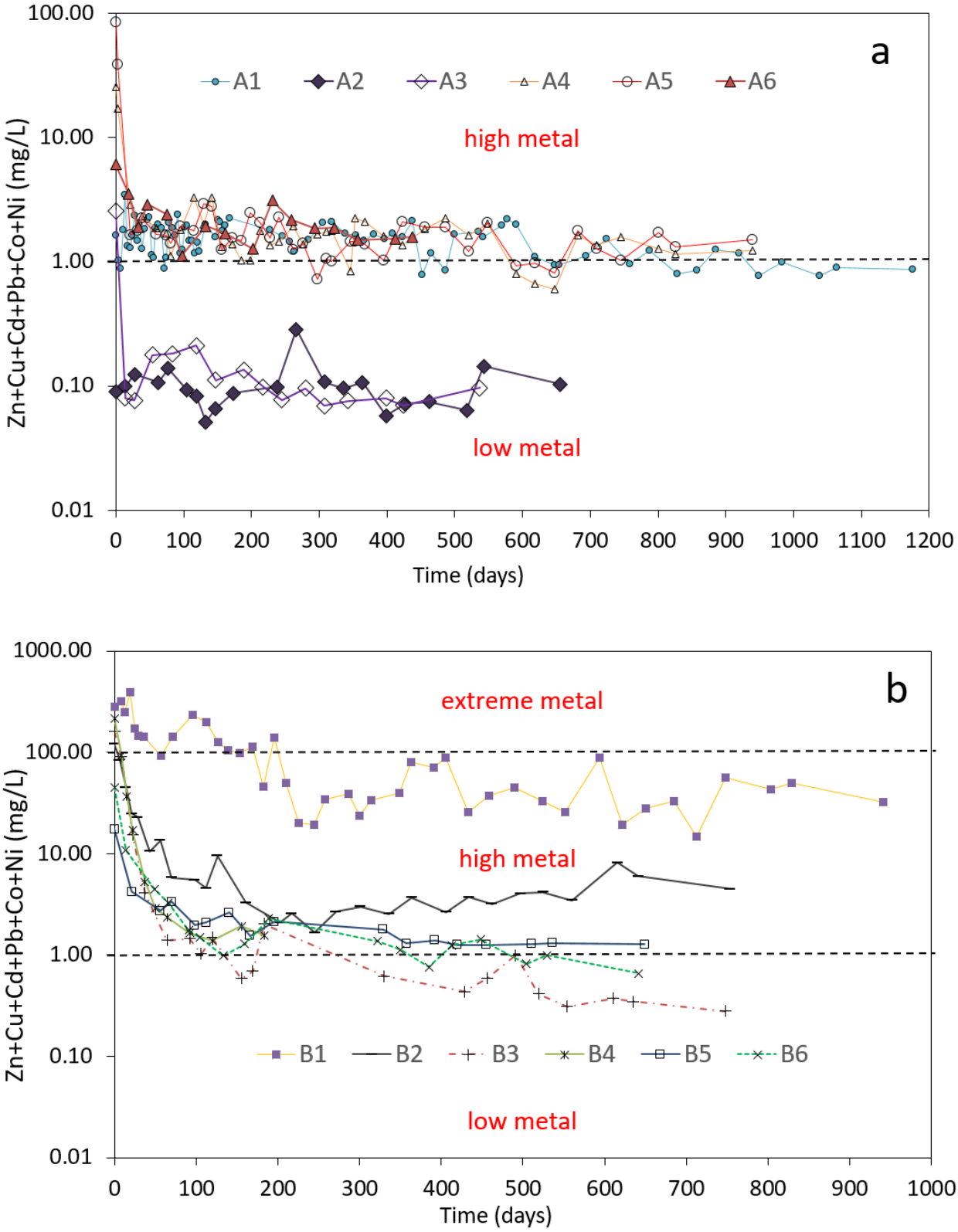

Figure 3.5. Adapted Flicklin diagram for the a) alkaline and b) acidic columns.

Figure 3.5a shows the adapted Flicklin diagram for the alkaline columns (group A).It is observed that most of the columns have the metal concentrations close to the threshold (i.e., 1 mg/L) that separates the high metal region from the low metal region. For columns A2 (i.e., with vegetation) and A3 (i.e., with sand layer), all the values are located inside and at the bottom part of the low metal region (< 0.15 mg/L). Moreover, column A1, the longest one (~1200 days), is in the low metal region for around the last 250 days of measurements. Similar to pH behavior, the general case in the A group columns is that, as long as a sufficient alkalinity amount is provided (i.e., > 3% AC, according to the acid base accounting test), the dissolved base metals concentrations will be similar among these columns and they will be on the lower side (i.e., inside or close to the low metal region). If additional variables (e.g., vegetation and sand layer) that enhance the neutralization potential of the system are introduced, these concentrations tend to be even lower.

Figure 3.5b shows the adapted Flicklin diagram for the acidic columns (group B). It is observed that the control column (B1) started in the "extreme metal" region (i.e. > 100 mg/L) and remained there for around 200 days, and, for the rest of the time (~750 days) it remained in the "high metal" region (>10 mg/L). Most of the remaining acidic columns also started in the "extreme metal" region, but only for few days, and, for the rest of the time they were located in the "high metal" or "low metal" regions (i.e. 1 – 100 mg/l, <1 mg/l, respectively). However, a remarkable similarity was found between the two groups of columns: the columns with vegetation (i.e. A2 and B3) and/or sand layer (i.e. A3 and B6) had better performances, in their respective groups, in terms of metals immobilization. In the case of columns B3 and B6, it was noted that even with the bottom CR layer, which controlled pH *[Figure 3.4a]*, their base metals concentrations are located in the lower metal region. In addition, it is evident that column B6 has the best performance of all the

acidic columns, achieving lower metal concentrations while keeping a higher pH (pH>5) than other columns in the B group. This constitutes another restriction when adopting an adequate amended layer depth that could ensure a high base metal immobilization and a near to neutral pH.

The relevance of the analysis of the columns with the bottom CR layer (i.e., B3 to B6) is that these scenarios are closer to the real-world conditions in the field, where there is a non-amended layer underneath the amended one. While both layers will contribute to subsurface runoff, these results emphasize the necessity to have an appropriate design of the amended layer in terms of depth, %AC and the presence of a complementary measure (i.e., vegetation or sand layer). Ultimately, it is desirable to guarantee an adequate acidic neutralization within the amended layer, while at the same time impeding water and oxygen diffusion downwards. Column B6 provides a good example of fulfilling those conditions.

In general, for both groups of columns, the order of metal mobility was the following: Zn > Cu > Ni > Co > Pb > Cd. The orders of magnitude of the first three metals are significant higher than the ones of the remaining metals. For instance, the reason because Zn is the most abundant dissolved base metals lies in the fact that Zn can become mobile even at moderate acidic pH (e.g. pH < 6) *[Sracek et al., 2010 and Jurjovec et al., 2002]*. The least dissolved metal, Cd, was below the detection limits (< 0.001 mg/L) in the majority of the columns. Only a few traces of Cd were found in some of the B columns.

3.4.4 Acidity, alkalinity and major ions (Fe, Al, Mn)

In mining environments, the drainages can be acidic or alkaline. In general, they have pH values between 2 and 9, and, in many cases they can degrade the aquatic habitat and change the water

quality due to their toxicity *[Morin and Hutt, 2001, Skousen et al., 2002 and Ziemkewicz et al., 2000]*. A drainage is acidic when acid minerals exceed the alkaline ones, it may contain high concentrations of SO_4, Fe, Mn, Al and other ions, it may or may not have low pH, but the presence of dissolved Fe, Al and Mn can generate H^+ and lower the pH. Alkaline mine drainages (alkalinity equal to or greater than acidity) may also have high concentrations of SO_4, Fe, Mn and other dissolved metals, but the dissolution of the carbonated minerals neutralize the acidity and remove Fe, Al and others metal ions, and yet does not significantly affect the concentration of SO_4. In acidic drainage the major cations are Fe, Mn and Al *[Skousen et al., 2002, Watlaf et al., 2002 and Ziemkewicz et al., 2000]*. In alkaline drainage, carbonates (e.g. $CaCO_3$) are more significant than SO_4 and the contents of Ca, Mg and Na are higher than those of Fe, Al and Mn *[Doye and Duchesne, 2003, Nordstrom and Alpers, 1999 and PlumLee et al., 1992]*.

In *Section1.4.2.3*, the procedure that was followed to determine the balance between acidity and alkalinity in the columns' leachate over time was detailed. This procedure was based on the approach made by *Kirby and Cravotta, [2005a,b]*, which used a titration method *[APHA, 1998a,b]* and the PHREEQC to calculate the alkalinity and *Eq.(1-1) [Kirby and Cravotta, 2005, Watzlaf et al., 2004 and Hedin et al., 1994]* to calculate the acidity. *Kirby and Cravotta, [2005a,b]* reproduced the data from *Hedin [2004]* and *Watzlaf et al. [2004]* and found good agreement between the measured and calculated acidity in large datasets with acidities up 15,000 mg/L as CaCO3 and with pH ranging from 1.6 to 8.5.

The calculation of the acidity using *Eq. (1-1)* was a relatively simple procedure, since the measured pH and concentrations of Fe, Mn and Al are the only input needed. However, the measurement of the alkalinity posed a major challenge, since it needed the use of all the collected sample (60 – 90 mL), so it was not possible to replicate the test. Since most of the alkalinity data

will be limited, the PHREEQC model was used to calculate the alkalinity in this study, based on the columns scenarios (amended: A1 and non-amended: B1). Moreover, the Standard Method alkalinity titration is constrained to yield positive values (alkalinity > 0). However, for low-pH samples, alkalinity can be negative due to negative contributions by dissolved metals that may oxidize and hydrolyze *[Kirby and Cravotta, 2005ab]*.

Figure 3.6a shows the alkalinity (measured and calculated with PHREEQC) and acidity (calculated) for column A1 (the amended scenario). For this scenario, the leachate remained with positive net alkalinity (alkalinity – acidity > 0) *[Eq. (1-2)]* during the entire time. After around 1100 days, the passive treatment with 10%AC (determined to be optimal) yielded a net alkalinity of >60 mg/L CaCO3, thus indicating that this treatment has been effective during the tested period. In addition, acidity data from columns A2 (10%AC + vegetation) and A3 (10%AC + sand layer) are included, showing lower acidity values (< 5 mg/L CaCO3), which is consistent with the lower concentrations of dissolved metals in these two columns. In summary, as expected, the net alkalinity in all A columns is controlled by the high pH *[Figure 3.4a]* and low levels of dissolved Fe, Mn and Al *[Figure 3.7 and Figure 3.8]*, since the negative contribution of metal species to alkalinity in near-neutral pH mine water is negligible *[Kirby and Cravotta, 2005ab]*.

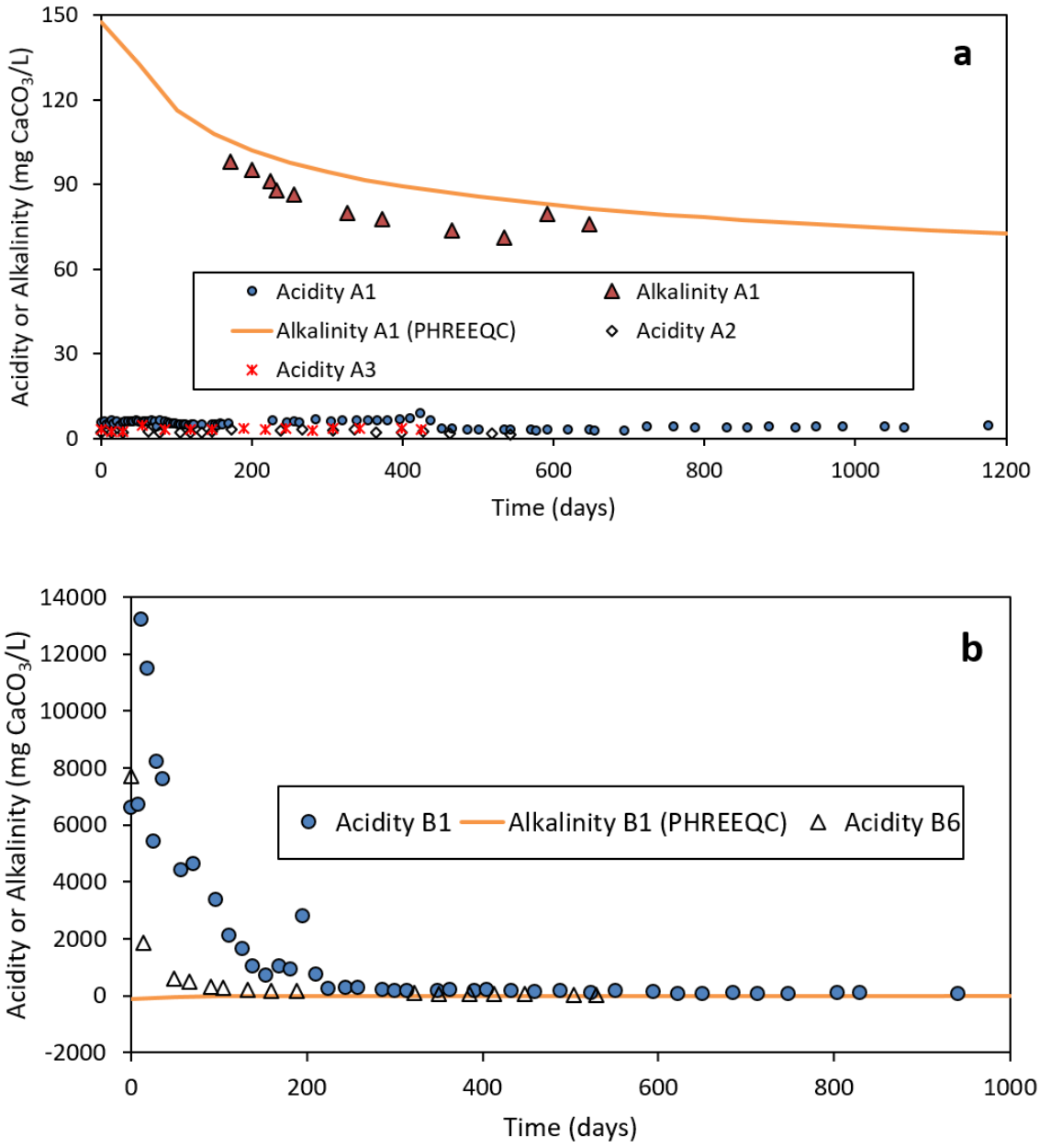

Figure 3.6. Leachate alkalinity and acidity for the a) alkaline and b) acidic columns.

Similarly, *Figure 3.6b* shows the alkalinity (measured from the column experiments and calculated with PHREEQC) and acidity (calculated) for column B1. After almost 900 days, the control scenario (no remediation) yielded a negative net alkalinity (alkalinity – acidity < 0) that approximately varied from -200 to -14,000 mg/L CaCO3, indicating that this drainage needed

alkaline addition as expected. In addition, for reference purposes, data from column B6 is included, showing the same order of magnitude in the alkalinity values. Despite the fact that some of the columns in the B group had a drainage with low concentrations of base metals (*Section 3.4.3*), their acidic pH (< 4.5) *[Figure 3.4a]* and their high levels of acidic metals (ie., Fe, Mn and Al) *[Figure 3.7 and Figure 3.8]* controlled the negative net alkalinity in the leachate. As a reference, *Pennsylvania DEP, [1998]* provides chemical data for water samples from 749 mine discharges in Pennsylvania, where more than 90% of the samples have a net alkalinity ranging from -500 to 500 mg/L $CaCO_3$, with the corresponding pH ranging from 3 to 7.

Figure 3.7 shows boxplots of Fe and Mn concentrations for some of the columns in groups A and B, respectively, as a function of the %AC and the presence of vegetation and sand layer. This analysis was based on the total number of samples collected from each of the columns, as seen in *Figure 3.5*, ranging from 700 to 1200 days of sampling, approximately. It was clearly observed that the amount of the alkaline remediation material had a great incidence in the mobility of these acidic metals. *Figure 3.7a* shows clearly that the addition of only 1%AC to the coal waste (3500 to 30 mg/L, considering the maximum values in columns B1 and B2, respectively) significantly immobilizes Fe. In this case, the addition of the alkaline material (i.e., AC) increased pH levels from about 2.5 – 3.5 to about 3.5 – 4.5, immobilized the metals, and reduced the activity of Fe(III) via the precipitation of Fe oxyhydroxide. In addition, the addition of the AC material may also have some effects of reducing the proliferation of bacteria as indicated by previous studies *[Doye and Duchesne, 2003]*.

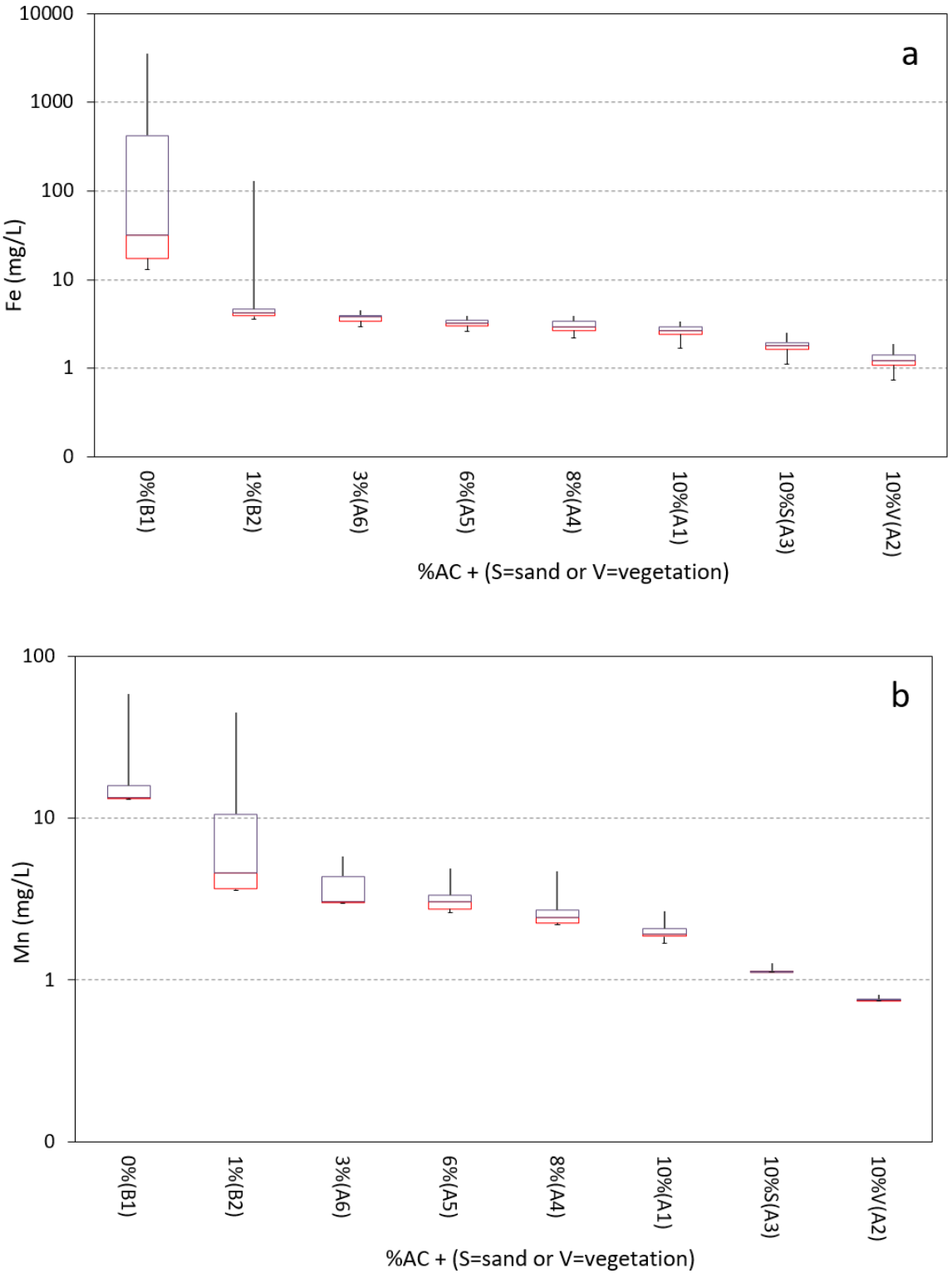

Figure 3.7. Boxplots for a) Fe and b) Mn concentrations for several %AC and the presence of vegetation and saturated sand layer.

Moreover, the impact of vegetation and sand layer in immobilizing Fe and Mn was clearly present as a result of the extraction/accumulation by vegetation and the oxygen/water diffusion blockage by the saturated sand layer. The column experiment results also showed that there is a large variability of metal mobility in the non-amended scenario over time, especially having their highest levels *[Figure 3.5 – 3.8]* at the beginning period of time of the experiments. Such high levels of metal concentrations demonstrate a critical need not only to implement a mine remediation strategy but also to implement the remediation as soon as the coal waste is disposed on the site to avoid the generation and drainage of significant amounts of dissolved metals.

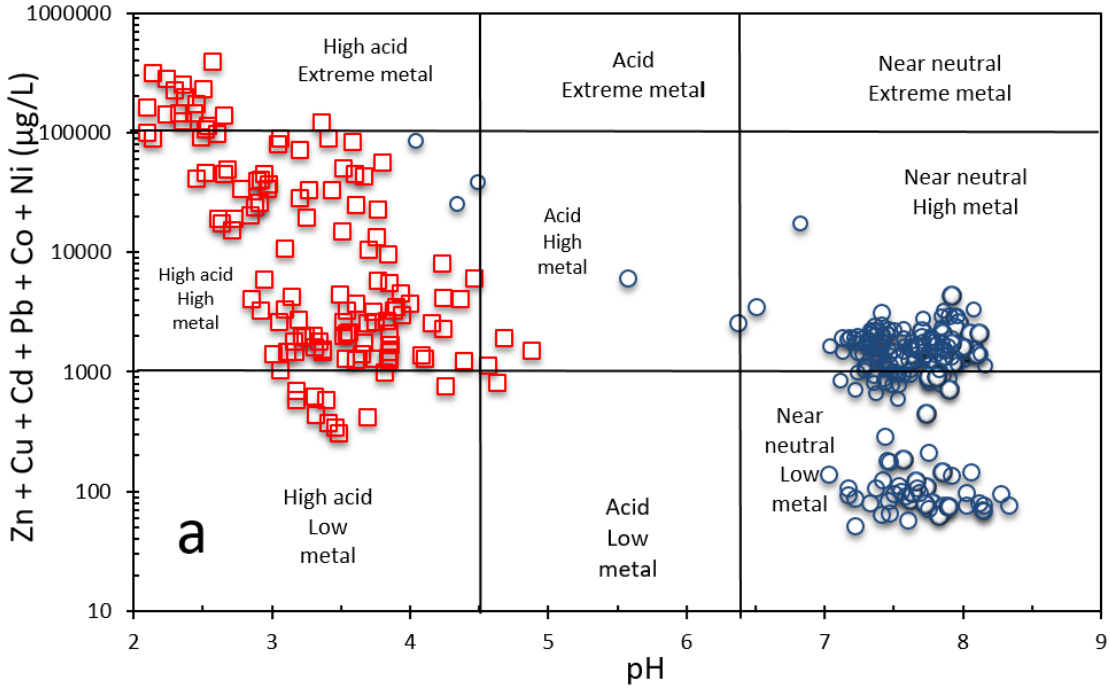

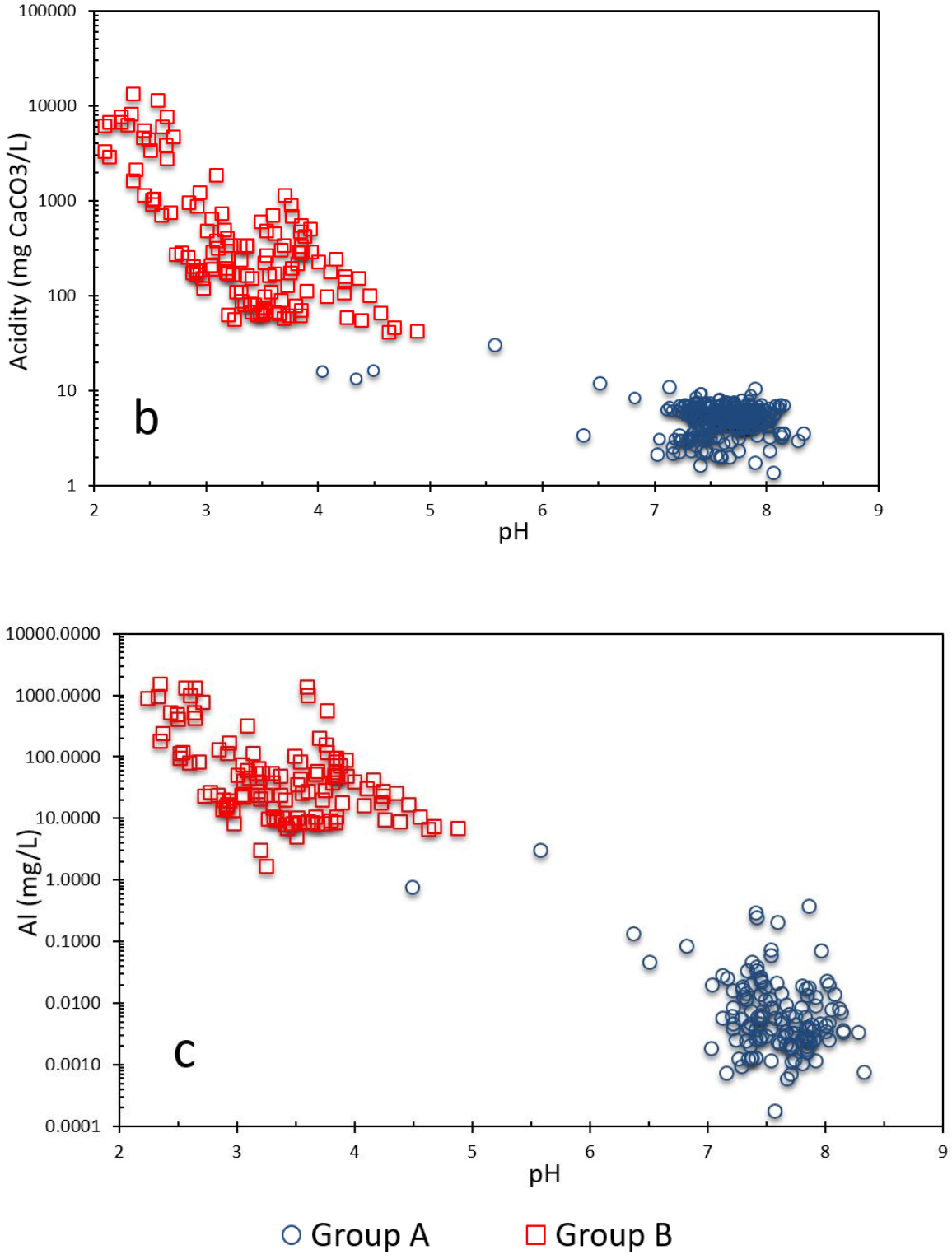

Figure 3.8. a) Ficklin diagram, b) acidity and c) Al related to pH, for alkaline and acidic columns

Finally, *Figure 3.8* shows two distinguished groups, alkaline group (group A, blue circles) and acidic group (group B, red squares) based on the relations among pH, dissolved metals, acidity and Al. *Figure 3.8a* is basically a Ficklin diagram, where pH showed a good agreement on the relationships between metal concentrations and pH for most of the columns. It was also observed that a small number of columns in group A had high metal concentrations with acidic pH and, conversely, some columns in the B group had low metal concentrations with high acidic pH. This indicates that pH is not the only determinant for metal mobility. The relations between pH and metal concentrations can also be controlled by the interactions of other factors such as the dilution of acidic water by alkaline water (e.g., the columns with a bottom CR layer) and solubility controls of Fe, Mn and Al *[Cravotta, 2006]*.

Figure 3.8b and *c* show the relationships between pH and acidity (based on pH, Fe, Mn, Al) and between the pH and an acidic metal (i.e., Al), respectively. Al is a good indicator as Al minerals are insoluble at near-neutral pH *[Cravotta, 2008 ab]*, having their minimum solubility at pH 6 to 7 *[Nordstrom and Ball, 1986 and Bigham and Nordstrom, 2000]*. Likewise, acidity is a good indicator as well since the solubility of Fe and Mn becomes very limited at neutral pH *[Valente et al., 2012, Hammarstrom et al., 2005, Nordstrom and Alpers, 1999 and PlumLee et al., 1992]*.This is clearly presented in the relationship between acidity and pH.

In summary, this analysis has shown that the relationships between the pH and concentrations of the major and trace elements in coal mine discharges vary among the constituents, which is consistent with other studies *[Kirby and Cravotta, 2005ab, Cravotta, 2006, Cravotta, 2008ab and PlumLee et al., 1999]*. All of these factors are important to be used to identify the potential environmental impacts of ARD. Moreover, the concentration levels of these factors/parameters are crucial in assessing the effectiveness of an ARD remediation design. As

indicated by *[Cravotta, 2006]* the appropriateness of a particular treatment method depends on the alkalinity and acidity balance among other variables. Finally, It is important to mention that the amended scenario, and, moreover, the amended scenario with complementary measures such as vegetation and saturated sand layer, ensured a drainage with low pH, positive net alkalinity and low metals concentrations

3.4.5 Metals/metalloids accumulation in vegetation: environmental impacts and implications for the amended layer depth

In general, metals (e.g., Fe, Pb, Zn, Cu, Cd, Al, Mn) are naturally present in soil and vegetation and, moreover, contamination also might come from other sources, such as the agriculture industry (e.g., irrigation with polluted water, contaminated manure and pesticide containing heavy metals) *[Aghamirlou et al., 2015]*. One of the main risks associated with metal accumulation in plants relies on the facts that some elements such as Cd are considered to be highly mobile in the food chain *[Chaney, 1989]*. Therefore, in terms of utilizing the vegetation as a complementary measure to enhance the remediation proposed in this study, it is important to do an analysis of the contamination magnitude suffered by vegetation growing in a potentially acidic environment and, furthermore, the tolerance of this vegetation before reaching metal intoxication.

Since the desired role of vegetation in this proposed ARD remediation study is to provide an additional "metal-immobilization/stabilization" factor, to have an additional natural barrier between the environment and the non-amended layer (e.g., vegetation grown in a topsoil above the amended layer serves as a retain water or water-movement-limiting agent, thus decreasing the influx of atmospheric oxygen into the underlying amended and non-amended layers, which in turn increases the neutralization capacity); and to have an environmentally-friendly solution with a

positive visual impact (i.e., green-vegetated area, as opposed to bare soil), while the primary goal is to neutralize the ARD through AC, it is not the focus of this study to test the suitability of several vegetation species to fulfill the remediation design requirements, or, even more, a study about phytoremediation, but to test one common grass species and perform the above-mentioned analyses.

The selected species for this study was the centipede grass (*Eremochloa ophiuroides munro*), one of the most popular turf grasses around the world *[Barampuram et al., 2009, Islam and Hirata, 2005]*, which is widely distributed in North America *[Hook et al. 1992, Duble 1996, Liu et al. 2008]*. Two important properties of centipede grass, for the purposed of this study, is that it can tolerate moderately acidic environments (pH ~ 4 – 6) and needs relatively low maintenance *[McCarty 1995, Landry and Murphy 2002, Islam and Hirata 2005]*.

Table 3.2 shows the trace elements concentrations (mg/kg of dry matter) in grass shoots for two different amended mixtures (5%AC+95%CR and 10%AC+90%CR) and a control scenario (i.e. grass grown in regular soil), that were collected 30, 90 and 190 days after the seeds were planted. To provide an additional scenario, it was intent to grow grass in 100%CR, but this test was unsuccessful, due to the high acidity of the soil. The results shown in *Table 3.2a* represent the average of the triplicated tests, based on both 0.25 g and 0.5 g of dry grass, which was observed (from their concentrations) to proportionally achieve similar digestion levels (see *Section 1.4.2.4*). In decreasing order, the trace elements concentrations were found to be Ca > Mg > Al > Fe > Na for the higher values (71000 to 1000 mg/kg) and Mn > Zn > Cu > Cr > Ni > Pb > As > Co > Cd for the lower values (180 to 0.3 mg/kg).

Table 3.2. a) Trace element concentrations (mg/kg of dry matter) in centipede grass shoots extracted 30, 90 and 180 days after the seeding. b) Normal ranges in plants, phytotoxic concentrations and toxic levels for livestock of several trace elements (*Chaney [1989]* and other authors, see table footnotes); levels in parentheses were estimated (by NRC) by extrapolating between animal species (*Madejon et al., 2002*)

a)

Element (mg/kg_{DW})	30 days			90 days			180 days		
	control	5%AC + 95%CR	10%AC + 90%CR	control	5%AC + 95%CR	10%AC + 90%CR	control	5%AC + 95%CR	10%AC + 90%CR
Al	100.55	613.94	569.37	179.22	1701.64	1646.16	231.47	2778.05	2541.04
Ca	880.88	5497.11	5558.38	1475.01	25451.80	25334.72	1853.40	35580.11	38654.11
Cr	0.30	0.51	0.47	0.66	2.86	2.70	0.79	5.88	5.61
Mn	2.45	16.89	15.65	7.57	49.26	44.16	10.43	91.02	79.77
Fe	54.41	520.91	490.31	101.09	1457.57	1357.36	141.22	2046.04	2035.77
Co	0.02	0.14	0.13	0.04	0.38	0.37	0.05	0.68	0.70
Ni	0.10	1.09	0.97	0.28	1.61	1.39	0.32	3.80	3.25
Cu	0.66	4.30	3.52	0.95	11.70	10.04	1.36	19.92	15.50
Zn	1.86	8.90	7.46	3.20	19.40	17.23	3.83	29.66	23.08
Cd	0.01	0.02	0.02	0.02	0.07	0.07	0.03	0.14	0.16
As	0.04	0.29	0.27	0.04	1.04	0.91	0.07	1.47	1.39
Na	32.95	5109.80	6061.75	64.83	11052.38	11564.10	94.52	17948.47	20753.27
Mg	76.61	498.81	464.89	226.99	1630.04	1568.11	296.40	4472.27	4302.06
Pb	0.08	0.26	0.22	0.13	1.19	0.98	0.19	1.79	1.39

b)

Element	**Normal levels (mg kg^{-1} dry foliage)**	**Phytotoxic levels (mg kg^{-1} dry foliage)**	**Maximum levels tolerated by livestock (mg kg^{-1} dry diet)**			
			Cattle	**Sheep**	**Swine**	**Chicken**
$As_{inorg.}$	0.01–1	3–10	50	50	50	50
Cd	0.1–1	5–700	0.5	0.5	0.5	0.5
Cu	3–20	25–40	100	25	250	300
		10–70[a]			300–500[b]	
Fe^{2+}	30–300	–	1000	500	3000	1000
					5000[b]	
Mn	15–150	400–2000	1000	1000	400	2000
					1000[b]	
Ni	0.1–5	50–100	50	(50)	(100)	(300)
Pb	2–5	–	30	30	30	30
Zn	15–150	500–1500	500	300	1000	1000
				1000	2000[b]	

a Toxic levels for crops according to *Gupta and Gupta [1998]*.

b Toxic levels according to *Annenkov [1982]*.

The analysis of metal accumulation in plants and their toxicity is usually linked to the vegetation potential use (e.g. livestock consumption, recreation). As a reference, *Chaney [1989]* and NRC [1980] have estimates of normal and toxic levels of some elements in plant foliage (crops), along with tolerable levels for domestic livestock *[Table 3.2b]*. In the control scenario of *Table 3.2a*, as previously expected, all concentrations are within the normal levels, which was consistent with a visual examination, were the grass was observed to be in healthy conditions (e.g., green leaves and no dead leaves). On the other hand, in the ARD amended scenarios (AC + CR mixture), Fe and $As_{inorganic}$ concentrations were higher than the normal levels, while other elements such as Ni and Cu were close to the upper threshold beyond which they would not to be considered as normal metal concentrations. From the livestock tolerance perspective, high quantities of Fe (>1000 mg/kg) would make this grass not suitable for most livestock types.

Madejon et al. [2002] studied the bioaccumulation of As, Cd, Cu, Fe and Pb in two species of wild grass affected by a mine spill in Spain. Comparing the results from *Madejon et al. [2002]* and the ones presented in this study, the metals concentrations in *Table 3.2a* for the AC+CR mixture scenarios, have similar order of magnitude but are however lower. For instance, Fe and Cu concentrations in this study range from around 500 to 2000 and 4 to 20 mg/kg, respectively, while in *Madejon et al. [2002]* they range from around 600 to 4,000 and 12 to 28 mg/kg, respectively. Many other studies *[Reilly and Reilly, 1973, Madejon et al., 2006, Yan et al., 2012, Qu et al., 2003]* clearly show the impact of partially and highly contaminated soils in vegetation. In conclusion, this experiment has indicated that there has been occurring metals/metalloids accumulation in the grass, under the amended scenario, which can be previously inferred from a mass balance perspective in the kinetic experiments, where column A2 has had the best performance in terms of metals/metalloids immobilization in the leachate *[Figure 3.5 and 3.7]*.

Moreover, the fact that the accumulation has not reached toxicity levels that could pose irreversible damage for the vegetation, showed that this is an effective approach for phytostabilization (i.e. grass acting as a metal mobility control factor). Therefore, a vegetated amended area has a beneficial impact that exceeds its potential risk (i.e. phytointoxication or wildlife consumption).

Other elements that are important to analyze in terms of their toxic effect on plants and animals are Al and Na. Due to the abundance of Al in most soils, it is largely dependent on pH, which controls Al solubility. In natural soils, where the pH is moderately acidic (4 – 6), Al has little solubility and its toxicity is rarely reported; and there is no evidence of Al toxicity suffered by grazing animals *[Gough et al., 1979]*. Moreover, there is some experimental evidence about the Al levels that some animal species (e.g., rats) can tolerate *[Bowen, 1966]*, but there is no relationship with the animal consumption of Al directly from the plant. However, further investigation is required to establish normal and toxic Al levels in vegetation and their impact on livestock or wildlife.

In the case of Na, it is widely known that its presence in soils (in soluble form) significantly reduces the plant normal growth, which causes adverse economic impacts on industries such as the agriculture *[Kopittke, 2012, Pitman and Läuchli, 2002]*. Under natural conditions, Na has been measured in plants and concentrations have been found to vary between 3000 to 24000 mg/kg_{DW} *[Tavakkoli et al., 2011]*. In the case of our experimental study, Na concentrations for the amended scenario (10% AC + 90% CR) reached a magnitude of approximately 20700 mg/kg_{DW}. This relatively high concentration makes this element an important parameter to evaluate because it could adversely affect the vegetation growth. Further study is required to search for a grass species that can tolerate high Na levels.

The outcome of these tests, jointly analyzed with the ones from the column experiments *[Plaza et al., 2018]* may also have a significant implication on the search for an adequate amended layer depth. *Xu [2013]* performed a sensitivity analysis of the amended layer depth from a modeling perspective using the HTGCM. The amended layer depths were set from 0 to 2.6 m. Judging by SO_4 and Fe results, it was determined that even a shallow amended layer of 0.40 m exerts an important influence to around 3 m depth, which means that SO_4 and Fe are also reduced in the underneath non-amended layer. As expected, the 2.6 m amended layer achieved a major reduction of contaminants, but no as significant to have a very thick amended layer. Finally, the model calibration was done based on a 61 cm amended layer depth, same as in the amended plots in Mather. The original HTGCM does not consider oxygen diffusion reduction by pyrite coating, which could strengthen the hypothesis of not needing to have a thick amended layer.

Based on the results from the columns with a CR layer at the bottom, there is a significant reduction of metals even though the pH remains on the acidic side. In the column with a bottom CR layer and vegetation, the metal reduction is more significant, and a slightly higher pH is achieved. However, the grass shows signs of metal intoxication *[Fig 3.9]*.

This fact points out that the root length is a very important constraint when determining an adequate amended layer depth, because vegetation has been proved to be beneficial in the remediation. On the modeling side, the inclusion of a pyrite coating effect through an oxygen diffusion reduction over time, could dramatically improve the water quality underneath the amended layer. Based on previous studies *[Murphy et al., 2017, Holdo and Brocato, 2015, Mazzacavallo and Kulmatiski, 2015, Han and Young, 2014, Mueller et al., 2013, Nippert and Wieme, 2012, Kumar et al., 2010]*, it was found that, on average, for most grass species, the root

length ranges from 0.8 m to 1.5 m. However, the majority of the studies about grass root length consider that the roots are located within 1 m depth.

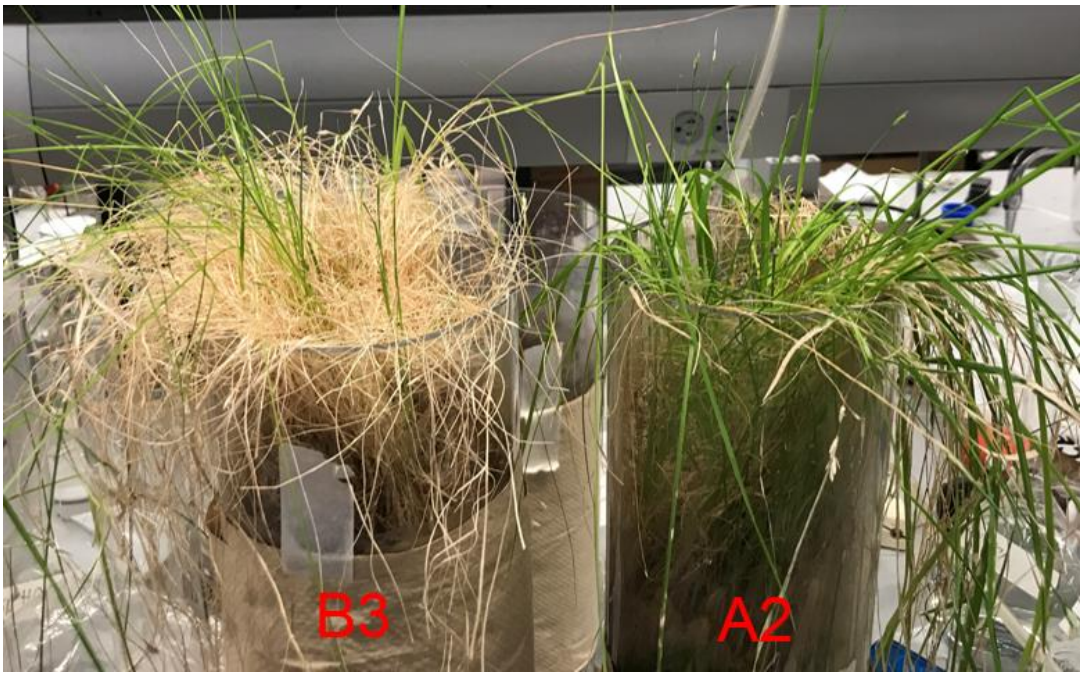

Figure 3.9. Comparison between grass conditions in alkaline and acidic column

From the hydro-geochemical analysis, it has been demonstrated that it is not necessary to have a very thick amended layer for two main reasons: the drainage of neutralized and low metal water from the upper amended layer and the continuous decrease of the oxygen diffusion downwards due to the pyrite coating and other precipitates such as sulfate precipitates (e.g., gypsum) that will no longer produce acidity.

However, from the experimental analysis, it has been established that the root length is a very important restriction factor - having a too shallow an amended layer might cause plant metal intoxication. Based on previous studies that have characterized the root depth of several grass species, the majority of the root biomass is located from the surface to 60 to 80 cm depth, approximately. Therefore, for the purpose having a "safe" amended layer depth that could jointly

enhanced the acidic neutralization properties of AC and grass, an adequate amended layer depth could be established between 0.8 m to 1 m.

3.5 CONCLUSIONS

This study has presented an assessment of an ARD remediation approach from several perspectives: amount of acid neutralization material, acidity and alkalinity in the leachate, acidity and alkalinity balance in the mineral phase, complementary measures that could add up to the neutralization properties of the AC such as vegetation and saturated sand barrier.

In general, AC has demonstrated to be an effective acidic neutralization agent. All columns with >3% AC have achieved major metal immobilization and a neutral pH. Moreover, the results from the kinetic experiments (columns) are consistent with the outcome from the acid base accounting test, namely, that the columns with a %AC $\geq$ 3 remain on the neutral side, while columns with less %AC are on the acidic side. It is likely that for the optimal amended scenario (10%AC + 90%CR) the alkalinity supply will be sufficient to maintain a neutral pH and lower metals/metalloids concentrations in the long term. The high net alkalinity resultant drainage is also a strong evidence of an effective ARD remediation. It is worth emphasizing that the context of the term “optimal mixing ratio” used through this study is to determine the approximate minimum amount of the remediation material (i.e., AC) that can guarantee a long-term ARD remediation in a coal waste pile. Further investigation should evaluate (e.g., based on a kinetic approach) the impacts of having higher amounts of AC (e.g., > 10%) applied in the amended layer.

Vegetation seems to enhance the dissolved metals/metalloids immobilization. Results from microwave-digested grass, grown in an AC+CR mixture, shows evidence of phytostabilization, in

which the vegetation acts as a trace element accumulation sink, without reaching severe toxicity levels. However, in order to minimize the potential risks linked to metal accumulation in plants, future work should involve establishing the necessity to do a revegetation after certain period of time, in case the pollution levels become intolerable for the plants. It is also necessary to make a more detailed study about normal or toxic levels of metals in plants.

The saturated sand layer seems to create a barrier that blocks oxygen and water diffusion through the soil and increases retention times, thus maintaining higher pH values over longer times. However, future work should consider the study of lower-cost, environmentally friendly alternatives to sand (e.g., a porous waste material). Another aspect that requires further investigation is the implementation and the effectiveness of this buffer layer under real field conditions, where many climatic factors are difficult to predict and impossible to control. For instance, it may be necessary to investigate how fast this layer can get saturated under wet and dry climatic conditions and what significant impacts can be distinguished from the implementation of this strategy in the field, as opposed to only having one amended layer (AC+CR) over a non-amended layer (CR).

The next stage of this research will focus on the simulation of the ARD remediation processes under a more physically-based modeling framework.

4.0 ACID ROCK DRAINAGE PASSIVE REMEDIATION USING ALKALINE CLAY: IMPLEMENTATION OF THE REMEDIATION AT A WATERSHED SCALE UTILIZING A SOPHISTICATED HYDRO-THERMAL GEOCHEMICAL MODEL

4.1 INTRODUCTION

In *Section 1.4.3.2*, it is briefly explained the final stage of the modeling framework using a modified version of the Hydro-Thermal-Geochemical Model (HTGC), originally developed by *Xu [2014]* to simulate the acid rock drainage and alkaline neutralization processes in an amended and non-amended plots in the Mather mine site. As previously mention, the HTGCM model couples the hydrological model DHSVM with the following thermal and geochemical modules:

- ***Pyrite Oxidation module***: calculates pyrite oxidation produced by oxygen (i.e., SO_4, $Fe_{(total)}$, and pH) based on a shrinking-core principle *[Davis and Ritchie, 1986]*.

- ***PHREEQC module***: calculates pH, soil temperature, oxygen concentrations, cations and anions in aqueous and mineral phases.

- ***Advection-Dispersion module***: calculates chemical transport.

- ***Thermal Transport module***: calculates the soil temperature profile influenced by solar radiation and heat generation from pyrite oxidation.

Figure 4.1 shows a flowchart of the original HTGCM model. The proposed improvements will result in a modification of the Pyrite Oxidation and PHREEQC modules.

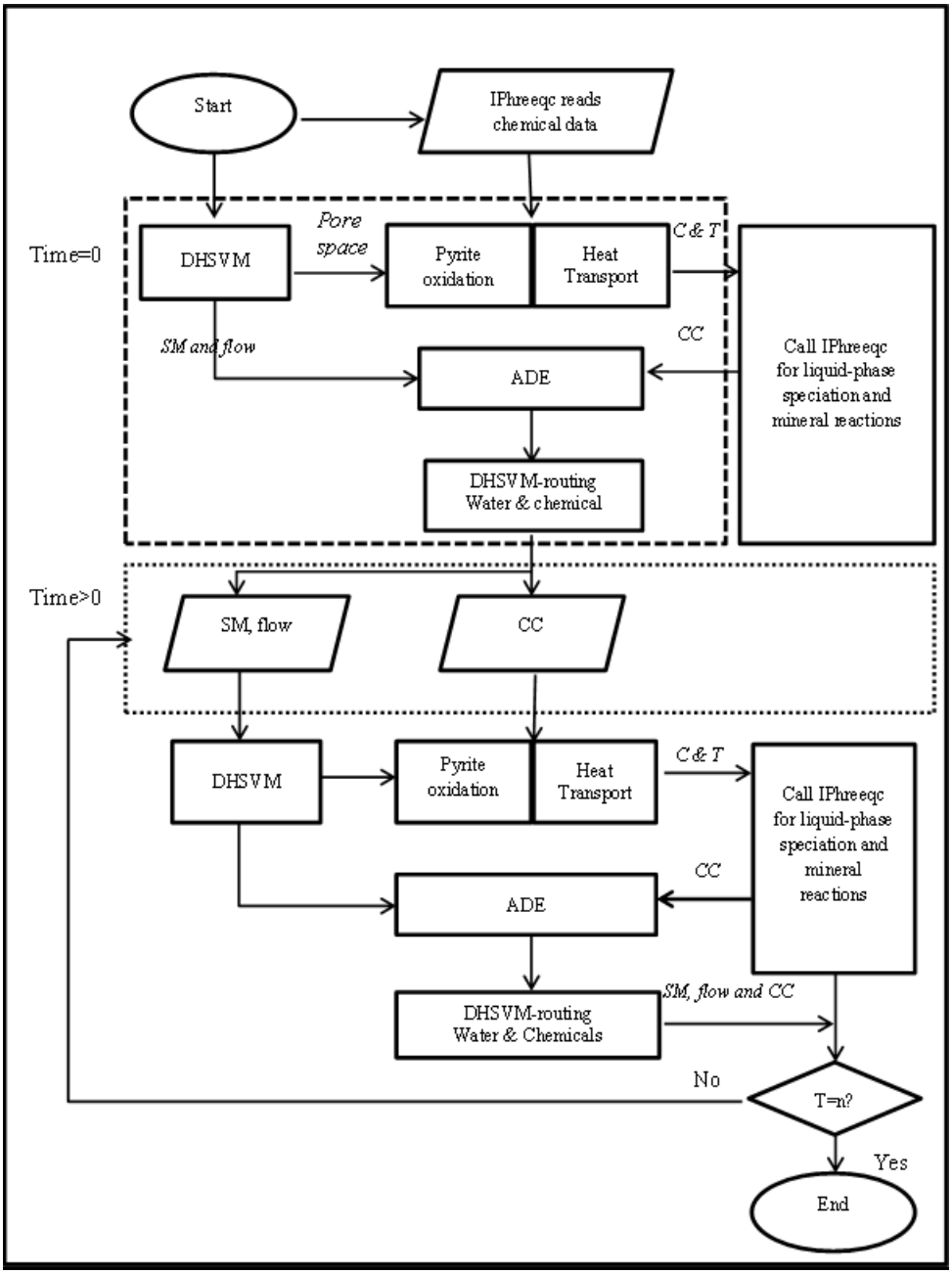

Figure 4.1. Flowchart of coupling HTGCM with PHREEQC *(Source: Xu, [2014])*. CC represent the concentrations of Fe (total), S (total), O (total), H (total), Al (total), Ca (total), Na (total), Mg (total), K (total), Si (total), P (total), Cl (total) and Mn (total) in solutions; C indicates the concentrations of Fe (total), S (total), O (total) and H (total) in solutions; SM is soil moisture, T is temperature, n is the ending time step and ADE is advection-dispersion equation.

In the following sections, the proposed changes and improvements to the current version of the model will be explained in detail. Finally, the resultant improved version of the HTGCM model will be tested in two different watersheds that have waste coal piles.

4.2 DESCRIPTION OF THE CHANGES AND IMPROVEMENTS TO THE ORIGINAL HTGCM MODEL

4.2.1 Model Scale

For the purposes of testing and calibrating the originally developed HTGCM model, it was limited to only the Mather site scale, approximately 0.038 km^2 *[Figure 4.2]*. This configuration helped to performed more complete and detailed calculations (e.g. sensitivity analysis) in several aspects of the model: PYROX, advection – dispersion, thermal transport and PHREEQC modules.

Moreover, the field measurements within the study site (i.e. meteorological and geochemical data) provided valuable inputs for the model development. This justified the focus only on the site's experimental plots to run the model.

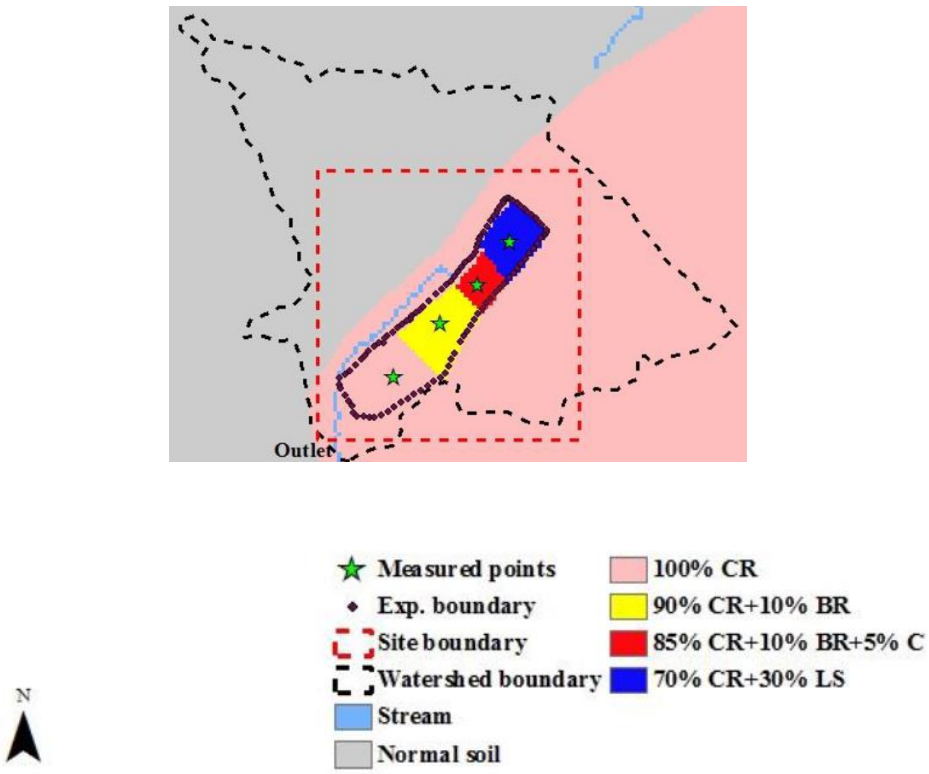

Figure 4.2. HTGCM study watershed in Mather, Pennsylvania *(Source: Xu, [2014])*. The modeled area corresponds to the four experimental plots.

Besides the Mather site, it is intended to implement the HTGCM model to other watersheds with AMD impacts. This involves having to deal with some important limitations: the lack of water quality data within the mine sites (the usual best case scenario is to have these kind of data on a stream discharge, a little bit far from the coal piles) and, the lack of subsurface water quality data (at the best, the data are limited to surface water). In terms of the model geographical scale, the general case to be modeled would be the one shown in *Figure 4.3*, below.

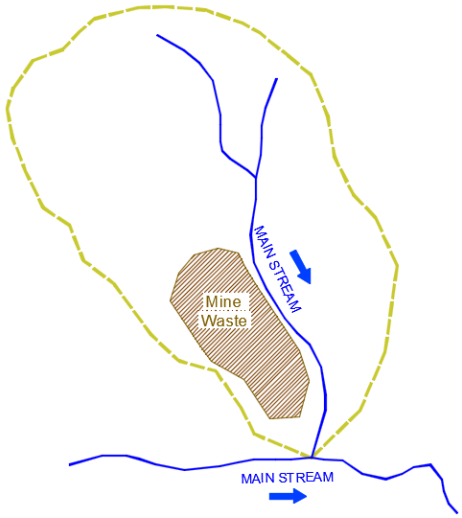

Figure 4.3. General case of a mine-impacted watershed

In this general case, the mine site is located within a certain watershed *[Figure 4.3]*. The discharge of this abandoned mine can impact secondary streams and the mainstream inside the watershed and, furthermore, can impact another mainstream at the watershed's discharge. By adding the model the capability to run from a watershed scale, some of the previously mentioned impacts can be assessed and, moreover, a comparison can be made against the retrieved water quality data, even if it's located outside the coal pile limits. Finally, the influence of the drainage upstream of the mine site can be determined. *Figure 4.4* illustrates the current and the proposed scales of the HTGCM model.

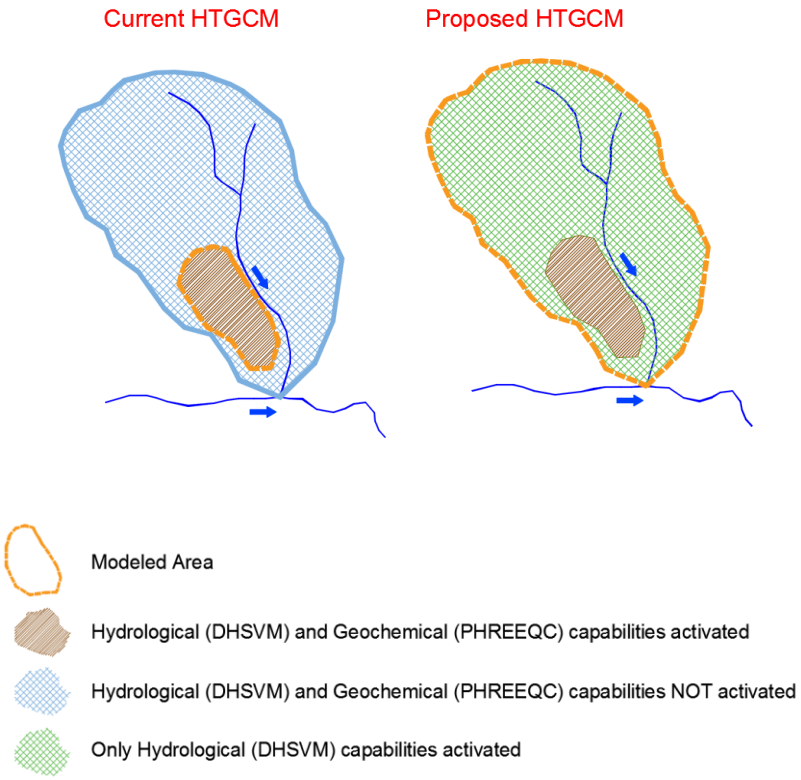

Figure 4.4. Spatial scales comparison between the current and modified HTGCM

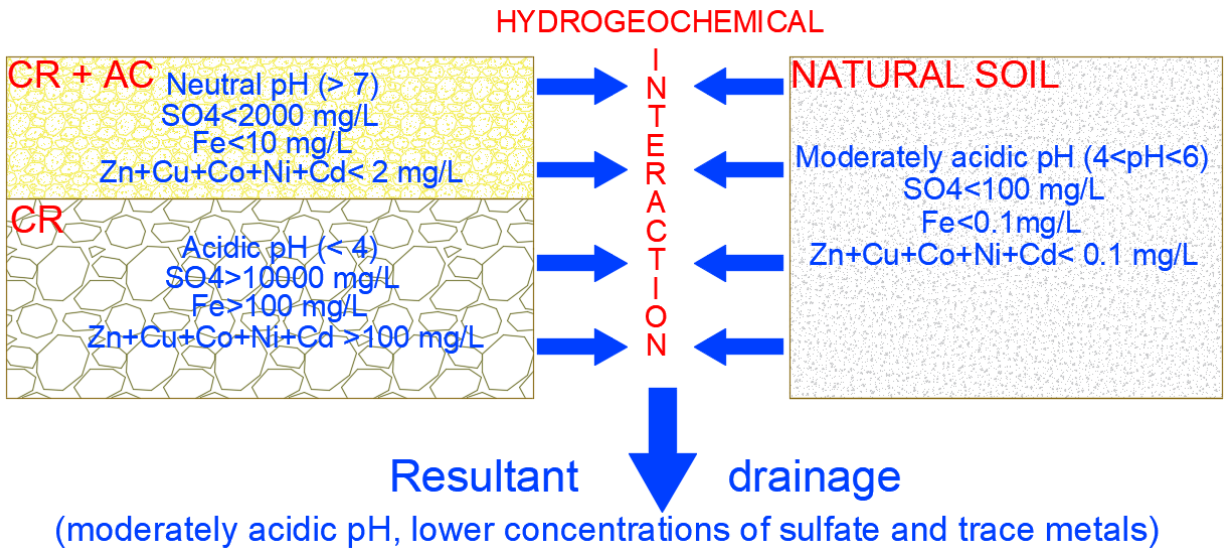

Figure 4.5. Schematic representation of the hydro-geochemical interaction between mine soil (amended and non-amended) and non-mine soil

One additional modification in the model settings can be made in order to enhance the watershed scale simulation advantages, that is, to activate the PHREEQC capabilities (geochemical simulation) in the entire watershed *[Figure 4.5]*. This added feature will result in a more realistic representation of a mine-impacted watershed, where surface and subsurface flow have contributions from the coal pile and from outside the coal pile, especially at the outlet (the importance of this feature will be especially observed in the second case study, the Ernest mine).

4.2.2 Addition of new chemicals and reactions into the model

Besides pH, sulfate and Fe, clearly the most important chemicals to analyze regarding pyrite oxidation and acid mine drainage, HTGCM has the capability to calculate dynamicly other important trace metals such as Ca, Na, Mg, K, Si, P and Al. It is worth mentioning that during the initial stages of the model development, experimental and field data was still very limited (i.e., a more complete characterization was needed), therefore, the model output (i.e., pH, sulfate and trace metals/metalloids) had to be assumed based on technical literature. All these elements are allowed to be transported in the model and are updated each time step. In other words, the model calculates the aqueous concentrations of these metals over time, wherever the PHREEQC is activated within the watershed. Moreover, the main reactions concerning pyrite oxidation that are included in the model are the following:

$$FeS_2 + H_2O + 7/2O_2 \Rightarrow Fe^{2+} + 2SO_4^{2-} + 2H^+ \quad (4\text{-}1)$$

$$Fe^{2+} + 1/4O_2 + H^+ \Rightarrow Fe^{3+} + 1/2H_2O \quad (4\text{-}2)$$

$$FeS_2 + 1/2H_2O + 15/4O_2 \Rightarrow Fe^{3+} + 2SO_4^{2-} + H^+ \quad (4\text{-}3)$$

$$CaCO_3 + 2\,H^+ \Leftrightarrow CO_2 + Ca^{2+} + H_2O \quad (4\text{-}4)$$

$$CaSO_4 \cdot 2H_2O \Leftrightarrow Ca^{2+} + SO_4^{2-} + 2\,H_2O \quad (4\text{-}5)$$

$$KAl_3Si_3O_{10}(OH)_2 + 10\,H^+ \Leftrightarrow K^+ + 3\,Al^{3+} + 3\,H_4SiO_4 \quad (4\text{-}6)$$

$$Al_2Si_2O_5(OH)_4 + 6\,H^+ \Leftrightarrow H_2O + 2\,H_4SiO_4 + 2\,Al^{3+} \quad (4\text{-}7)$$

$$SiO_2 + 2H_2O \Leftrightarrow H_4SiO_4 \quad (4\text{-}8)$$

$$Fe_2O_3 + 6H^+ \Leftrightarrow 2Fe^{3+} + 3H_2O \quad (4\text{-}9)$$

$$Ca_2SiO_4 + 4H^+ \Leftrightarrow 2Ca^{2+} + H_4SiO_4 \quad (4\text{-}10)$$

$$Ca_2Al_2SiO_7 + 10H^+ \Leftrightarrow H_4SiO_4 + 2Al^{3+} + 2Ca^{2+} + 3H_2O \quad (4\text{-}11)$$

Complete hydrochemical data for coal mine discharges are rarely reported *Cravotta et al. [2008-Part 1]*; in this lies the need to have a more detailed water characterization. Freshwater and drinking water standards *[U.S. EPA, 2002]* requires the analysis of trace elements suchs as Cr, Co, Cu, Mn, Ni and Zn. Moreover, these dissolved metals are frequently present in the discharges of many coal piles (e.g. in Pennsylvania) at levels that can be harmful to aquatic and terrestrial ecosystems *[Cravotta et al., 2006]*. Data from the Mather site and from the laboratory experiments have shown the presence of the above-mentioned elements in significant concentrations, thus it is important to extend the capabilities of the HTGCM model to calculate concentrations of these important elements. The final goal would be the acquisition to sufficient chemical data for a better evaluation of the AMD remediation. Furthermore, the addition of these new chemicals as output

will allow to evaluate correlations and geochemical controls on element concentrations *[Cravotta et al., 2008-Part 1]*. It has been found *[Cravotta et al., 2008-Part 2]* that bituminous mine discharges, which are located in western Pennsylvania, have higher concentrations of Mn, Ni and Zn than anthracite discharges (i.e. eastern Pennsylvania) *[Cravotta et al., 2015]*. With the inclusion of the new metals, the HTGCM model will include the calculation of most of the identified priority pollutants in coal mine discharges in Pennsylvania

New reactions can also be added in the chemical database within the HTGCM model: reactions involving the new chemicals that are going to be included (i.e. Zn,. Cu, Pb, Cd, Co and Ni) and other reactions that can complement the ones in the original model. For instance, Ca concentrations in the experimental columns (i.e. amended scenario) could be an indication of acid mine drainage neutralization by the dissolution of Ca carbonates, such as calcite ($CaCO_3$), due to the alkaline additive, thus releasing Ca *[Eq. (4-12)]*.

$$CaCO_3 + H_2SO_4 \rightarrow Ca^{2+} + SO_4^{2-} + CO_{2(g)} + H_2O \quad (4\text{-}12)$$

Usually, Ca dissolution is identified with acidic neutralization and high pH, enabling various metal removal mechanisms *[Sun et al., 2013]*. However, high dissolution rates of Ca minerals could also occur in active mine tailings (e.g. CR).

Another reaction that is worth including, especially based on our PHREEQC modeling under the column scenario, is the dolomite dissolution. Dolomite was calculated as a neo-formed mineral phase in the amended column.

$$CaMg(CO_3)_2 + 2H^+ \rightarrow Ca^{2+} + Mg^{2+} + 2HCO_3^- \quad (4\text{-}13)$$

Moreover, pyrite is commonly associated with other sulphide minerals such as chalcopyrite, which dissolution reaction is also acid generating:

$$CuFeS_2 + 16Fe^{3+} + 8H_2O \rightarrow 17Fe^{2+} + Cu^{2+} + 2SO_4^{2-} + 16H^+ \quad (4\text{-}14)$$

Another important reaction is the precipitation of Mn as a carbonate, especially in alkaline environments (i.e. amended scenario):

$$Mn^{2+} + HCO^{3-} \rightarrow MnCO_3 + H^+ \quad (4\text{-}15)$$

In summary, reactions like the ones shown above *[Eq. (4-11) to Eq.(4-15)]* can be added to the HTGCM chemical database to be taken into account in the calculations. Further research will be done to establish what other relevant reactions are to be included in the model.

4.2.3 Including real chemical proportions into the model

One of the first versions of the HTGCM model included hydro-geochemical coupling, formed by the hydrological model DHSVM, the advection-dispersion module (AD) and the oxygen diffusion - shrinking core module (OD-SC). OD-SC is used to calculate the production (i.e., SO4 and total Fe) of pyrite oxidation. This is the input for the AD, which is coupled with the DHSVM.

The key connections between the AD and DHSVM are soil moisture, θ, and water flow, q. These two variables respond to the forcing data and the hydrological processes and are updated at each time step. After the soil moisture is updated in each layer, these two variables are passed to the AD. The ADE starts to run the solute transport process, which includes pyrite oxidation.

The interaction of chemical concentrations between grids is achieved by the surface and subsurface routing. Assuming the chemical concentrations are immediately mixed with input water, the concentration can be expressed by the mass balance:

$$C_{in,i,j}Q_{in,i,j} = \sum_{k=0}^{7} F_k C_{out,k} Q_{out,k} \tag{4-16}$$

where $C_{in,i,j}$ and $Q_{in,i,j}$ are the chemical concentration and inflow at the grid (i, j) respectively (in kg/m^3), F_k is the weight of the flow in each direction (unitless) [Wigmosta and Lettenmaier, 1999], $C_{out,k}$ is the concentration in the k_{th} direction and $Q_{out,k}$ is the flow in the k_{th} direction.

The final stage of HTGCM comprises the coupling with the PHREEQC model [Parkhurst et al.,1999] in order to perform more complete geochemical calculations. One of the main inputs is the initial solid and liquid compositions within the soil layer. The solid composition is assumed to be initially in equilibrium with the solution. For the purpose of taking into account the total availability of the main chemicals (e.g. Fe, S, K, Al, Mn and so on) involved in AMD, that are forming the mineral composition of the coal piles (i.e. CR) and the remediation materials (i.e. AC), it was introduced in the HTGCM model an input file with the proportion of all these chemicals in the solid phase (kg element / kg of total soil). Currently, these chemical proportions that were utilized for the model testing and calibration are based on the technical literature and not on the real measurements of these elements. Moreover, jarosite was neglected from the mineral analysis, which could underestimate the Fe mineral availability. Although this initial assumption is valid, there can be made an improvement to the model if we can use more realistic chemical proportions in the solid phase, based on our XRD measurements.

The calculations of the "real" chemical proportions in the solid phase for both the mine waste (i.e. coal refuse or CR) and the remediation material (i.e. alkaline clay or AC) can be performed using the XRD analysis obtained from Alcoa. Given the detected percentages of each mineral found in the soil, the amount of moles of each element is is determined from the chemical formula of the mineral. Then, using the molecular weight of each element, their proportions in the mineral phase (kg/kg) are calculated. Finally, these proportions are weighted by the mineral proportion (XRD) in either CR and AC. Once we have these two outputs, we can calculate the proportions for any CR/AC mixing ratio (e.g. 90%CR/10%AC). The detailed calculations are shown below *[Table 4.1 to Table 4.3]*.

Table 4.1. Calculation of chemical proportions in CR

		# moles of each element												
mineral	**proportion**	H	O	S	K	Mn	Mg	Fe	Ca	Ti	Al	Si	Na	Cl	C
Quartz	0.5562		2									1			
K-mica	0.24	2	12		1						3	3			
Jarosite	0.099	6	14	2	1			3							
Kaolinite	0.0826	4	7								2	2			
Calcite	0.01		3						1						1
Gypsum	0.0092	4	6	1					1						
Pyrite	0.003			2				1							

proportion of each element in the mineral compound (kg/kg)

H	O	S	K	Mn	Mg	Fe	Ca	Ti	Al	Si	Na	Cl	C
	0.53									0.47			
0.005	0.48		0.1						0.2	0.21			
0.012	0.45	0.13	0.08			0.33							
0.018	0.5								0.24	0.25			
	0.48						0.4						0.12
0.023	0.56	0.19					0.23						
		0.53				0.47							

Table 4.1 (continued)

proportion of each element in the CR composition (kg/kg)

H	O	S	K	Mn	Mg	Fe	Ca	Ti	Al	Si	Na	Cl	C
	0.296									0.26			
0.001	0.116		0.024						0.049	0.051			
0.001	0.044	0.013	0.008			0.033							
0.001	0.041								0.02	0.021			
	0.005						0.004						0.001
2E-04	0.005	0.002					0.002						
		0.002				0.001							

TOTAL proportion of each element in the CR composition (kg/kg)

0.0041	**0.5070**	**0.0160**	**0.0313**	**0.0000**	**0.0000**	**0.0345**	**0.0061**	**0.0000**	**0.0685**	**0.3313**	**0.0000**	**0.0000**	**0.0012**
H	O	S	K	Mn	Mg	Fe	Ca	Ti	Al	Si	Na	Cl	C

Table 4.2. Calculation of chemical proportions in AC

		# moles of each element												
mineral	**proportion**	H	O	S	K	Mn	Mg	Fe	Ca	Ti	Al	Si	Na	Cl	C
Quartz	0.03		2									1			
Dicalcium silicate	0.57		4	1					2						
Sodalite	0.12		24								6	6	8	12	
Gehlenite	0.1		7						2		2	1			
Hematite	0.08		3					2							
Calcium aluminium sulfate	0.02	12	24	3					6		2				
Titanium dioxide	0.02		2							1					
Gibbsite	0.01	3	3								1				
Calcite	0.03		3						1						1
calcium titanium oxide	0.02		3						1	1					

proportion of each element in the mineral compound (kg/kg)

H	O	S	K	Mn	Mg	Fe	Ca	Ti	Al	Si	Na	Cl	C
	0.53									0.47			
	0.36	0.18					0.45						
	0.29								0.12	0.13	0.14	0.32	
	0.41						0.29		0.2	0.1			
	0.3					0.7							
0.015	0.49	0.12					0.31		0.07				
	0.4							0.6					
0.039	0.62								0.35				
	0.48						0.4						0.12
	0.35						0.29	0.35					

Table 4.2 (continued)

proportion of each element in the AC composition (kg/kg)													
H	O	S	K	Mn	Mg	Fe	Ca	Ti	Al	Si	Na	Cl	C
	0.016									0.014			
	0.253	0					0.317			0.222			
	0.035								0.015	0.015	0.017	0.039	
	0.041						0.029		0.02	0.01			
	0.024					0.056							
3E-04	0.01	0.002					0.006		0.001				
	0.008							0.012					
4E-04	0.006								0.003				
	0.014						0.012						0.004
	0.007						0.006	0.007					
TOTAL proportion of each element in the AR composition (kg/kg)													
0.0007	**0.4141**	**0.0024**	**0.0000**	**0.0000**	**0.0000**	**0.0560**	**0.3702**	**0.0190**	**0.0392**	**0.2616**	**0.0167**	**0.0386**	**0.0036**
H	O	S	K	Mn	Mg	Fe	Ca	Ti	Al	Si	Na	Cl	C

Table 4.3. Calculation of chemical proportions in CR – AC mixtures

90 %	CR	**0.0038**	**0.4931**	**0.0250**	**0.0282**	**0.0000**	**0.0000**	**0.0367**	**0.0368**	**0.0019**	**0.0656**	**0.3021**	**0.0017**	**0.0039**	**0.0014**
10 %	AC	H	O	S	K	Mn	Mg	Fe	Ca	Ti	Al	Si	Na	Cl	C
99 %	CR	**0.0041**	**0.5056**	**0.0169**	**0.0310**	**0.0000**	**0.0000**	**0.0347**	**0.0092**	**0.0002**	**0.0682**	**0.3284**	**0.0002**	**0.0004**	**0.0012**
1 %	AC	H	O	S	K	Mn	Mg	Fe	Ca	Ti	Al	Si	Na	Cl	C

There are some elements such as Cu or Mn that were not detected in the XRD analysis but they where detected as dissolved metals/metalloids in the leaching-column experiments. To take into account these mineral phases, it will be assumed a minimum chemical proportion based on the technical literature.

4.2.4 Variable oxygen diffusion to simulate pyrite coating of iron precipitates

The HTGCM model includes a pyrite oxidation – shrinking core module that is based on *Davis and Ritchie [1986]* and applies the PYROX model algorithm of *Wunderly et al. [1996]*. The main assumption of this model is that spherical sulphide mineral (e.g. pyrite) particles with radius *R* are surrounded by a thin inmobile water film. Oxygen within the pore space diffuses through the water

film and through the porous oxidized coating towards the unreacted core of the particle (i.e. radius = r_c) *[Figure 4.6]*. All oxidation reactions are assumed to occur in the aqueous phase in contact with or near a reacting solid.

The diffusion of oxygen into the particles is driven by the oxygen concentration gradient between the surface and the core of the particles *[Wunderly et al., 1996]*. In this model, pyrite oxidation is assumed to occur only within the unsaturated zone, as oxygen diffusion is considered to be negligible under saturated soil conditions *[Gerke et al., 1998]*.

The two main reactions included in the model are the following:

$$FeS_2 + H_2O + 7/2\ O_2 \Rightarrow Fe^{2+} + 2SO_4^{2-} + 2H^+ \qquad (4\text{-}17)$$

$$Fe^{2+} + ¼\ O_2 + H^+ \Rightarrow Fe^{3+} + 1/2H_2O \qquad (4\text{-}18)$$

These reactions can be combined into a single one:

$$FeS_2 + 1/2H_2O + 15/4\ O_2 \Rightarrow Fe^{3+} + 2SO_4^{2-} + H^+ \qquad (4\text{-}19)$$

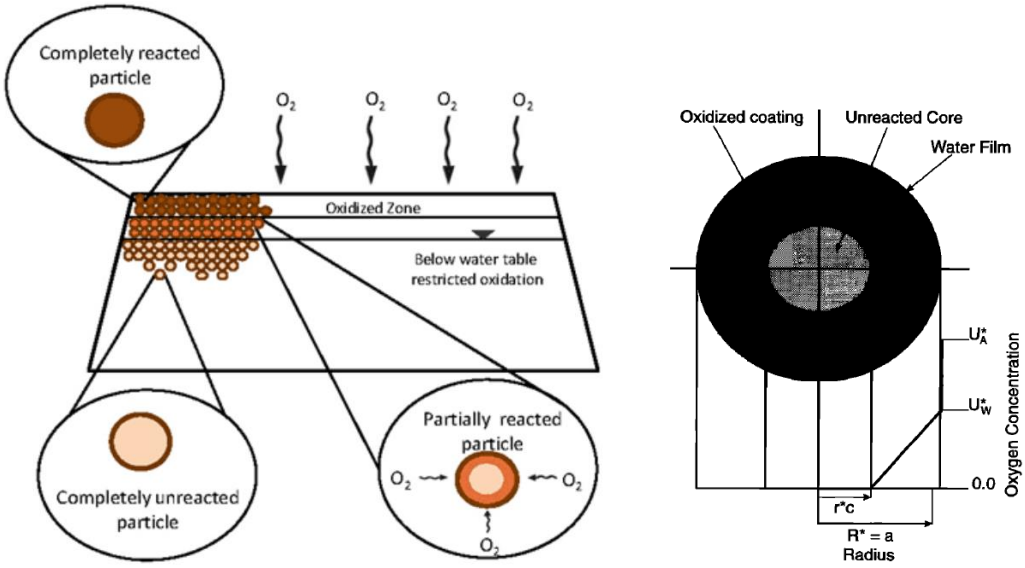

Figure 4.6. Schematic of oxidation-shrinking-core conceptual model *(Source: Wunderly et al., [1996] and INAP-The International Network for Acid Prevention)*

In the model, it is assumed that the sulphide mineral particles are spherically shaped and homogeneously distributed throughout the coal pile. The shrinking of the unreacted particle is represented by:

$$\frac{dr_c}{dt} = -\frac{D_w(1-\theta_s)}{\varepsilon\rho_s}\frac{R}{r_c(R-r_c)}\frac{[O_2]_a}{H} \qquad (4\text{-}20)$$

where D_w is the effective oxygen diffusion coefficient containing the diffusion properties of the water and the oxidized mineral particle [$L^2 \cdot T^{-1}$] and is equal to 3.2×10^{-11} m^2/s *[Gerke et al., 1998]*, ρ_s is the sulfur bulk density [$M \cdot L^{-3}$] which is equal to $f \times \rho_b$ where ρ_b is soil bulk density [$M \cdot L^{-3}$] and f is the proportion of sulfur in the soil [M·M-1], ε is the mass ratio of the consumption of oxygen to the consumption of sulfur based on the reaction stoichiometry and it is determined by:

$$\varepsilon = \frac{Mass\ of\ oxygen}{Mass\ of\ sulfur} = \frac{\frac{7}{2}\cdot W_{O_2}\cdot ratio + \frac{15}{4}\cdot W_{O_2}\cdot(1-ratio)}{2\cdot ratio\cdot W_s + (1-ratio)\cdot 2\cdot W_s} = \frac{\frac{15}{4}\cdot W_{O_2} - \frac{1}{4}\cdot W_{O_2}\cdot ratio}{2\cdot W_s} \tag{4-21}$$

Where W_{O2} and W_s are the molar mass for oxygen and sulfur respectively and ratio denotes the concentration of Fe^{2+} to total Fe:

$$ratio = \frac{[Fe^{2+}]}{[Fe(total)]} = \frac{1}{\left[K_{eq}\times\left(\frac{[O_2]_a}{H}\right)^{0.25}\times 10^{-pH}+1\right]} \tag{4-22}$$

where $K_{eq} = 10^{7.7549}$ at 25°C [*Wunderly et al.*, 1996].

In addition, in the oxygen diffusion sub-module, the advection-dispersion of oxygen in the pore space is described by:

$$\frac{\partial\theta_a\cdot[O_2]_a}{\partial t} = \frac{\partial}{\partial z}\left(\theta_a D_a\frac{\partial[O_2]_a}{\partial z}\right) - D_w\frac{3(1-\theta_s)}{R^2}\left(\frac{r_c}{R-r_c}\right)\frac{[O_2]_a}{H} \tag{4-23}$$

where $\theta_a(z)$ is the air content [$L^3\cdot L^{-3}$], $D_a(z)$ a is the oxygen diffusion coefficient [$L^2\cdot T^{-1}$] in the pore space, $[O_2]_a$ is the concentration of oxygen in the pore space [$M\cdot L^{-3}$], z is soil depth [L], and t is time [T]. $D_a(z)$ is calculated by the method of *Elberling et al. [1993]*:

$$D_a(z) = \alpha\cdot D_a^{O_2}\cdot(1-\phi)^{\beta} + \frac{\phi\cdot D_w^{O_2}}{H} \tag{4-24}$$

where α is equal to 0.273 and β is equal to 3.28, D_a^{O2} is the oxygen diffusion coefficient in air [$L^2 \cdot T^{-1}$], D_w^{O2} is the oxygen diffusion coefficient in water [$L^2 \cdot T^{-1}$], Φ is the relative water saturation which is equal to $\theta \cdot (\theta_s - 0.01)^{-1}$ where θ_s is porosity [$L^3 \cdot L^{-3}$] and the residual water content is 0.01, H is equal to 2.63 (Henry's constant), D_a^{O2} and D_w^{O2} are equal to 1.8 × 10-5 m^2/s and 2.1 ×10-9 m^2/s, respectively, based on the data provided by *Gerke et al. [1998]*.

Eq. (4-20) and *Eq. (4-23)* (i.e. shrinking core and oxygen diffusion modules, respectively) allow to solve the unreacted particle radius (r_c) and the oxygen concentration ($[O_2]_a$) for each soil layer. Consequently, this will allow the estimation of total sulfate and total Fe produced by pyrite oxidation at each time step. Using a finite difference method, *Eq. (4-20)* and *Eq. (4-23)* can be expressed as follows:

$$r_c\big|_m^{n,j} = r_c\big|_m^{n,j-1} - \frac{\left(r_c\big|_m^{n,j-1}\right)^2\left(\frac{R\big|_m}{2} - \frac{r_c\big|_m^{n,j-1}}{3}\right) - \left(r_c\big|_m^{n-1}\right)^2\left(\frac{R\big|_m}{2} - \frac{r_c\big|_m^{n-1}}{3}\right) + \frac{D_w\left(1-\theta_s\big|_m\right)R\big|_m}{\varepsilon\big|_m^n \rho_s\big|_m H}\frac{[O_2]_a\big|_m^{n-1} + [O_2]_a\big|_m^{n,k}}{2}\Delta t}{r_c\big|_m^{n,j-1}\left(R\big|_m - r_c\big|_m^{n,j-1}\right)} \tag{4-25}$$

$$\frac{(\theta_a \cdot [O_2]_a)\big|_m^n - (\theta_a \cdot [O_2]_a)\big|_m^{n-1}}{\Delta t} = (\theta_a D_a)\big|_m^n\left(\frac{[O_2]_a\big|_{m+1}^n - 2[O_2]_a\big|_m^n + [O_2]_a\big|_{m-1}^n}{\Delta z^2}\right) + \frac{(\theta_a \cdot D_a)\big|_m^n - (\theta_a \cdot D_a)\big|_{m-1}^n}{\Delta z} \cdot \frac{[O_2]_a\big|_m^n - [O_2]_a\big|_{m-1}^n}{\Delta z} - \left[D_w \frac{3(1-\theta_s)}{R^2}\left(\frac{r_c}{R-r_c}\right)\right]\Bigg|_m^n \frac{[O_2]_a\big|_m^n}{H} \tag{4-26}$$

where the superscripts n and m are the current time step and the number of the soil layer. j denotes the j_{th} iterative step of the shrinking-core equation and k denotes the iteration step of *Eq. (4-26)*. The upper boundary of oxygen concentration in the air is set to be a constant with 0.31 kg/m^3 which is obtained based on a standard air condition. In the soil, an initial oxygen

concentration profile, which decreases with depth, is assumed. The pH value is assumed to be a constant over time. At the first time step, an initial value of rc should be estimated using *Eq. (4-27)*.

$$r_c\big|_m^n = 2r_c\big|_m^{n-1} - r_c\big|_m^{n-2} \tag{4-27}$$

In order to solve $[O_2]_a$ and r_c at the m_{th} layer at the n_{th} time step, one should peform the following iterative process: 1) Calculate intial r_c with *Eq. (4-27)* and solve for $[O_2]_a$ in *Eq. (4-26)*; 2) Calculate new r_c using *Eq. (4-25)*, with $[O_2]_a$ from the previous step (i.e., *Eq. (4-26)*) and with ε from *Eq. (4-21)*; 3) Calculate the ratio of [Fe^{2+}] to Fe(total) using *Eq. (4-22)* with a constant pH and the solved $[O_2]_a$, then update ε with *Eq. (4-21)*; 4) Use the r_c from step 2) to calculate $[O_2]_a$ in *Eq. (4-26)*; 5) Repeat steps 2), 3) and 4) until r_c and $[O_2]_a$ are converged. Finally, the production of aqueous sulfur per time step can be calculated using:

$$\Delta C^{oxid}_{S,liquid} = \frac{\rho_s\big|_m((r_c\big|_m^n)^3 - (r_c\big|_m^{n-1})^3)}{R\big|_m^3\theta\big|_m} \tag{4-28}$$

Where $\Delta C^{oxid}_{S,liquid}$ is the amount of sulfur produced by the pyrite oxidation from the solid phase into the liquid phase at one time step [$M\cdot L^{-3}$] and θ is the soil moisture at the m_{th} layer [$L\cdot L^{-1}$]. In addition, the concentrations of Fe(total) in the liquid can be derived by the following:

$$\Delta C^{oxid}_{Fe,liquid} = \frac{W_{Fe}\cdot\Delta C^{oxid}_{S,liquid}}{2.0\times W_s} \tag{4-29}$$

where W_{Fe} is the molar mass for iron. *Eqs. (4-28)* and *(4-29)* do not consider solid precipitates, however, the products from pyrite oxidation may precipitate.

When sulfide minerals within a coal pile, such as pyrite, oxidize and produce acidity in a faster way than it is neutralized by the surrounded alkalinity (e.g., minerals such as calcite), AMD is generated. However, at neutral or near-neutral pH conditons caused by the presence of sufficient alkalinity in the system, Fe minerals might precipitate and Fe oxyhydroxide coatings might form in the pyrite grain's surface. As these coatings grow thicker and denser they block oxidant transport from the solution to the pyrite surface and reduce the rate of pyrite oxidation *[Huminicki et al. 2009]*.

Huminicki et al. [2009] developed conceptual and quantitative model of declining pyrite oxidation rate caused by the formation of a Fe oxyhydroxide coating under high alkalinity conditions. Experiments were conducted to measure reaction rates for the underlying minerals, as coatings grew thicker. These experimental data were fit to a diffusion model to estimate diffusion coefficients of reactants through pore spaces in coatings. This model was extrapolated to longer times to predict the behavior of the coated grains under field conditions.

The conducted experiments measured oxidation rates that were considered to represent two stages of iron oxyhydroxide coating formation: (1) the initial coating development and (2) the densification and inward propagation of the coating *[Figure 4.7]*.

The obtained data supports the idea that during the first stage of coating formation of a thin, highly porous and permeable layer of colloidal iron oxyhydroxide particles attach to the pyrite surface. The data also supports the idea that during the second stage of coating formation there is a transition from reaction-limited to diffusion-limited rates as coatings grow inward and become

thicker and denser. Their experimental results indicated that when Fe oxyhydroxide coatings grow on pyrite the rate of pyrite oxidation declines as a function of $t^{-1/2}$.

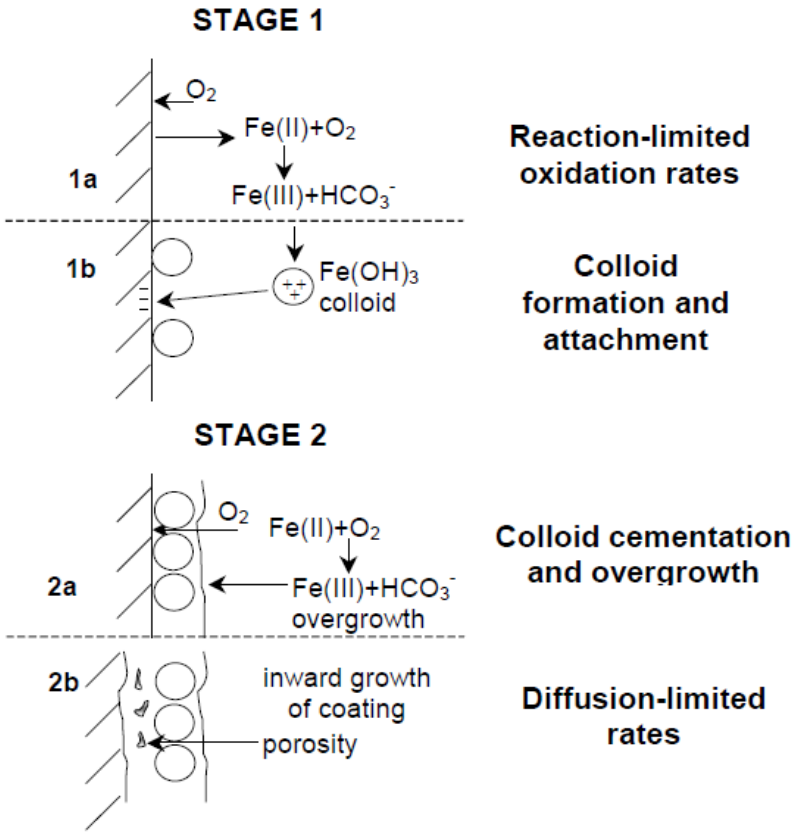

Schematic diagram showing the steps leading to the replacement of pyrite by goethite. Stage 1a and b show the initial formation of a porous and permeable iron oxyhydroxide coating by the formation and attachment of colloidal iron oxyhydroxide. Stage 2 shows the densification and thickening of the coating leading to the transition from reaction-limited to diffusion-limited rates.

Figure 4.7. Pyrite coating by Fe precipitates. *(Source: Huminicki et al., [2009])*

Based on Fick's first law, this model predicts the rate of H^+ production over time:

$$r_{H^+} = 2\left(\sqrt{\frac{2000 m_{(sol)} D_i A(1-\phi)}{\nu_i f_{ppt} V_m}}\right) t^{-1/2} \quad (4\text{-}30)$$

A	surface area, m^2
D_i	diffusion coefficient, m^2/s
m_i	concentration of species i, molal
r_i	specific rate of reaction of species i, $mol/(m^2s)$
V_m	molar volume, m^3/mol
t	time, s
ϕ	porosity, unitless ratio from 0 to 1
f_{ppt}	fraction of reactant that precipitates as pyrite coating
v_i	stoichiometric coefficient

In general, this model predicts how coatings form, and how long it takes for coatings to become thick enough to effectively reduce alkalinity demand required to neutralize acid produced by pyrite oxidation. They determined the diffusion coefficient of oxygen through the pore spaces in the iron oxyhydroxide coating and used that value to calculate the rate of acid production by coated pyrite as a function of time.

The coating thicknesses were calculated from the fraction of Fe reprecipitated on the pyrite surface, the molar volume of the coating, the surface area of pyrite, and the porosity of the coating:

$$x = \frac{n_{Fe} f_{ppt} V_m}{A(1-\phi)} \tag{4-31}$$

Where n_{Fe} is the total amount of Fe produced and f_{ppt} was observed to be approximately 3% of the total Fe. Finally, Φ, the coating's porosity, was estimated to be around 0.1. Similarly as in *Eq. (4-30)*, it was derived an equation to estimate the total Fe production, n_{Fe}:

$$n_{Fe} = \left(\sqrt{\frac{2000 m_{(sol)} D_i A(1-\phi)}{\nu_i f_{ppt} V_m}} \right) t^{1/2}, \tag{4-32}$$

The time derivative of *Eq. (4-32)* yields the rate of pyrite oxidation as a function of time:

$$r_{FeS_2} = \frac{1}{2} \left(\sqrt{\frac{2000 m_{(sol)} D_i A(1-\phi)}{\nu_i f_{ppt} V_m}} \right) t^{-1/2} \tag{4-33}$$

Therefore, it is expected that because of the growth of the iron oxyhydroxide coatings, the rate of pyrite oxidation will decline as a function of $t^{-1/2}$. Making the slope of the linear regression *r vs* $t^{-1/2}$ is ½ *c* so that we can solve for the diffusion coefficient from the relationship:

$$D_i = \frac{1}{2000} \frac{\nu_i f_{ppt} V_m}{m_{(sol)} A(1-\phi)} c^2 \tag{4-34}$$

Where *c* was found to be 9.3 x 10^{-10}. Therefore, using values from the slopes of *r vs* $t^{-1/2}$ and substituting in the appropriate values for the constants into equation *Eq. (4-34)* yields diffusion coefficients for DO through Fe coating.

In the oxygen diffusion – shrinking core model, D_w represents the effective oxygen diffusion coefficient containing the diffusion properties of the water and the oxidized mineral

particle [$L^2 \cdot T^{-1}$]. In HTGCM, this coefficient is set to be constant and is equal to 3.2×10^{-11} m^2/s *[Gerke et al., 1998]*. Therefore, to take into account the pyrite coating by Fe precipitates, it is proposed to introduce a variable diffusion coefficient using the model developed by *Huminicki et al. [2009]*. The coefficient every time step will be derived from *Eq. (4-32)*. Finally, in the HTGCM model, the term D_w will be assumed to be D_i from the pyrite coating model.

Solving *Eq. (4-32)* for we D_i have

$$D_i = \left[\frac{n_{Fe}{}^2 v_i f_{ppt} V_m}{2000\, m_{(sol)} A\, (1-\emptyset)}\right] t^{-1} \tag{4-35}$$

Considering that n_{Fe} is the total amount of Fe produced by pyrite oxidation, per time step and m(sol) in the reactant concentration in the solution carriet out of the system, we can simplify *Eq. (4-35)* given that Fe is the reactant. According to the experimental data from *[Huminicki et al., 2009]*, Fe concentration in the solution was found to be around 40% of the total amount of Fe produced, the final equation for calculation oxygen diffusion is the following:

$$D_i = \left[\frac{Fe_{(sol)}\, v_i\, f_{ppt} V_m}{320\, A\, (1-\emptyset)}\right] t^{-1} \tag{4-36}$$

Where

D_i = oxygen diffusion coefficient (D_w in HTGCM), m^2/s

$Fe_{(sol)}$ = Fe concentration in the solution (calculated in HTGCM each time step), mol/kg

v_i = stoichiometric coefficient. For oxygen diffusion, v_i = 3.5

f_{ppt} = fraction (from 0 to 1) of reactant that precipitates as pyrite coating. In *Huminicki et al. [2009]* measured to be around 0.03. However, it can be adjusted.

V_m = molar volume of the pyrite coating (e.g. geothite), in m^3/mol

A = surface area of pyrite, in m^2. It can be calculated each time step, according to the unreacted particle with radius r_c.

Φ = porosity of the coating, from 0 to 1. In *Huminicki et al. [2009]* assumed to be 0.1. However, it can be adjusted.

t = time, s

320 = conversion factor

The coupling strategy of the variable diffusion coefficient with the oxygen diffusion – shrinking core model will begin assuming an initial diffusion coefficient $D_{w(t)}$ and applying the above mentioned algorithm (i.e. steps 1 to 5). At the end of the first time step it will be obtained the aqueous Fe concentration and the new unreacted core radius r_c, which can be used to calculate the particle's surface area. Finally, *Eq. (4-36)* will give us the new oxygen diffusion coefficient $D_{w(t+1)}$ that will be used for the next time step and so forth.

A basic example was performed to show the difference between the sulfate concentrations from the original oxygen diffusion – shrinking core module included in HTGCM and the sulfate concentrations considering a variable oxygen diffusion coefficient as in *Huminicki et al. [2009]*. This exercise was considered for only one pyrite particle with an inicial radius (R_c) of 2 mm (same as in HTGCM). The other assumptions were the following:

- The soil is homogeneus. In other words, the soil layers above and below the particle share the same properties, which leads to the neglection of some terms in *Eq. (4-26)*.
- The coating of the pyrite grain is formed by geothite, an Fe oxyhydroxide with a molar volume V_m = 2.2 x 10^{-5} m^3/mol.
- The porosity of the coating Φ and the fraction of reactant that precipitates as pyrite coating f_{ppt} are the same as in *Huminicki et al. [2009]*: 0.1 and 0.03, respectively.
- The surface area of pyrite is updated each time step, assuming an spherical particle with radious $r_{c(t)}$. Thus, the surface ares is equal to $4\pi r_{c(t)}^2$.
- The initial diffusion coefficient $D_{w(t)}$ is assumed to be 1.27 x 10^{-11} m^2/s and is updated each time step.

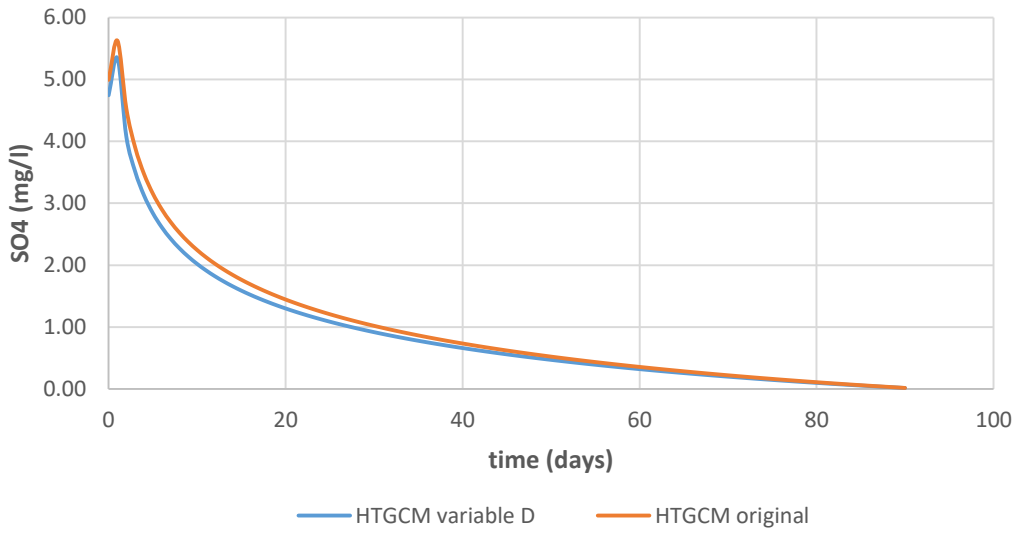

Figure 4.8. Sulfate concentrations produced by pyrite oxidation in one spherical pyrite particle with an initial radius Rc=2 mm

Figure 4.8 shows the difference in sulfate concentrations in one particle, considering the original oxygen diffusion – shrinking core model and the one with the variable oxygen diffusion coefficient, in order to take into account the pyrite coating, and, *Figure 4.9* shows the variation of

the oxygen diffusion coefficient D_w. The first figure shows the usual behavior of the sulfate concentrations in this model: as the pyrite particle shrinks down, less surface area is available for reaction, thus the production of sulfate and iron has a decreasing trend and, at some point, it is asymptothic to 0. The results show that including a variable (i.e. decreasing) oxygen diffusion coefficient due to the iron coating makes the concentrations to be smaller. This allows to simulate at the same time the effect of acid generation and acid neutralization processes.

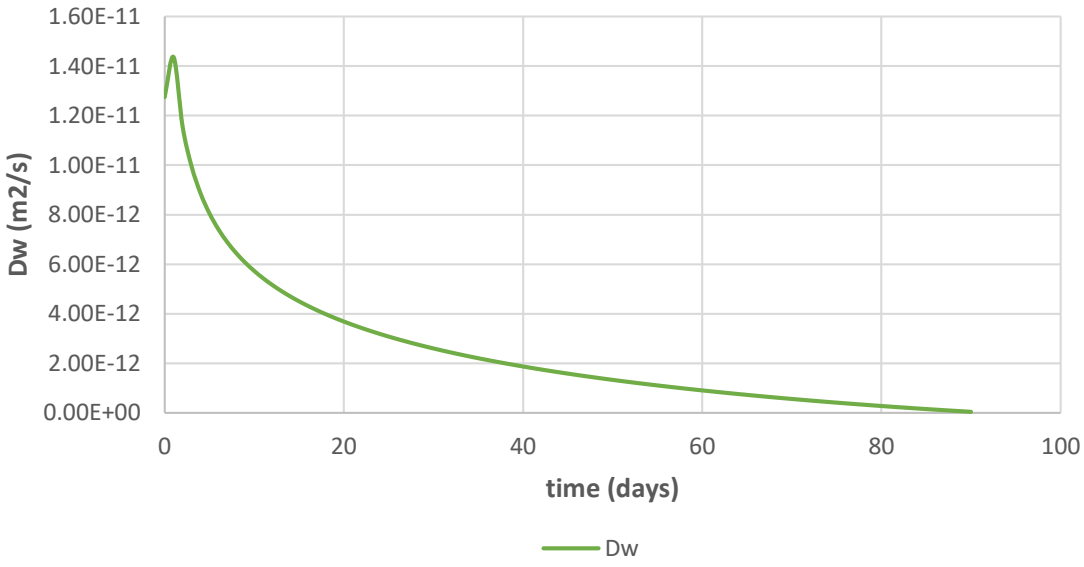

Figure 4.9. Variation of the oxygen coefficient Dw

It is worth mentioning that this exercise was performed considering only one single particle. In the watershed scale, the effect of all the particles are summed up, thus resulting in the total sulfate and iron concentrations at a certain location and at a certain depth. In summary, the outcome of this example indicates the feasibility of including this oxygen diffusion variability in the HTGCM model. However, to thoroughly investigate the significance of the model improvement, a watershed simulation is recommended.

4.2.5 Hydrogeological parameters for HTGCM calibration and validation

The understanding of the hydrogeological properties of the waste mine piles is essential for an adequate characterization and prediction of mine drainage quality. For instance, groundwater is considered to be an important chemical component in ARD formation because, among other things, it serves as the contaminant transport medium *[Pennsylvania DEP, 1998]*.

Since the HTGCM model utilizes the DHSVM model hydrological framework, some parameters such as soil porosity, hydraulic conductivity and bulk density are part of the model's input. During the HTGCM development, some laboratory tests were conducted to determine the magnitude of the above mentioned parameters. These measurements were used to test and calibrate the model, but they were never crosschecked with the technical literature and/or previous studies. Therefore, the objective of this section is to establish if the adopted values (i.e., from laboratory measurements) for the hydrogeological input parameters of the HTGCM model were reasonable.

Table 4.4. Adopted hydrogeological parameters for HTGCM (original model) calibration

Paramenter	Value
Porosity	0.45 - 0.52
Ks (m/s)	$6x10^{-5}$ - $8.5x10^{-4}$
Bulk density (kg/m^3)	1360

Table 4.4 shows the measured soil parameters used for HTGCM calibration. In waste coal piles, hydraulic conductivity (*Ks*) is considerably larger than that of the surrounding soil *[Xu, 2014]*. *Aljoe and Hawkins, [1994]* indicated that the range of *–log Ks* in mine spoils is approximately 3 – 7, while for the HTGCM the measured range was 3.1 – 4.3. *Pennsylvania DEP, [1998]*, based on measurements in 103 monitoring sites from 15 surface mines in northern West

Virginia and Western Pennsylvania, determined that *Ks* (m/s) ranged from 4.2 x 10^{-9} to 7.6 x 10^{-2}. Regarding porosity, this parameter is very important to mine drainage quality characterization and prediction in terms of determining groundwater storage volumes and predicting water level changes stemming from recharge to discharge *[Pennsylvania DEP, 1998]*. Laboratory – measured porosity on Eastern Ohio waste mine samples ranged from 0.41 to 0.48 with a mean of 0.44 *[Mezga, 1973]*. Measured values in Mather *[Xu, 2014]* ranged from 0.45 to 0.52. Finally, soil bulk density is the most common way to evaluate soil compactation. *Delong et al., [2012]* determined, based on four methods and five surface mine soils in West Virginia, that the bulk density ranged from 1350 to 1760 kg/m^3. Moreover, *Sheoran et al., [2010]* shows that the characteristic bulk density in mine surface soils ranges from 1100 to 1500 kg/m^3. In summary, previous investigations around the study area (i.e., Western Pennsylvania) have confirmed that the hydrogeologic parameters measured in Mather and utilized for the HTGCM model calibration and validation were adequately adopted. Moreover, it is worth mentioning that *[Xu, 2014]* made a sensitivity analysis for the calibration on these parameters in the HTGCM model.

4.3 CASE STUDY 1: IMPLEMENTATION OF THE MODIFIED HTGCM MODEL IN THE MATHER COAL PILE WATERSHED

4.3.1 Model Scale

As previoulsy mentioned, the Mather coal pile, located in Greene County, Pennsylvania, USA, was the study site based on which the original HTGCM model was tested and calibrated, but only considering the experimetal plots described in *Section 1.4.1.1*, with approximately 0.038 km^2.

Since one of the objectives of this study is to validate the HTGCM model beyond the plot scale (i.e., watershed scale), a sensitivity analysis was performed to test the model capabilities to predict the impact of the ARD generation and remediation in the watershed (e.g., at the outlet) where the coal pile is located.

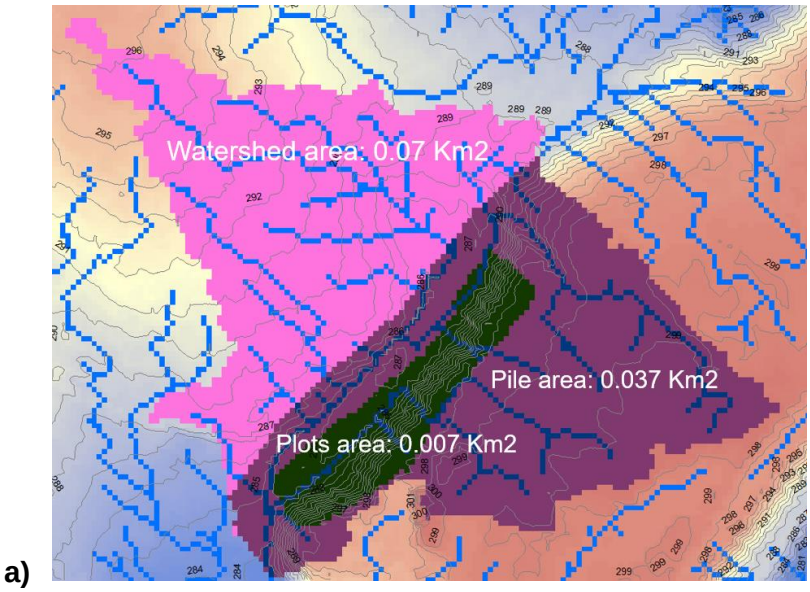

a)

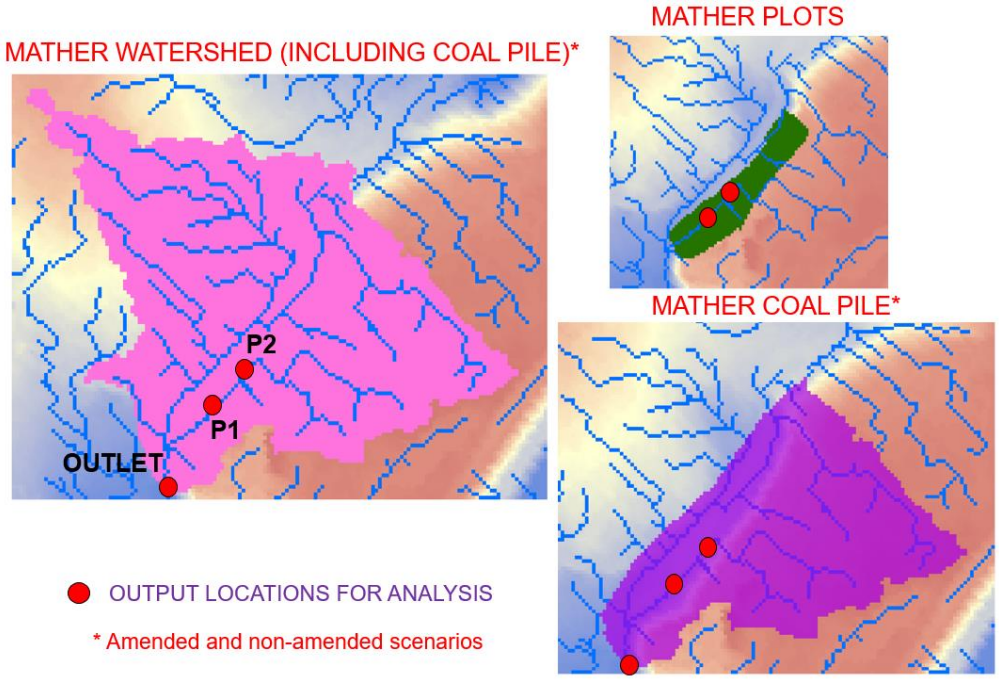

b)

Figure 4.10. a) Mather watershed, coal pile and experimental plots. b) HTGCM model spatial scenarios and output locations

Three main spatial scenarios have been created : 1) the entire watershed (0.07 km^2), 2) total coal pile area (0.037 km^2) and 3) experimental plots (0.007 km^2). At the same time, the model output will be analyzed from three different locations: 1) plot 1 (100% CR or the non-amended plot), 2) plot 2 (90% CR + 10%AC up to 61 cm depth or the amended plot) and 3) the watershed outlet (only possible for the first spatial scenario). The spatial scenarios and the output locations are shown in *Fig 4.10*. In addition, *Table 4.5* shows the initial solutions that are included in the PHREEQC module input, for the amended and non amended scenarios, and for regular soil (outside the coal pile), based on the technical literature *[Agnieszka et al., 2012, Billett and Cresser, 1992, Klaminder et al., 2011, Lidman et al., 2017, Meers et al., 2006, Tack et al., 2002, Vandecasteele et al., 2002]*.

Table 4.5. Mather simulations initial solutions

	Amended Scenario	Non-amended Scenario	Outside Coal Pile
Description	Concentration (mg/l)	Concentration (mg/l)	Concentration (mg/l)
SO_4	1880	5880	4.9
Fe	5	1200	1.4
Ca	570	430	0.9
Na	280	200	2.2
Mg	100	65	100
K	7.2	8	0.3
Si	60	178	8.4
P	0.5	15	0.5
Al	1.6	280	1.7
Cl	155	100	0.001
Mn	0.7	9	0.007
Zn	0.8	100	0.009
Cr	0.004	0.6	0.002
Ni	0.04	6	0.003
Co	0.001	2	0.001
Cu	0.04	100	0.002
pH	6	2.5	5.5

Figure 4.11 shows the modeling results (1-year simulation) for the below-described scenarios, in terms of spatial scale (watershed, piles and experimental plots) and output locations (plot 1, plot 2 and the watershed outlet). The main objective of this set of simulations is a sensitivity analysis to determine if the model properly captures the incidence of the spatial scale and the output location (inside or outside the mine site).

It is observed that, in all cases, the drainage at the outlet has lower sulfate and metals concentrations than in plots 1 and 2, which indicates the model's capability to capture real field conditions, by taken into account the surface and subsurface drainage from outside the coal pile (approximate 0.03 km^2) and, consequently, producing a dilution effect with the regular soil's pore water composition (see *Table 4.5*). The change in pH is less noticeable due to similar conditions both inside (the amended scenario) and outside the coal pile. Even though there is not observed data to compare with, the outlet modeling results fall within the expected magnitudes, due to the drainage from outside the Mather site.

Moreover, the model is sensible to small scale changes. For example, in the plots simulations, it is observed that there is a difference between modeling the plot spatial scale and modeling the watershed scale (including the plots). As can be seen in *Fig 4.10*, there is a small drainage area upstream of both plots that contributes to the surface and subsurface drainage downstream (i.e., the plots). However, from the environmental assessment perspective, both modeling approaches are equally valid, compared to the observations. This justifies the original HTGCM development, testing and calibration only considering a plot scale.

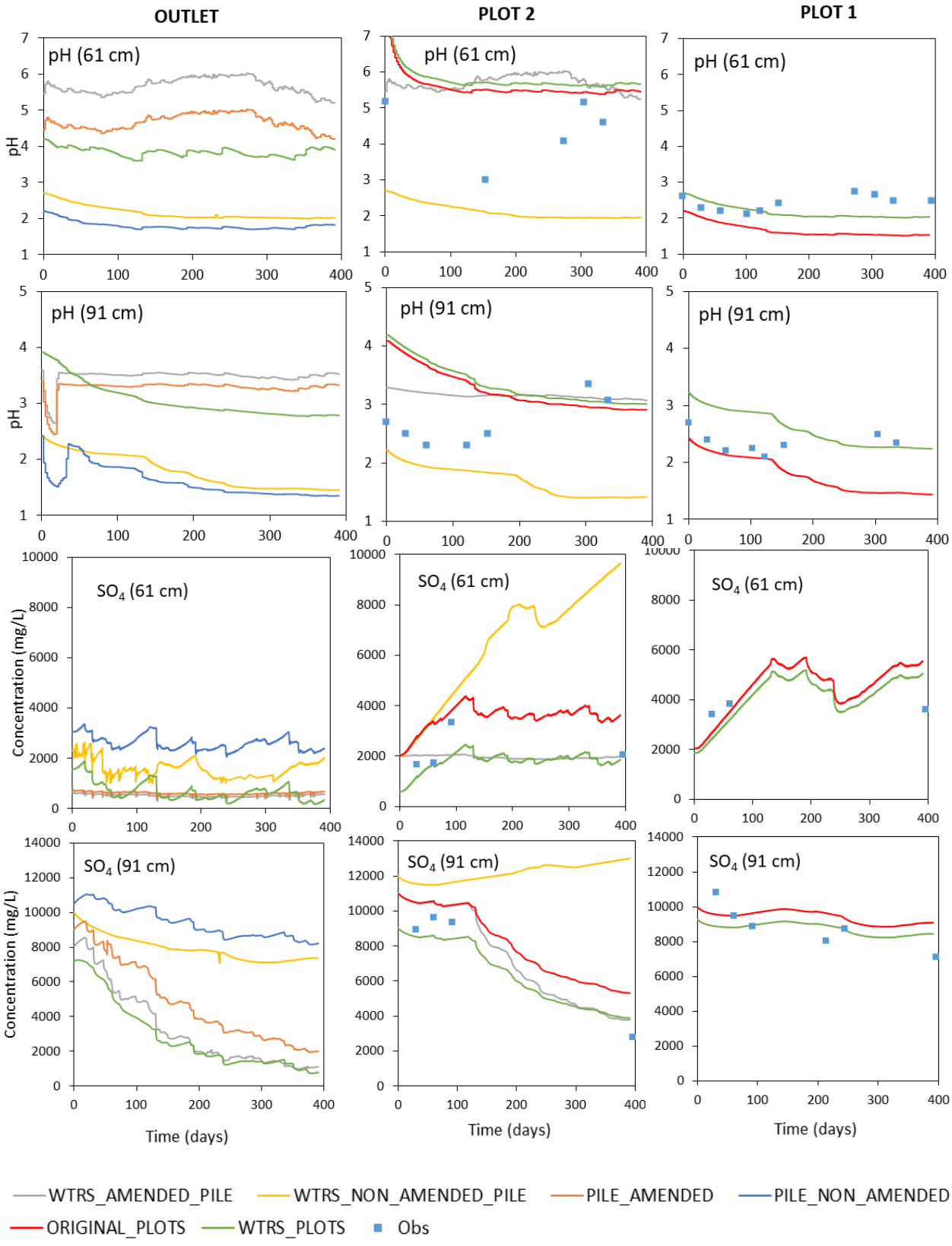
OUTLET
PLOT 2
PLOT 1
pH (61 cm)
pH (91 cm)
SO4 (61 cm)
SO4 (91 cm)
pH
Concentration (mg/L)
Time (days)
WTRS_AMENDED_PILE
WTRS_NON_AMENDED_PILE
PILE_AMENDED
PILE_NON_AMENDED
ORIGINAL_PLOTS
WTRS_PLOTS
Obs

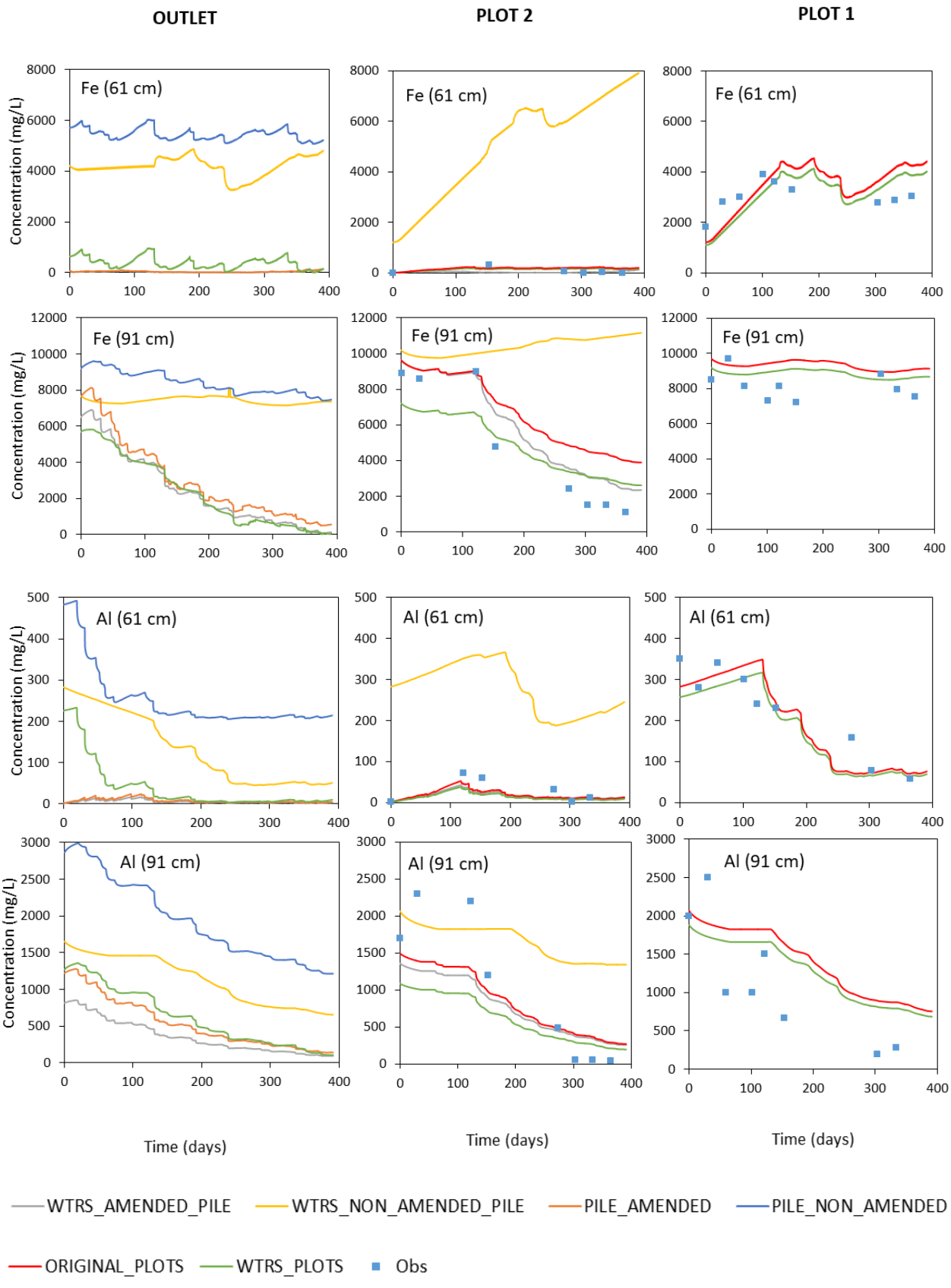
OUTLET
PLOT 2
PLOT 1
Fe (61 cm)
Fe (91 cm)
Al (61 cm)
Al (91 cm)
Concentration (mg/L)
Time (days)
WTRS_AMENDED_PILE
WTRS_NON_AMENDED_PILE
PILE_AMENDED
PILE_NON_AMENDED
ORIGINAL_PLOTS
WTRS_PLOTS
Obs

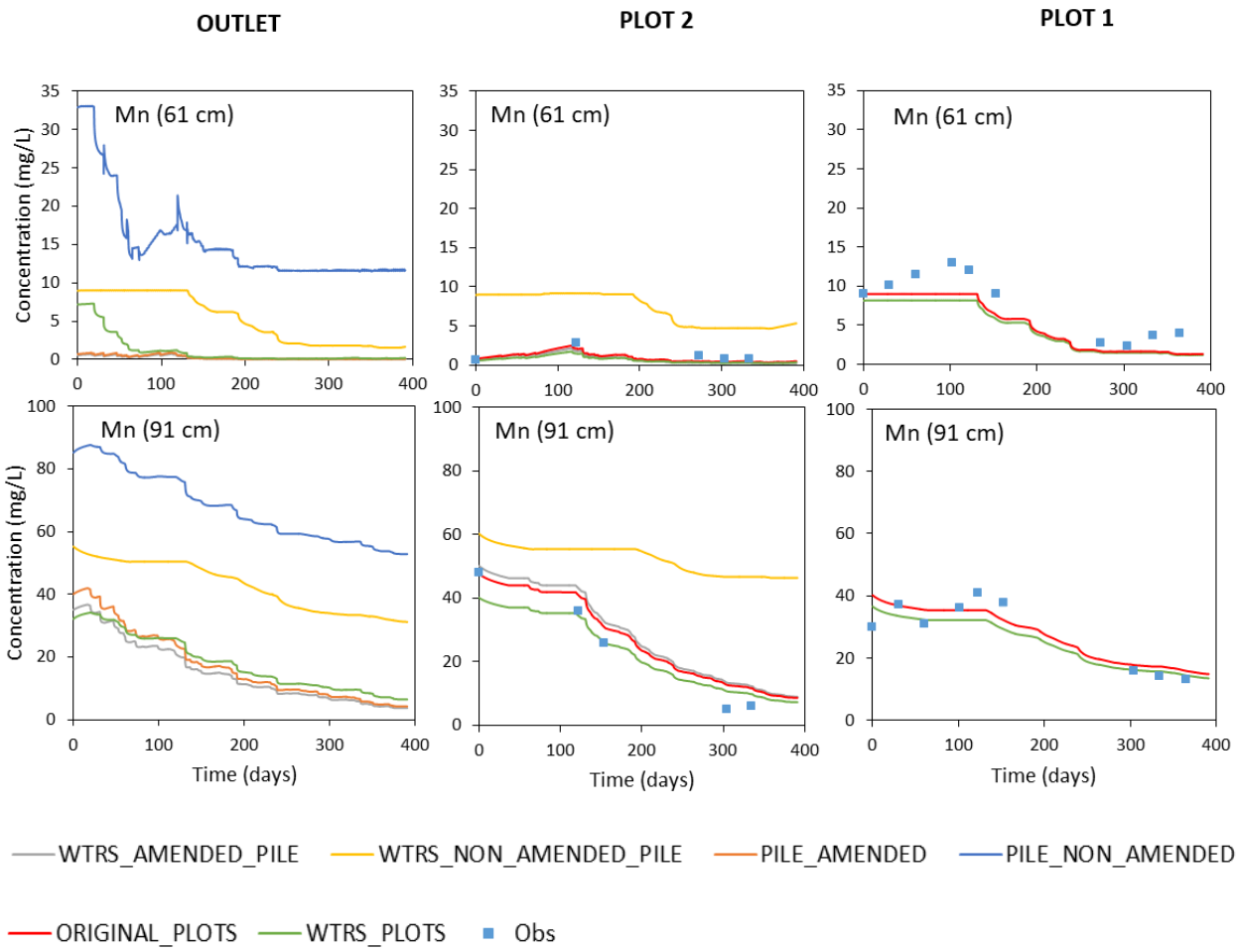

Figure 4.11. 1-yr simulation in Mather watershed for several scenarios varying the spatial scale (WTRS = watershed, PILE = only coal pile) and the output location (OUTLET, PLOT 1 and PLOT 2). Observed field data shown in some plots were measured from June 2009 to May 2010

In summary, the analysis presented in this section has emphasized the importance of the spatial scale regarding ARD modeling. By giving the model the possibility to simulate small and large areas and analyze the output from many desired locations, a more complete environmental assessment is achieved. It is possible, for instance, to determine the impact of a watershed that has a coal piles and other areas with different uses (e.g. agriculture, livestock). However, this could need the modification of the proper modules to characterize the water quality from other sources other than mine drainage. Likewise, it is possible to establish the impact of a neighboring watershed that receives the drainage from the watershed that is being studied.

4.3.2 Calculation of new metals: Zn, Cu, Ni, Cr, Co

In the previous section, the model was setup to be able to run the entire Mather site watershed. In this section, a new improvement has been made to the model: the addition of new chemicals to be calculated in the model, which implied the modification of the PHREEQC module and database, along with the update of chemicals paremeters (see *Figure 4.1*). *Figure 4.12* shows the modeling results (5-year simulation) for both plot 1 (100% CR or the non-amended plot) and plot 2 (90% CR + 10%AC up to 61 cm depth or the amended plot) locations, at 61 and 91 cm. The observations from Mather lysimeters are also included. For an additional comparisson, the results from the column experiments are also included: the amended scenario of plot 1 at 61 cm is compared to column A1 and the non-amended scenario of plot 2 at 61 cm is compared to column B1.

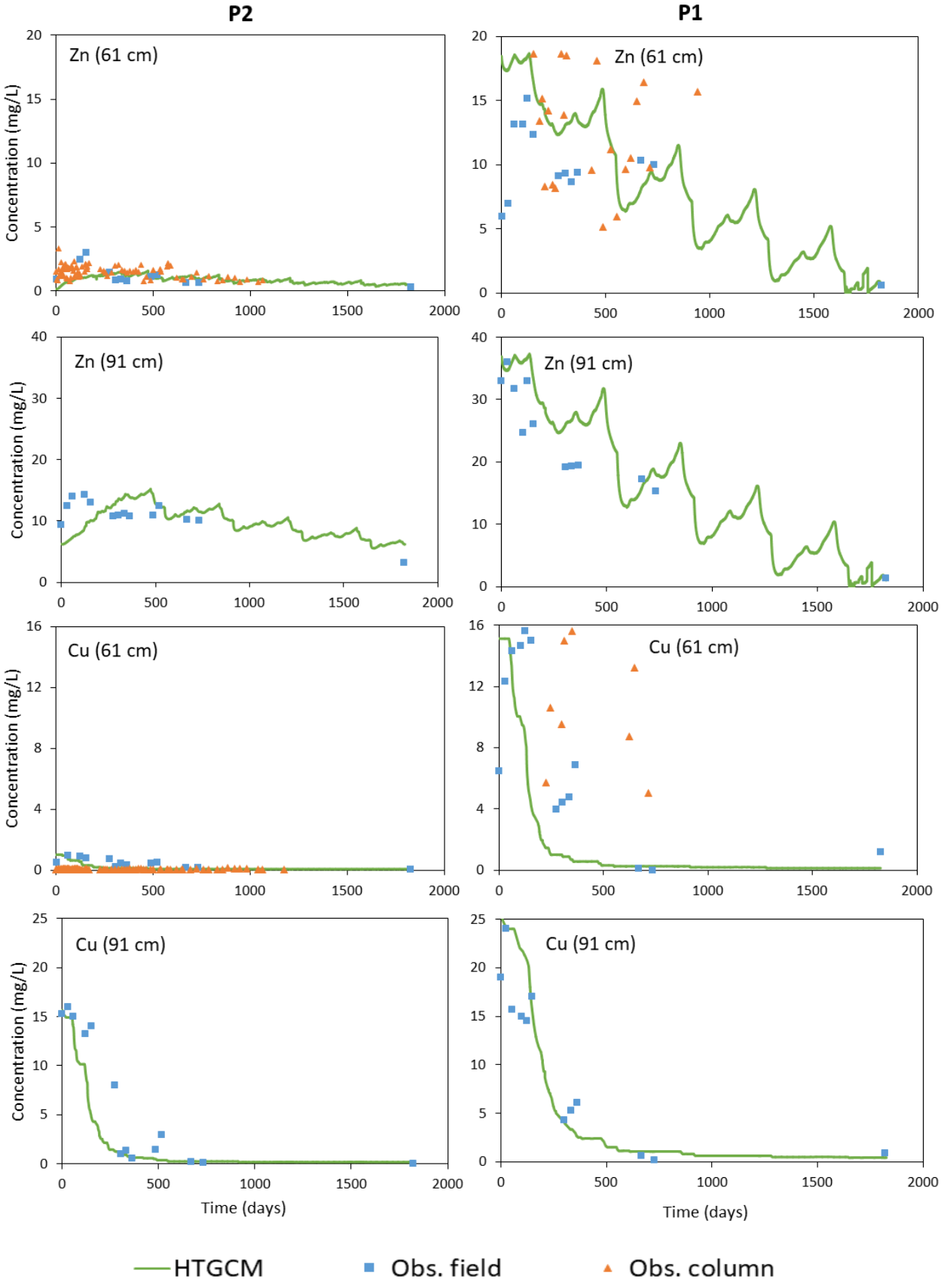
P2
P1
Zn (61 cm)
Zn (91 cm)
Cu (61 cm)
Cu (91 cm)
Concentration (mg/L)
Time (days)
HTGCM
Obs. field
Obs. column

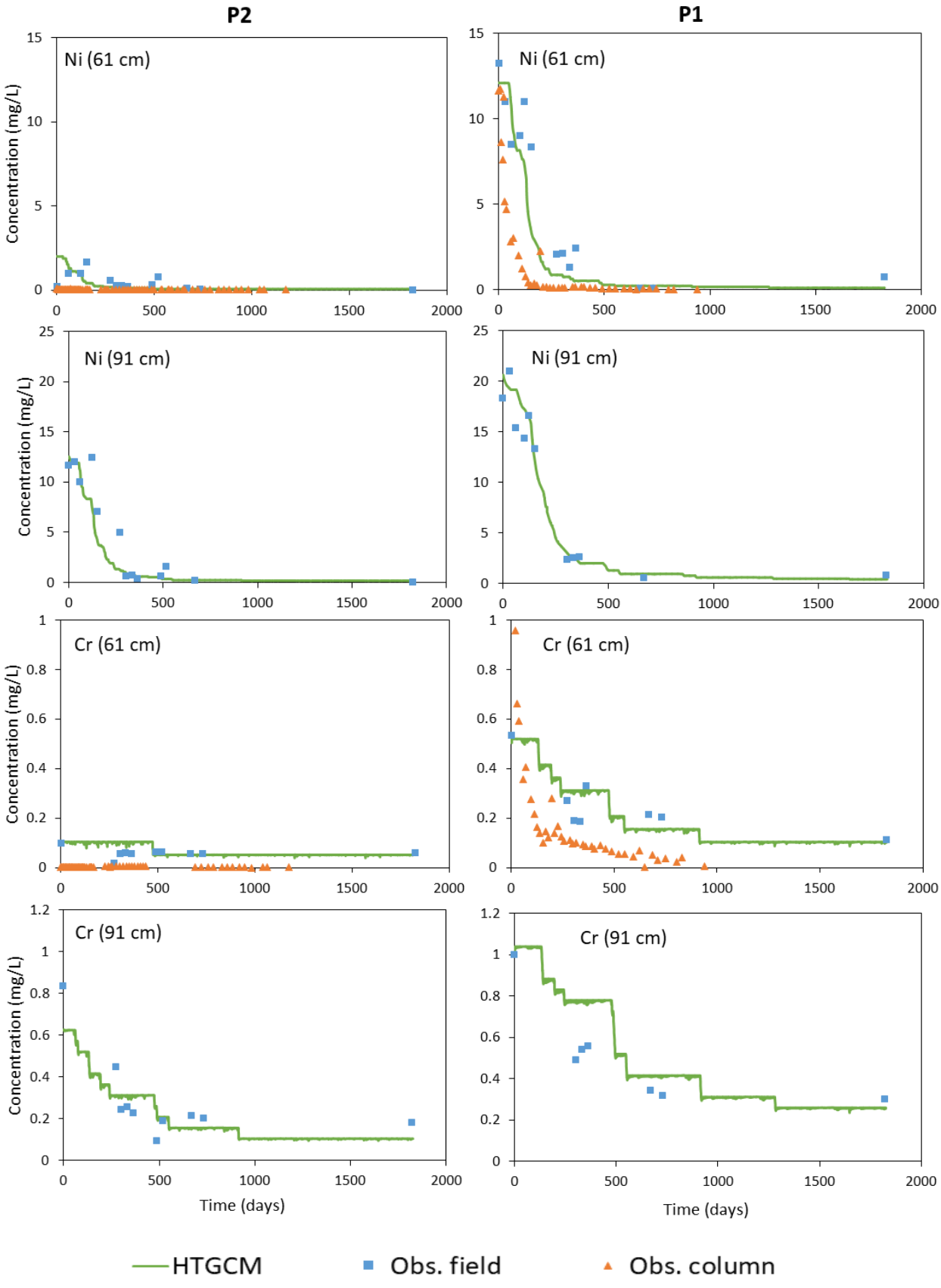
P2
P1
Ni (61 cm)
Ni (91 cm)
Cr (61 cm)
Cr (91 cm)
Concentration (mg/L)
Time (days)
HTGCM
Obs. field
Obs. column

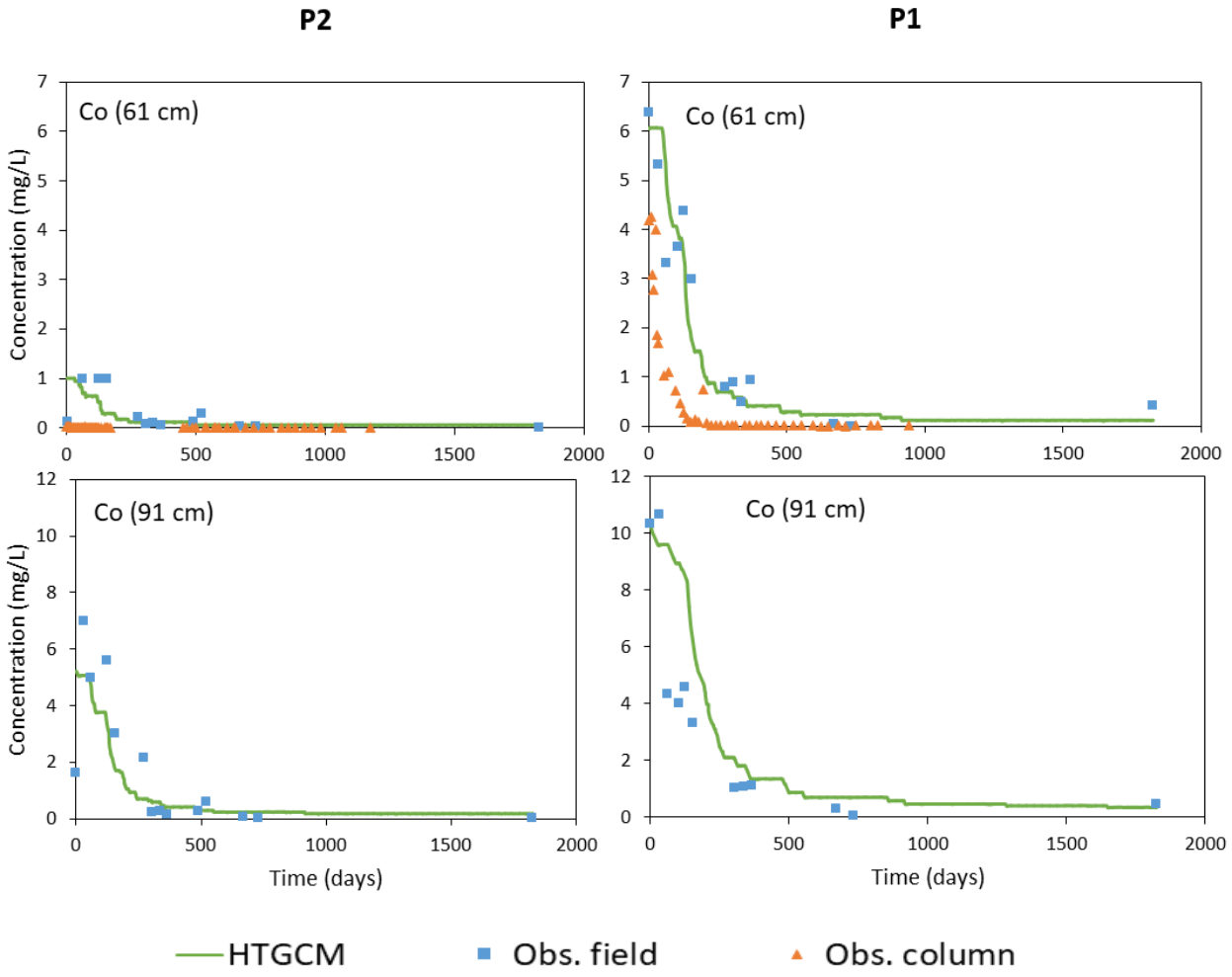

Figure 4.12. 5-yr simulation in Mather watershed for the new metals added into the HTGCM model, compared to the field and columns observations. Observed field data shown in the plots were measured from June 2009 to June 2014

It is observed, in general, that the model properly replicates the observed behavior of these chemicals. For instance, the model is able to reproduce the oscillating behavior of Zn in the non-amended plot 1, which has been measured both in the field and in the laboratory. In the case of Zn, this is a very important mine water pollutant whose aqueous concentrations are controlled by various hydro-geochemical processes acting at the same time: pH, soil moisture, soil texture, evaporation, particle size, secondary mineral formation and even the presence of nutrients (e.g., phosphorus) *[Gutierrez et al., 2016, Plumlee et al., 1999, Blowes et al., 2003]*. High acid neutralization (i.e., neutral pH, mineral precipitation) exerted by AC in the amended plot controls

the Zn concentrations and keeps them to be relatively low with a conservative behavior (< 3 mg/L); however, in the non-amended plot, high acidic conditions combined with low alkalinity supply makes Zn to be highly soluble and, at the same time, more sensitive to the variations of the above-mentioned hydro-geochemical factors. Furthermore, from previous studies about mine-impacted natural waters *[Plumlee et al., 1999]*, it has been observed that Zn shows the same oscillating behavior that has been observed in Mather.

In addition, the model also replicates the initial steep decrease and subsequent flattening of the observation curve for some metals such as Cu, Ni, Cr and Co. Cr, specifically, shows a very particular behavior in the modeling curve, making it similar to stairs; however, the overall performance of this curve is adequately described the observed data and, moreover, the concentrations magnitudes are relatively low for this particularity to have a significant adverse impact in the overall simulation.

Finally, the results from the kinetic experiments (i.e. columns) showed a surprising similarity (both behavior and magnitude wise) to the field-observed and modeling data. This fact helped to validate the adoption of the kinetic experimental design and setting, which were intent to mimic the field conditions.

4.3.3 Variable oxygen diffusion in the PYROX (shrinking-core module)

The last proposed improvement to the HTGCM model is to introduce a factor that can take into account the decrease in pyrite oxidation rates due to the iron precipitates coating developed in the pyrite particle's surface over time, especially under alkaline pH conditions. This condition was introduced to the model and tested for one single particle (see *Section 4.2.4*). Since the variable

diffusion coefficient will be introduced in the PYROX module (shrinking-core module), only pH, SO_4 and Fe will be affected by this modification, since these are the only chemical parameters linked to this module (the other chemicals are calculated in the PHREEQC module).

Fig 4.13 shows the modeling results (5.5-year simulation) for SO_4, including both the HTGCM with the original and the modified PYROX modules, along with the observation in plot 2 (amended). It is clearly observed the incidence of the decreasing oxygen diffusion in the generation of SO_4. Even though both simulation curves start around the same concentrations, due to having the same initial conditions, at some point they begin to diverge from each other. There is an observed data limitation in the case of SO_4 (less than 500 days of data), which does not allow to assess the behavior of the simulation curves in the long term. However, preliminarily, the modified HTGCM yielded the expected results (i.e. steeper depletion curve). The performance of the model in the long term is confirmed with the other two parameters, pH and Fe.

Regarding Fe, the availability of more observed data (5 years) allowed a better assessment of the modified model in the long term. Similarly to Fe, the modified HTGCM model properly simulates the long-term pH conditions. In the modified HTGCM simulations, there is a clear indication of the pyrite oxidation inhibition as a consequence of the Fe precipitate coatings, and the resulting reduction of H^+ concentrations. These pH modeling results utilizing the new version of the model is also more consistent to the data retrieved from the kinetic experiments and the field measurements and, moreover, it is consistent with the technical literature, where even in a highly acidic environments, there is a decrease of the alkalinity demand over time, thus a rise in the pH is produced.

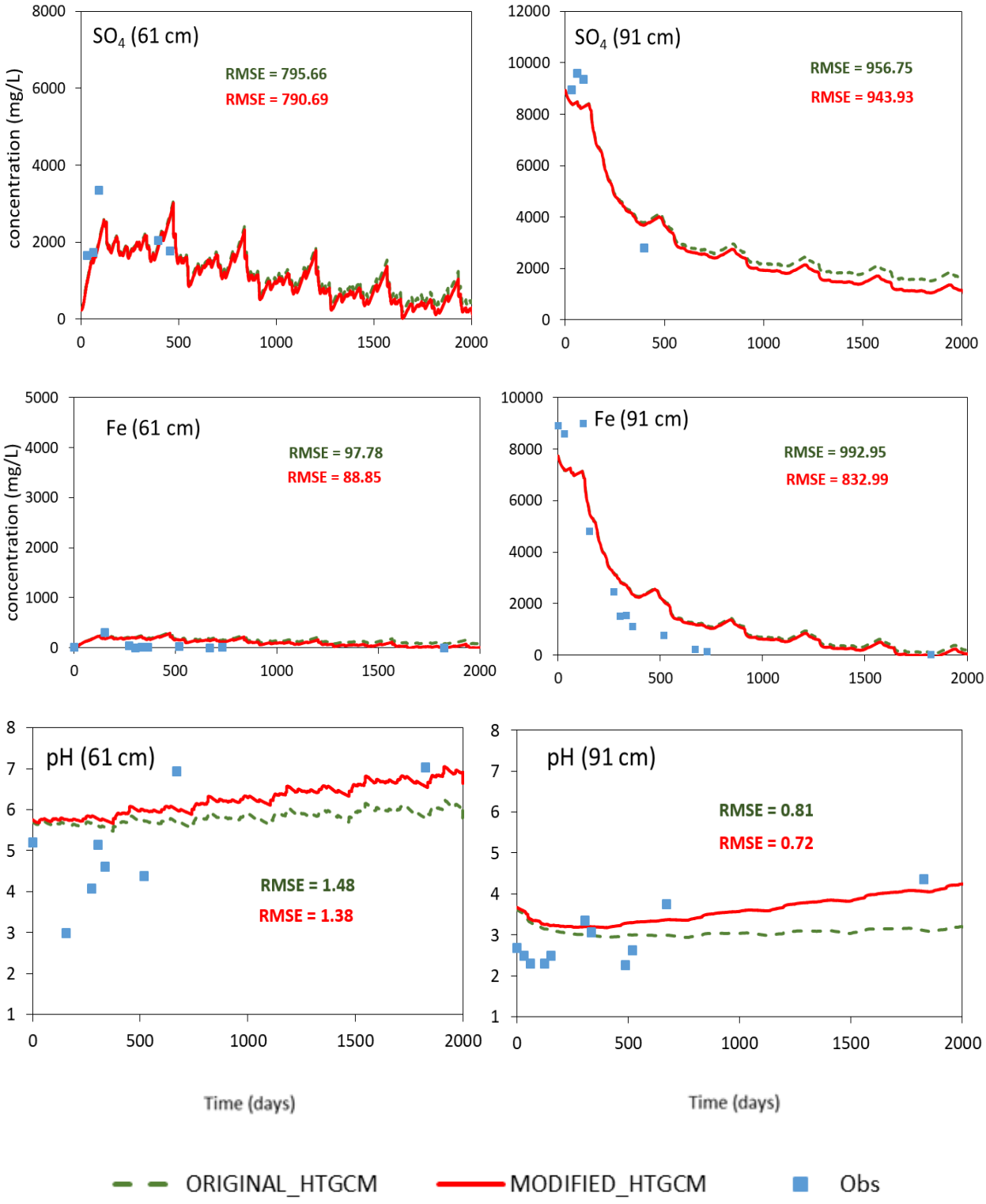

Figure 4.13. 5.5-yr simulation of the amended scenario (plot 2) in the Mather watershed for the variable oxygen diffusion added into the HTGCM model, compared to the field observations. Observed field data shown in the plots were measured from June 2009 to June 2014

Even though the oxygen diffusion model included in the PYROX module is based on high alkaline conditions, one can hypothesize about the case of low alkaline conditions just like the ones found in the non-amended scenario. The high solubility of Fe mineral phases at low pH conditions makes less likely for the precipitates to produce and encapsulate the pyrite grain. Nonetheless, in this study the simulation of variable oxygen diffusion will also be implemented in the non-amended scenario. Moreover, it is worth mentioning that the settings in plot 1 (the non-amended scenario) were modified after approximately two years to be identical as plot 2 (10%AC+90%CR amended layer of 61 cm); so, in a way, a pyrite coating might have been also occurring at this plot after the amendment. However, one parameter will be modified in order to make the precipitation rates lower than in the case of the amended scenario. The proportion of Fe that is likely to precipitate will be decreased from 3% to 1%.

Fig 4.14 shows the modeling results (5.5-year simulation) for SO_4, including both the HTGCM with the original and the modified PYROX modules, along with the observation in plot 1 (non-amended). For example, in the case of Fe, at 61and 91 cm, it is noticed that the modified model captures more adequately the steeper decrease in Fe concentrations, after the initial two years, approximately. However, in plot 1 at 91 cm, the observed data after two years is still lower than the simulation curve, which could show the influence of the amended layer in plot 1 after that period of time, but which also could imply that there is another factor that plays a role in the decreasing of Fe and that the model is not able to capture. Future research is needed to identify any new buffering factor that can be included in the model calculations.

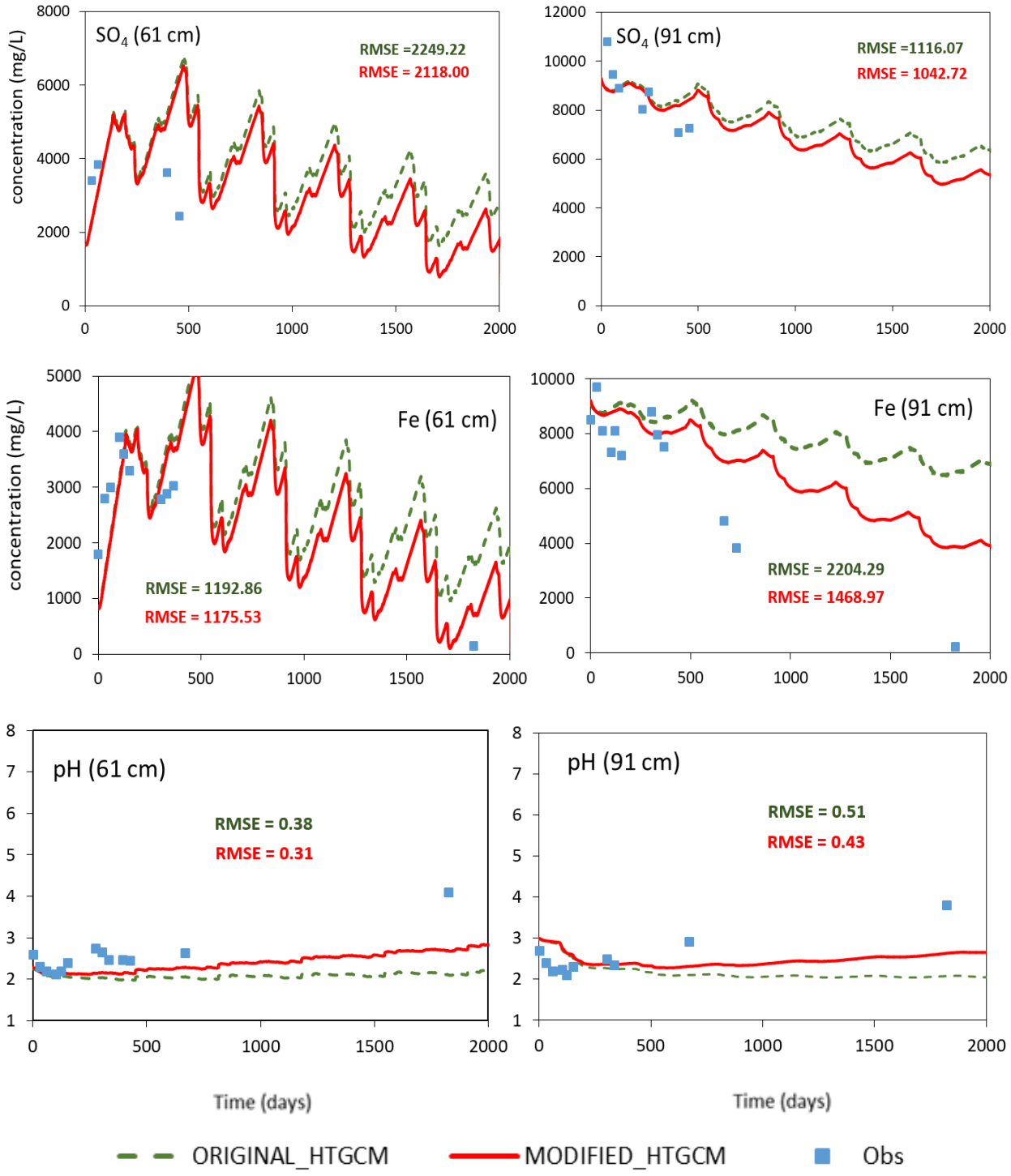

Figure 4.14. 5.5-yr simulation of the non-amended scenario (plot 1) in the Mather watershed for the variable oxygen diffusion added into the HTGCM model, compared to the field observations. Observed field data shown in the plots were measured from June 2009 to June 2014

In order to have a more objective evaluation about the model performance, a statistical analysis was done to compare the original HTGCM (i.e. with constant oxygen diffusion in the PYROX module) and the modified HTGCM (i.e. with variable oxygen diffusion in the PYROX module) against the observations in plots 1 and 2, at 61 and 91 cm, retrieved over 5 years. The used assessment parameter was the root mean square error (RMSE). For all the scenarios presented in *Figure 4.13* and *Figure 4.14*, the RMSE is shown for both original (top) and modified (bottom) model. It is observed that, in all cases, the RMSE is lower for the modified HTGCM simulations, thus indicating that, the inclusion of the pyrite coating factor through the decrease of the oxygen diffusion in the PYROX module, is an important added value that significantly improves the model performance for long-term simulations, in which the role played by this factor is even more influential in the ARD generation/neutralization processes.

Additionally, *Figure 4.15* shows a long-term simulation (i.e., 20.5 years) in the amended plot 2, at 61 and 91 cm. The input forcing data (i.e., meteorological) available for this simulation was from 2009 to 2017. For the remaining period of time (i.e., 2018 – 2029), the data from the previous period of time was repeated. The objective of this exercise is to observe, in the long term, how divergent from each other are the simulation curves with the original shrinking-core module and the modified one (i.e., with variable oxygen diffusion), although there is no observed data beyond 5 years. The divergence of the two simulation curves is more evident at 91 cm, because the orders of magnitude of the chemicals (i.e., SO_4 and Fe) are higher. It is also noticed that, at all times, the simulation curve of the HTGCM with the modified shrinking core module has lower concentrations of SO_4 and Fe and higher pH, thus confirming the direct incidence of the variable (i.e., decreasing) oxygen diffusion over time. This module has been successfully calibrated against the observed data over 5 years (*Figure 4.13*, *Figure 4.14* and *Table 4.5*), meaning that the iron

coating of the pyrite grain has been taken into account. However, more measured data is needed to adjust the parameters of this module for longer simulations.

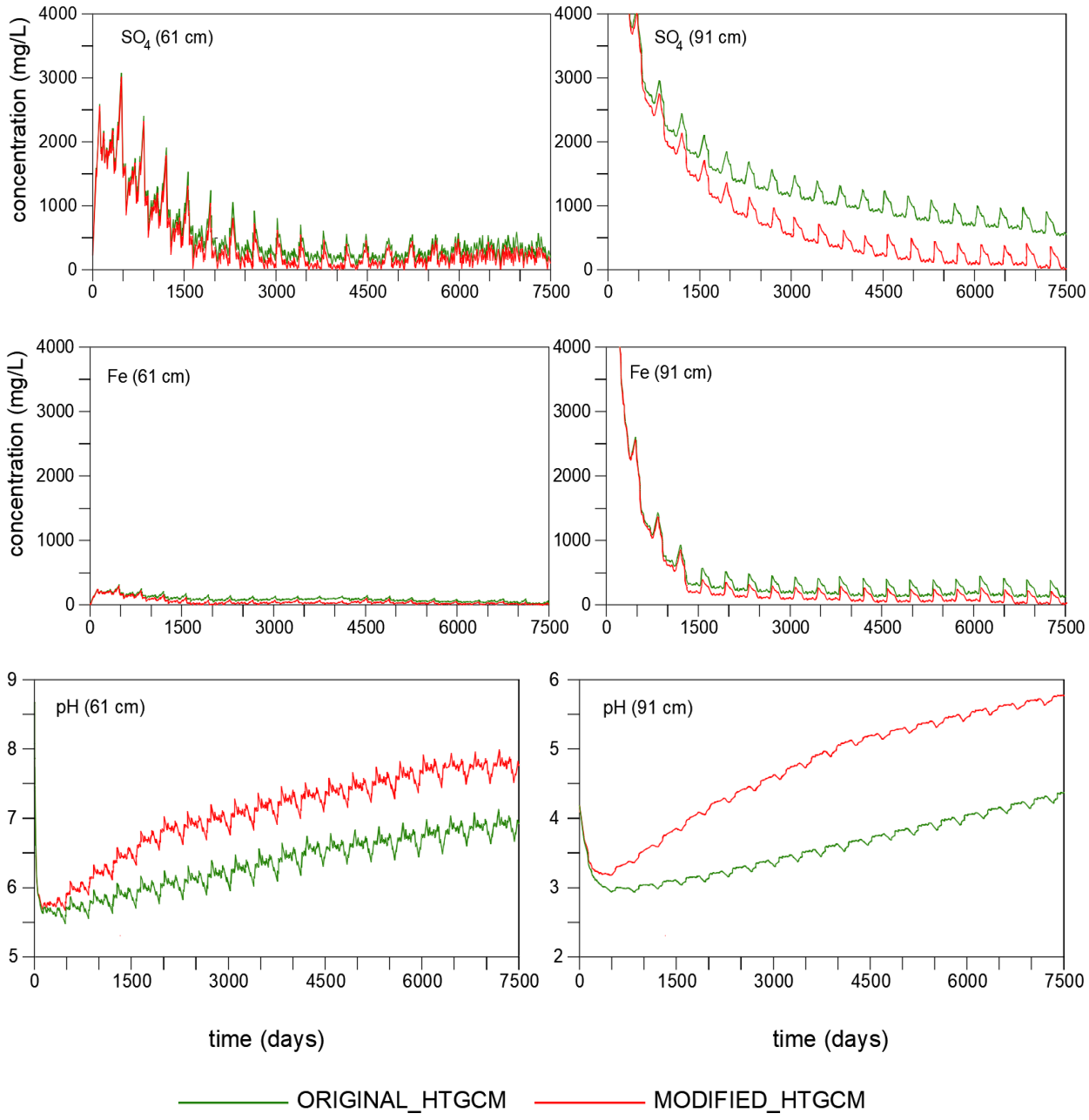

Figure 4.15.Long-term (20.5-yr) simulation of the amended scenario (plot 2) in the Mather watershed for the variable oxygen diffusion added into the HTGCM model.

One final statistical analysis was made by using a hypothesis testing approach to evaluate whether the differences between the original and modified models are statistically significant or not. Both scenarios were considered as independent variables; the null hypothesis was that there is no significant difference between the two modeled scenarios (i.e.,$\mu_1=\mu_2$) and the alternative hypothesis was that these scenarios are different (i.e.,$\mu_1\neq\mu_2$), based on a significance level of 5%. Table 4.6 shows the hypothesis testing results for the original and modified models and for the short and long-term simulations (i.e.,≈5-year and ≈20-year, respectively). It is worth mentioning that the long-term simulations where only conducted for the amended scenario of plot 2.

Table 4.6. Hypothesis testing for short and long-term simulations, comparing the original model (constant oxygen diffusion) and the modified model (variable oxygen diffusion)

Parameter (depth)	5-year simulation		20-year simulation	
	PLOT 1	PLOT 2	PLOT 1	PLOT 2
pH (61 cm)	μ1 = μ2	μ1 = μ2		μ1 ≠ μ2
pH (91 cm)	μ1 = μ2	μ1 = μ2		μ1 ≠ μ2
SO_4 (61 cm)	μ1 ≠ μ2	μ1 = μ2		μ1 = μ2
SO_4 (91 cm)	μ1 ≠ μ2	μ1 = μ2		μ1 ≠ μ2
Fe (61 cm)	μ1 ≠ μ2	μ1 = μ2		μ1 = μ2
Fe (91 cm)	μ1 ≠ μ2	μ1 = μ2		μ1 ≠ μ2

In the 5-year simulation, it is observed that there is no statistical difference between the original and modified models for the amended scenario of plot 2. This might be explained by the fact that the pyrite coating is a long-term process that depends on several hydrological and geochemical factors (e.g., rainfall, soil moisture, particle size, pH, presence of Fe minerals). For instance, pyrite coating in early formation can be partially or totally washed off due to the rainfall / runoff weathering effect *[Huminicki et al. 2009]*. For the same simulation period, results are different for the non-amended scenario of plot 1. In this case, the presence of higher amounts of sulfur and iron minerals lead to higher aqueous concentrations of SO_4 and Fe, thus making this

scenario more sensible to oxygen diffusion variations (i.e., decrease). In addition, it is observed that there is no significant change of pH in the short term as well.

In the 20-year simulation, it is noticed that for all cases, except for SO_4 and Fe at 61 cm, the difference between the original and modified models is statistically significant. This confirms the long-term nature of the pyrite grain coating by iron precipitates and, at the same time, enhances the necessity of taking into account this coating effect for long-term ARD remediation prediction and assessment through physically-based hydro-geochemical models (e.g., HTGCM).

Once every proposed improvement to the HTGCM model has been successfully implemented and tested in the Mather site (Case Study 1), the next step was to replicate these results in another watershed with similar characteristics: the Ernest mine watershed (Case Study 2).

4.4 CASE STUDY 2: IMPLEMENTATION OF THE MODIFIED HTGCM MODEL IN THE ERNEST COAL PILE WATERSHED

The HTGCM model has been satisfactory tested and calibrated under different scenarios in the Mather site. However, it is fundamental to investigate the capabilities of the model to replicate the same type of results in other watersheds where coal piles are located. For this purpose, the Ernest coal pile, located in Indiana County, Pennsylvania, USA, was chosen as a second study site. Many shared similarities with Mather where identified as reasons to choose Ernest: both are coal refuse piles, with similar geographic locations (i.e. Western Pennsylvania, in the Northern Appalachian Coalfield) and fairly well characterized. In the specific case of Ernest, this site has around 2-year

data of non-amended conditions and about 8-year data of amended conditions (addition of fluidized bed combustion or FBC ash). The sampling site (MW-1) that was utilized for the HTGCM model implementation is located at the watershed outlet, at approximately 1.5 m depth. The parameters that were measured at this sampling site are pH, SO4, Fe, Al, Mn, Ca, Ni and Zn.

The HTGCM version that will be used in Ernest is the modified version of the model that includes all the proposed changes (i.e., spatial scale, new chemicals, variable oxygen diffusion), widely described and tested in the previous sections. *Figure 4.16* shows the entire Ernest watershed, including the mine site, the non-mine region and the location of MW-1 sampling site. The implementation of the watershed scale in the HTGCM model is particularly important in this case study, because the sampling site is located at the watershed outlet, and has an important drainage contribution from outside the mine region.

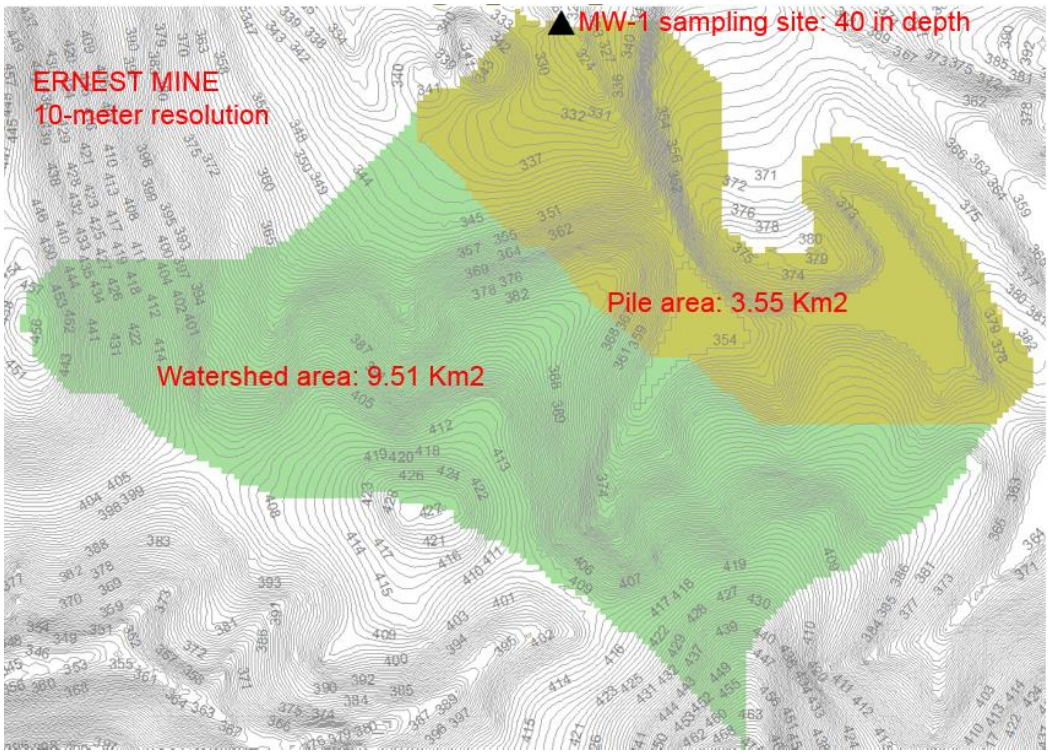

Figure 4.16. Ernest Mine Watershed.

As previously mentioned, there is evidence *[Pennsylvania Minefill Study, 2007]* pointing at the fact that the addition of FBC ash not only did not improve the water quality conditions, but caused water quality degradation. In June, 2002, the Pennsylvania Department of Environmental Protection (PADEP) issued a report on the Ernest site responding to public concerns about water quality degradation from this operation. The last recorded water quality data available for this site is from November 2004. In the model results, all the available data will be presented, however only the data before the FBC ash placement, when the site was an unaltered coal refuse pile (like the Mather site), will be utilized for the purposes of the model assessment.

Table 4.7. Ernest simulations initial solutions

	Amended Scenario	Non-amended Scenario	Outside Coal Pile
Description	Concentration (mg/l)	Concentration (mg/l)	Concentration (mg/l)
SO_4	1000	3000	4.9
Fe	2	400	1.4
Ca	550	400	0.9
Na	280	200	2.2
Mg	100	65	100
K	7.2	8	0.3
Si	60	178	8.4
P	0.5	15	0.5
Al	1.5	200	1.7
Cl	155	100	0.001
Mn	2.0	40	0.007
Zn	0.0	2	0.009
Cr	0.004	0.6	0.002
Ni	0.01	2	0.003
Co	0.003	6	0.001
Cu	0.01	16	0.002
pH	6	4.5	5.5

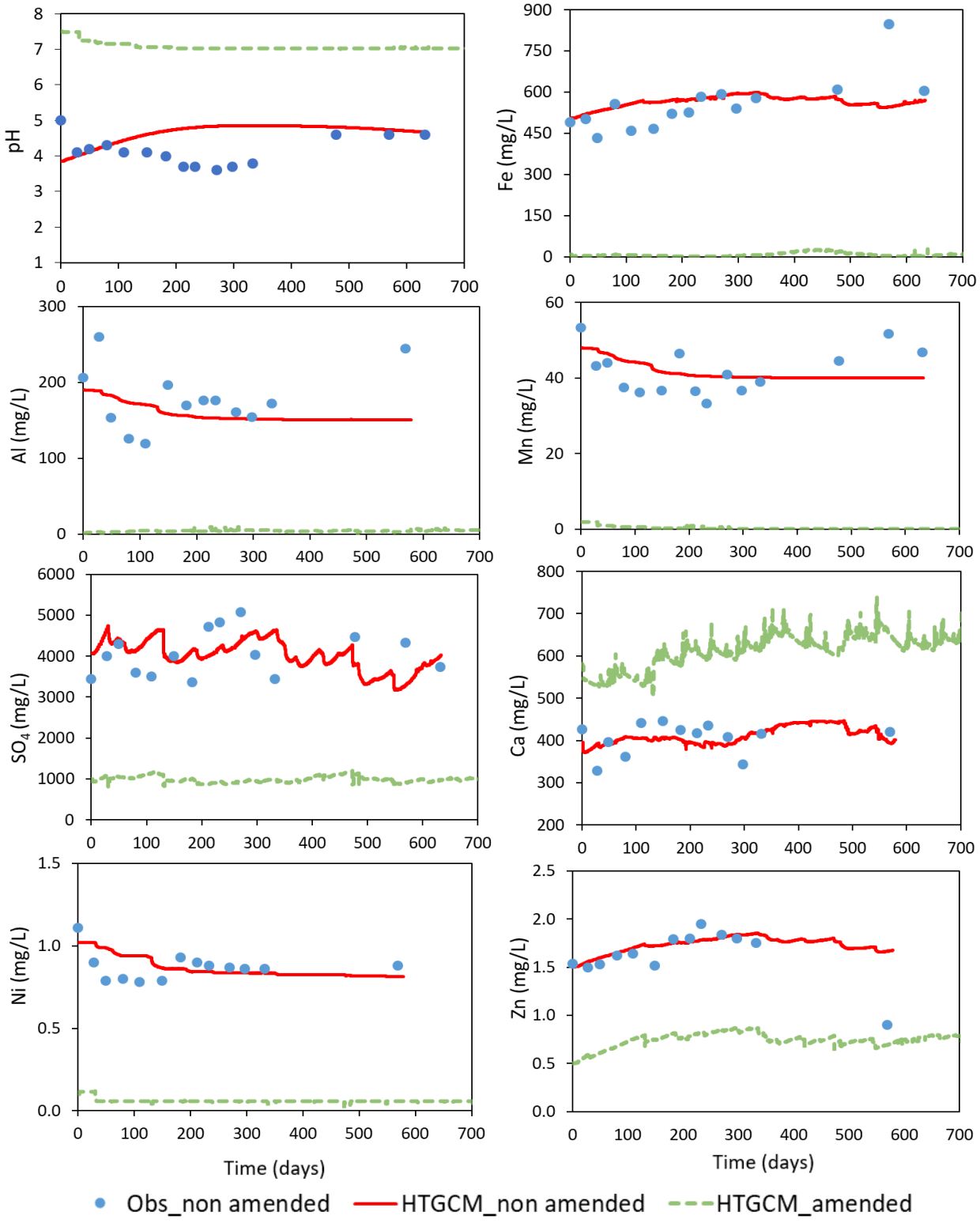

Figure 4.17. Ernest Mine Watershed HTGCM 2-yr simulations for amended and non-amended conditions. The observed data is for the non-amended scenario. Observed field data shown in the plots were measured from November 1994 to August 1996

Figure 4.17 shows the simulation results (approximately 2 years) in the Ernest mine watershed. *Table 4.7* shows the initial solutions in the PHREEQC module. The output location is the MW-1 sampling site, which data has also been included. In addition, even there is no observed data to compare with, a simulation considering the same remediation design as the one tested in Mather (10% AC + 90 % CR amended layer) is also presented. It is observed that the model properly captures the behavior of the system for the non-amended scenario in the Ernest mine site. Moreover, it is probable that the water quality in MW-1 is influenced by a dilution effect caused by the contribution of surface and subsurface drainage water from the non-mine region (9.51 km^2). This can be inferred by the relatively low chemical concentrations and higher pH in MW-1, compared, for example, to those from another coal refuse site like Mather. For instance, in Mather (non-amended plot 1 at 91 cm) the pH, SO_4, Fe, Ni and Zn concentrations range approximately from 3 – 2, 9000 – 7000 mg/L, 9000 – 5000 mg/L, 20 – 5 mg/L and 40 – 20 mg/L, respectively, while in Ernest (non-amended pile in MW-1 at 150 cm) the pH, SO_4, Fe, Ni and Zn concentrations range approximately from 4 – 4.5, 5000 – 3000 mg/L, 600 – 500 mg/L, 1 – 0.8 mg/L and 2 – 1.5 mg/L, respectively, considering the same period of time in both cases. This fact enhances the necessity to include the entire watershed in the simulation and the hydrogeochemical interaction of both mine and non-mine environments in the model, allowing to assess the environmental impacts in several locations, inside and outside the mine site.

In addition, special attention needs to be addressed regarding the pH field measurements. The pH seems to follow a very particular trend, decreasing until approximately 280 days, afterwards, increasing until around 500 days, and, finally, having a more stable behavior for the remaining measurements. One of the main reasons for this particular behaviour is that the pH was measured directly at the field and not at a lab, so the pH temperature dependence plays a very

important role. For example, at 60°C the neutral point is 6.51 while at 10°C it is 7.26, a difference of three fourths of a unit. Thus the pH of a sample measured at field temperature is more likely to represent the true pH in the site water than the pH measured in that sample at a different temperature in the laboratory *[Pennsylvania Minefill Study, 2007]*. This explains why the decreasing trend occurs during the fall and winter months and, the subsequent increase in pH occurs in the spring time. In the case of the Mather measurements, this behaviour is not observed because the measurements took place in the laboratory.

The amended scenario simulations in *Figure 4.17* should be taken only as a reference to idealize how would the conditions in Ernest have changed if a similar remediation design as the one applied in the experimental plots in Mather and tested in the laboratory experiments presented in this study would have been applied in Ernest as well: neutral pH and high immobilization of SO_4 and toxic metals. It is not necessary to extend this simulation, as there are no observed data to compared with. Since the initial conditions (i.e., initial aqueous solution) for this amended scenario was unknown, it was obtained by a simple mathematical relation based on the initial solutions of plots 1 and 2 in Mather.

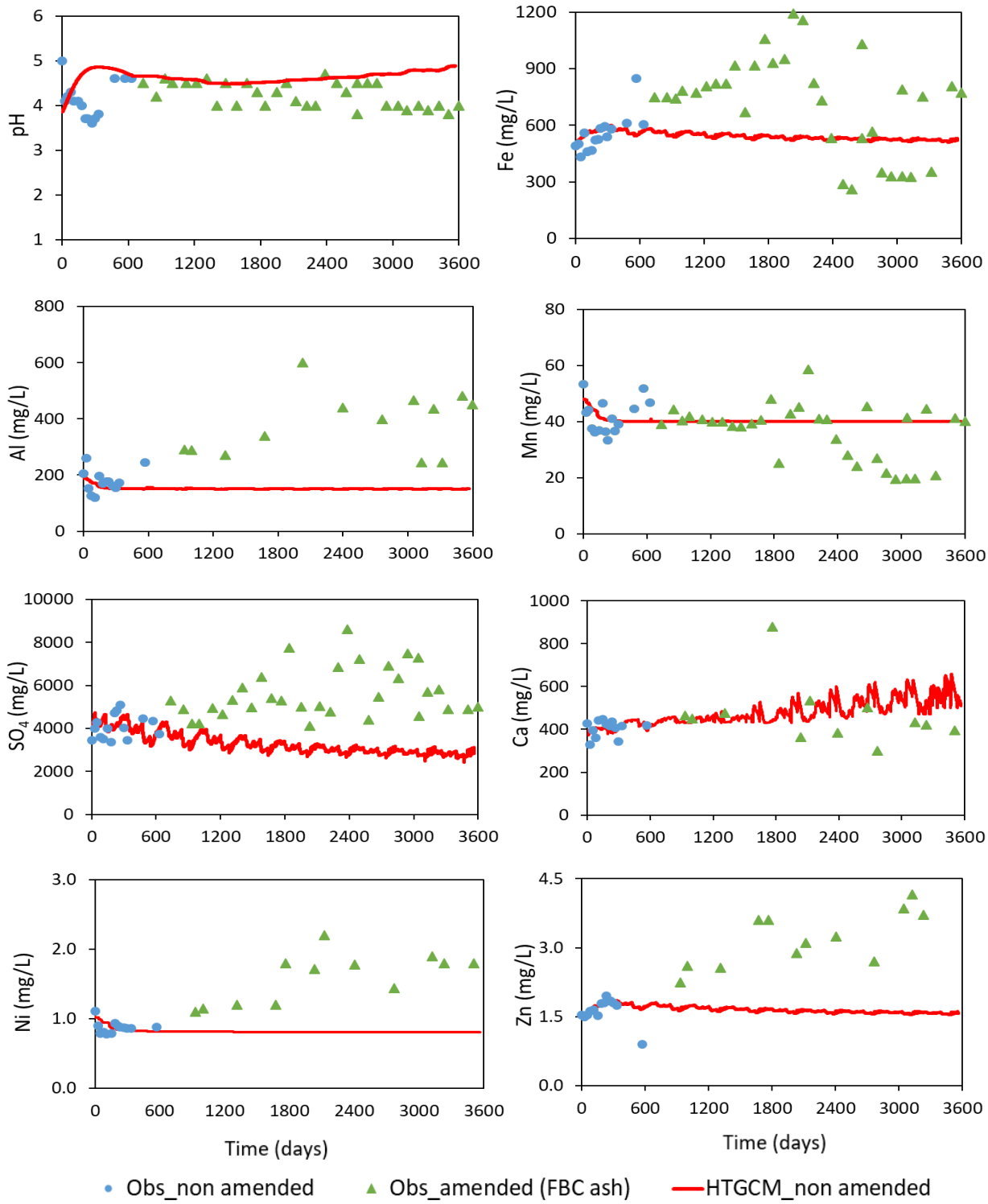

Figure 4.18. Ernest Mine Watershed HTGCM 10-yr simulations and observed data before and after the addition of FBC ash. Observed field data shown in the plots were measured from November 1994 to August 1996 (i.e., before FBC ash addition) and from November 1996 to September 2004 (i.e., after FBC ash addition).

In addition, an extended simulation (10-year) of the non-amended scenario is presented in *Figure 4.18* and includes the water quality data retrieved from MW-1 sampling site, after the addition of FBC ash. It is observed that some chemicals such as SO_4, Fe, Al, Ni and Zn reached higher concentrations after the remediation was applied in the site, which might imply a lack of characterization study of the FBC ash as a remediation material, based on the fact that apparently this material generated the mobilization of higher amounts of some chemicals compared to the case of the non-amended conditions. Hence the importance of an extensive hydro-geochemical analysis of the remediation material, just like in the case of the presented study, where AC has been exhaustively tested from several perspectives (i.e. field measurements, modeling, static and kinetic experiments). On the other hand, other parameters such as pH and Ca remained stable and the last one, Mn, was observed to have an oscillatory behavior. It is worth to mention that the model calibration was solely based on the observed data before the addition of the FBC ash and the long-term simulation is intent to replicate the conditions that would have experienced the site if no remediation has ever been made. This conditions happened to be, in most cases, less critical than the observed conditions with the addition of a ARD remediation agent.

4.5 CONCLUSIONS

In this chapter, two case studies have shown the feasibility of implementing an improved version of the HTGCM model at a watershed scale. The following findings related to the application of this improved model have been identified:

- The modification of the model scale (i.e. watershed scale) allowed the assessment of the ARD generation and remediation impacts, inside and outside the waste coal pile. Based on the results from both case studies, the model has shown an improved and more versatile performance. The addition of watershed simulation capabilities with the interaction of both mine and non-mine soils, allowed the analysis of the model output in several locations.
- The inclusion of new chemicals in the output allowed to have a much better water quality characterization, thus taking into account all the important pollutants in mine waters, some of which have been identified as priority pollutants in mine waters over Pennsylvania and other mine regions.
- The inclusion of new reactions in the PHREEQC database: reactions involving the added chemicals (e.g. Zn, Cr, Co) and buffer reactions (e.g. dissolution of calcite), resulted in a more complete hydrogeochemical module that is able to deal with the calculation of the most important pollutants in mine waters.
- The introduction of the Fe precipitation factor, through the continuous decrease of the oxygen diffusion in the pyrite grain, enhanced the physically-based component in the model.
- The testing of new remediation designs (e.g. amended layer depths) allowed the exploration of different remediation conditions.

In summary, the main contribution of the modified HTGCM is that this new version takes into account as posible all the factors that might cause pyrite oxidation and all the factors that might help to neutralize it.

On the downside, due to the larger model scale and the addition of the calculation of new metals and new chemical reactions, along with the consideration of the Fe precipitation, the running time increases (mainly depending on the watershed size and resolution) and, since HTGCM model strength relies in subsurface mine discharges, it is more difficult to retrieve this kind of data from other mine sites, for calibration/validation purposes. Usually, the availability of mine discharge data is very small, disperse, often limited to superficial discharges, and far enough from the mine site, thus causing the dilution of contaminants. In other words, although it has been shown, through the study of two watersheds, that the model is able to replicate real field conditions, it is always desirable to have measured data that can verify the model's performance.

Future work should include an exhaustive analysis about the impacts of different ameneded layer designs, especially in terms of the AC/CR mixing ratio (e.g., AC > 10%). However, additional field and experimental data are essential for such analyses.

5.0 CONTRIBUTIONS AND FUTURE WORK

5.1 CONTRIBUTIONS

An extensive study of ARD generation and remediation, from both experimental and modeling perspectives, have been presented. In addition, this study has also been supported by field measurements, which allowed to test the modeling stage and, at same time, validate the experimental design and results. A summary of the main identified findings, mostly aiming to address the proposed scientific questions, are listed below:

1) Alkaline clay (AC), a byproduct of the aluminum refining process, has demonstrated to successfully neutralize pyrite oxidation and the consequent ARD generation in a waste coal pile. Once mixed with coal refuse (CR), AC quickly reacts and produces a significant decrease in the alkalinity demand, resulting in a positive net alkalinity solution with neutral pH, low sulfate and low dissolved metals. Moreover, the addition of AC to the waste coal pile has proved to be environmentally sustainable: on one hand it allows the use of a waste as a remediation material and on the other hand it maintains the drainage that goes out to the amended region in water quality levels that fully comply with regulations and standards for mine discharges.

2) From several experimental and modeling designs, it has been found that a 10%AC/90%CR is an adequate mixing ratio that guarantees an effective ARD remediation with sustainable conditions in the long term. The static experiments (batch reaction and acid base

accounting) have indicated that with this mixing ratio the total amount of alkalinity exceeds approximately by double the total amount of acidity. The kinetic experiments and the modeling have confirmed that the acidity is likely to be consumed before the alkalinity does.

3) Defining the amended layer depth is crucial when designing an ARD remediation system. *Xu [2014]* has shown that an amended layer as shallow as 40 cm could be effective for ARD remediation. On the other hand, it is no feasible to have a much deeper amended layer (e.g., > 2 m). In this study, a new factor that plays an important role in the definition of the amended layer depth has been identified: the root depth. If a vegetated layer above the amended layer is intent to be applied, it is not desirable for the roots to reach a highly acidic environment (i.e., the non-amended region), otherwise the plats will likely reach harmful and irreversible toxicity levels. Several previous studies that have characterized the physiology of many grass species have determined that the usual root depth is from 0.8 to 1.0 m. Therefore, to guarantee both an effective amended layer depth (i.e., for ARD neutralization) and the safety of the planted vegetation, an amended layer of 1 m is recommended.

4) Two potential complementary measures to enhance the ARD remediation have been studied: a vegetation layer above the amended layer and a saturated sand layer within the amended region or underneath it. To have a vegetation cover on the amended region has determined to be highly beneficial from both biogeochemical and environmental perspectives. Biochemically, the vegetation plays the role of phytoaccumulation and phytoextraction factor, which means that it significantly lowers the levels of dissolved metals, which are extracted and accumulate in the plant tissue. From the kinetic experiments (i.e., columns) and the metal accumulation in plant experiments, it has been determined that as long as the roots don’t reach a highly acidic

environment (i.e., the non-amended layer), vegetation can accumulate higher amounts of metals but without reaching plant toxicity. Environmentally, it has been found that the accumulation of metals in plants is not significant high to have side impacts to the neighbor flora and fauna. Overall, the beneficial impacts of a vegetation cover exceeds its potential risks. The impact of the saturated sand layer is more direct and easy to predict. This saturated layer acted as a natural barrier that blocked oxygen and water diffusion to the underneath layer, thus lowering pyrite oxidation rates.

5) The improved version of the HTGCM model has been successfully tested to model the ARD generation and remediation processes in a watershed scale. Through two case studies, the environmental impacts of the amended and non-amended scenarios have been identified at various locations, inside (higher chemicals concentrations) and outside (lower chemicals concentrations, due to the dilution factor) the waste coal piles. The original elements included in the model (e.g., pH, SO4, Fe, Al, Mn, Ca) and the newly added ones (i.e., Zn, Co, Cu, Cr, Ni), which are considered among the priority pollutants in the Northern Appalachian Coalfield, allowed a complete hydrogeochemical characterization of the drainage in the watershed. The addition of the pyrite coating factor through a variable (i.e., decreasing) oxygen diffusion coefficient, added a new feature that enhanced the physically-based component of the model. Even though the model was calibrated using a fairly large amount of data (5 years in Mather and 2 years in Ernest), it should continuously feed with more data in order to improve its performance.

6) Finally, the experimental and modeling evidence strongly suggest that the proposed remediation has a sustainable and beneficial long term impact. The high ARD neutralization capability of AC ensures a sufficient alkalinity supply that will always exceed the existent acidity in the piles. Moreover, even in the non-amended scenario, the alkalinity demand tends to decrease,

and one of the main factor is the pyrite coating by iron precipitates. This has been observed both on the field and the column experiments, and replicated by the model as well. Also observed and replicated by the model, the addition of AC to the CR significantly lowers the dissolution of toxic metals into levels that are not harmful for the environment, thus resulting in a drainage with positive net alkalinity.

5.2 FUTURE WORK

The most important remaining work that has been identified through this study is listed below:

1) Since vegetation has demonstrated, from the experimental perspective, to play an important role in the ARD remediation process (i.e., acting as a phytoextraction and phytoaccumulation factor), it would be important to include in the HTGCM a biogeochemical module that can take into account the physical-chemical interactions between soil and plants.

2) A more complete mineralogical analysis (e.g., XRD analysis) could be useful to make a better assessment of the small-scale processes occurring in the acidic-alkaline mixture, such as secondary minerals formation, precipitates and pyrite coating. This analysis should be done under different scenarios, in terms of AC/CR mixing ratios and age of the mixture.

3) The assessment of the impact of the soil characteristics inside and outside the waste coal pile (e.g. porosity, hydraulic conductivity, soil density) on the pyrite oxidation rates.

4) Two complementary measures to enhance the ARD remediation have been proposed and analyzed in this study: the implementation of a vegetation cover over the amended layer and the introduction of a saturated sand layer over the non-amended layer. However, future work

should consider a deeper study about these two alternatives. For instance, in the case of vegetation, it would be fundamental to explore among several types of vegetation species in terms of their acidic tolerance, metal uptake or their capability to grow with no major maintenance. In the case of the saturated layer, it would be important to identify any other potential material that can replace the sand utilized in this study. In addition, a field study should be conducted to evaluate the impact of these complementary strategies under real field conditions.

BIBLIOGRAPHY

Adams, A., Raman, A. and Hodgkins, D., 2013. How do the plants used in phytoremediation in constructed wetlands, a sustainable remediation strategy, perform in heavy-metal-contaminated mine sites?. Water Environ J, 27: 373–386. doi:10.1111/j.1747-6593.2012.00357.x

Aghamirlou, H. M., Khadem, M., Rahmani, A., Sadeghian, M., Mahvi, A. H., Akbarzadeh, A., & Nazmara, S., 2015. Heavy metals determination in honey samples using inductively coupled plasma-optical emission spectrometry. Journal of Environmental Health Science & Engineering, 13(1), 39. doi:10.1186/s40201-015-0189-8

Agnieszka, J. and Barbara, G., 2012. Chromium, nickel and vanadium mobility in soils derived from fluvioglacial sands. J. Hazardous Mater., 237–238, 315–322, https://doi.org/10.1016/j.jhazmat.2012.08.048.

Aljoe, W. W. and J. W. Hawkins, 1994. Application of aquifer testing and surface and underground coal mines. In: Proceeding of the 5th International Mine Water Congress, Nottingham (U. K.), pp. 3-21.

Allison, J. D., D. S. Brown, and K. J. Novo-Gradac (1991), MINTEQA2/PRODEFA2, a geochemical assessment model for environmental systems :Version 3.0 User's ManualRep., Environmental Research Laboratory, Office of Research and Development, U. S. Environmental Protection Agency, Athens, Georgia,U.S.A.

American Public Health Association (APHA), 1998a. Acidity (2310)/Titration method. In: Standard Methods for the Examination of Water and Wastewater, 20th ed., American Public Health Association, Washington, DC.

American Public Health Association (APHA), 1998b. Alkalinity (2320)/Titration method. In: Standard Methods for the Examination of Water and Wastewater, 20th ed., American Public Health Association, Washington, DC.

Amos, R.T., Mayer, K.U., Blowes, D.W., Ptacek, C.J., 2004. Reactive transport modeling of column experiments for the remediation of acid mine drainage. Environ. Sci. Technol. 38 (11):3131–3138. http://dx.doi.org/10.1021/es0349608.

Annenkov, B.N., 1982. Mineral feeding of pigs. In: Georgievskii, V.I., Annenkov, B.N., Samokhin, V.I. (Eds.), Mineral Nutrition of Animals. Butterworths, London, pp. 355–389.

Appelo, C.A.J., Verweij, E., Schäfer, H., 1998. A hydrogeochemical transport model for an oxidation experiment with pyrite/calcite/exchangers/organic matter containing sand. Appl. Geochem. 13 (2):257–268. http://dx.doi.org/10.1016/S0883-2927(97)00070-X.

Banks, D., 2006. Assessment of the impact of the mine flooding process on groundwater quality; chemical and mineralogical analysis of rock samples recovered from Janina Mine. Hydrogeological Modelling of Water Evolution, Final report of WaterNorm Project, European Union Grant No. MTKD-CT-2004-003163 55Pp.

Barampuram, S., Chung, B. Y., Lee, S. S., An, B. C., Lee, E. M., & Cho, J., 2009. Development of an embryogenic callus induction method for centipede grass (eremochloa ophiuroides munro) and subsequent plant regeneration. In Vitro Cellular & Developmental Biology. Plant, 45(2), 155-161. doi:10.1007/s11627-009-9199-5

Batty, L.C., Baker, A.J.M., Wheeler, B.D., 2006. The effect of vegetation on porewater composition in a natural wetland receiving acid mine drainage. Wetlands 26(1):40-48.doi:10.1672/0277-5212(2006)26[40:TEOVOP]2.0.CO;2.

Bigham, J. M., and Nordstrom, D. K., 2000, Iron and aluminum hydroxysulfate minerals from acid sulfate waters, In Jambor, J. L., Alpers, C. N., and Nordstrom, D. K., (eds.), Sulfate minerals, crystallography, geochemistry and environmental significance: Mineralogical Society of America Reviews in Mineralogy and Geochemistry, v. 40, p. 351-403.

Billett, M. F. and Cresser, M. S., 1992. Predicting stream-water quality using catchment and soil chemical characteristics. Environ. Pollut., 77, 263–268, https://doi.org/10.1016/0269-7491(92)90085-O.

Blowes, D.W., Reardon, E.J., Jambor, J.L., and Cherry, A., 1991. The formation and potential importance of cemented layers in inactive sulphide mine tailings. Geochimica et Cosmochimica Acta, 55: 965-978.

Blowes, D.W., Ptacek, C.J., Jambor, J.L.,Weisener, C.J., 2003. The Geochemistry of Acid Mine Drainage. Treatise on Geochemistry. 9. 149-204. 10.1016/B0-08-043751-6/09137-4.

Borden, R.K., Black, R., 2005. Volunteer revegetation of waste rock surfaces at the Bingham Canyon Mine, Utah. J Environ Qual 34:2234–2242

Bowen, H. J. M., 1966, Trace elements in biochemistry: New York, Academic Press, 241 p.

Brady, K.B.C., Cravotta III, C.A., 1992. Acid-base accounting - an improved method of interpreting overburden chemistry to predict quality of coal mine drainage. Proceedings of the 13th Annual Meeting, West Virginia Surface Mine Drainage Task Force. WVU, Morgantown, West Virginia.

Britton, H.T.S., 1955. Hydrogen Ions. fourth ed. Chapman and Hall, London.

Chandra, A. P., & Gerson, A. R., 2010. The mechanisms of pyrite oxidation and leaching: A fundamental perspective. Surface Science Reports, 65(9), 293-315. doi:10.1016/j.surfrep.2010.08.003

Chaney, R. L., 1989. Toxic Element Accumulation in Soils and Crops: Protecting Soil Fertility and Agricultural Food-Chains. Inorganic Contaminants in the Vadose Zone pp 140-158.

Conesa, H. M., & Faz, Á., 2011. Metal uptake by spontaneous vegetation in acidic mine tailings from a semiarid area in south spain: Implications for revegetation and land management. Water, Air, & Soil Pollution, 215(1), 221-227. 10.1007/s11270-010-0471-4

Chaplin, J.J., Cravotta III, C.A., Weitzel, J.B., Klemow, K.M., 2007. Effects of Historical Coal Mining and Drainage from Abandoned Mines on Streamflow and Water Quality in Newport and Nanticoke Creeks, Luzerne County, Pennsylvania, 1999–2000. U. S. Geological Survey, Scientific Investigations Report 2007–5061.

Cravotta III, C.A., 2006. Relations among pH, sulfate, and metals concentrations in anthracite and bituminous coal-mine discharges, Pennsylvania. 7th International Conference on Acid Rock Drainage, 2006 pp 378-404. DOI: 10.21000/JASMR06020378.

Cravotta III, C.A., 2008. Dissolved metals and associated constituents in abandoned coalmine discharges, Pennsylvania, USA. Part 1: constituent quantities and correlations. Appl. Geochem. 23 (2):166–202. http://dx.doi.org/10.1016/j.apgeochem.2007.10.011.

Cravotta III, C.A., 2008. Dissolved metals and associated constituents in abandoned coalmine discharges, Pennsylvania, USA. Part 2: Geochemical controls on constituent concentrations, Appl. Geochem. 23 (2):203–226.http://dx.doi.org/10.1016/j.apgeochem.2007.10.003.

Cravotta III, C.A., Brady, K.B.C., 2015. Priority pollutants and associated constituents in untreated and treated discharges from coalmining or processing facilities in Pennsylvania, USA. Appl. Geochem. 62:108–130. http://dx.doi.org/10.1016/j.apgeochem.2015.03.001 (ISSN 0883-2927).

da Silva, J. C., E. do Amaral Vargas, and O. Sracek, 2009. Modeling multiphase reactive transport in a waste rock pile with convective oxygen supply, Vadose Zone J, 8(4), 1038-1050.

Daubert, L., & Brennan, R., 2007. Passive remediation of acid mine drainage using crab shell chitin. Environmental Engineering Science, 24(10), 1475-1480. doi:10.1089/ees.2006.0199.

Davis, G. B., and A. I. M. Ritchie, 1986. A model of oxidation in pyritic mine wastes .1. equations and approximate solution, Appl Math Model, 10(5), 314-322.

DeLong, C., Skousen, J., & Pena-Yewtukhiw, E., 2012. Bulk density of rocky mine soils in forestry reclamation. Soil Science Society of America Journal, 76(5), 1810-1815. doi:10.2136/sssaj2011.0380n

Dold, B., 2014. Evolution of acid mine drainage formation in sulphidic mine tailings. Minerals 4:621–641. http://dx.doi.org/10.3390/min4030621.

Doye, I., Duchesne, J., 2003. Neutralisation of acid mine drainage with alkaline industrial residues: laboratory investigation using batch-leaching tests. Appl. Geochem. 18 (8):1197–1213. http://dx.doi.org/10.1016/S0883-2927(02)00246-9.

Duble, R. L., 1996. Turfgrasses-Their management and use in the Southern Zone. 2nd ed. Texas A & M University Press, College Station, pp 1–336.

Elberling, B., R. V. Nicholson, and D. J. David, 1993. Field-evaluation of sulfide oxidation rates, Nord Hydrol, 24(5), 323-338.

Evangelou, V. P., 1995. Pyrite oxidation and its control: Solution chemistry, surface chemistry, acid mine drainage (AMD), molecular oxidation mechanisms, microbial role, kinetics, control, ameliorates and limitations, microencapsulation. Boca Raton, FL: CRC Press.

Ficklin, W.H., Plumlee, G.S., Smith, K.S., and McHugh, J.B., 1992, Geochemical classification of mine drainages and natural drainages in mineralized areas: Proceedings, 7th Internal Water-Rock Interaction Conference, Park City, Utah, 1992, pp. 381–384.

Garrels, R.M., Thompson, M.E., 1960. Oxidation of pyrite by iron sulfate solutions. Am. J. Sci. 258-A, 57–67.

Gerke, H. H., J. W. Molson, and E. O. Frind , 1998. Modelling the effect of chemical heterogeneity on acidification and solute leaching in overburden mine spoils, J Hydrol, 209(1-4), 166-185.

Gibert, O., de Pablo, J., Luis Cortina, J., & Ayora, C., 2003. Evaluation of municipal compost/limestone/iron mixtures as filling material for permeable reactive barriers for in-situ acid mine drainage treatment. Journal of Chemical Technology & Biotechnology, 78(5), 489-496. doi:10.1002/jctb.814.

Gough, L. P., Case, A. A., Shacklette, H. T., & Geological Survey (U.S.), 1979. Element concentrations toxic to plants, animals, and man: An appraisal of the toxicity hazard to plants, animals, and man from natural and manmade element concentrations of environmental concern. Washington, D.C.: United States Department of the Interior, Geological Survey.

Graupner, T., Kassahun, A., RammLmair, D., Meima, J. A., Kock, D., Furche, M., . . . Melcher, F., 2007. Formation of sequences of cemented layers and hardpans within sulfide-bearing mine tailings (mine district Freiberg, Germany). Applied Geochemistry, 22(11), 2486-2508. doi:10.1016/j.apgeochem.2007.07.002.

Gupta, U.C., Gupta, S.C., 1998. Trace element toxicity relationships to crop production and livestock and human health: implications for management. Commun. Soil Sci. Plant Anal. 29, 1491–1522.

Gutiérrez, M., Mickus, K., & Camacho, L. M., 2016. Abandoned pb zn mining wastes and their mobility as proxy to toxicity: A review. Science of the Total Environment, 565, 392-400. doi:10.1016/j.scitotenv.2016.04.143

Hammarstrom, J.M., Sibrell, P.L., Belkin, H.E., 2003. Characterization of limestone reacted with acid-mine drainage in a pulsed limestone bed treatment system at the Friendship Hill National Historical Site, Pennsylvania, USA. Appl. Geochem. 18 (11): 1705–1721. http://dx.doi.org/10.1016/S0883-2927(03)00105-7 (ISSN 0883-2927).

Hammarstrom, J.M., Seal, R.R., Meier, A.L., Kornfeld, J.M., 2005. Secondary sulfate minerals associated with acid drainage in the eastern US: recycling of metals and acidity in surficial environments. Chem. Geol. 215 (1):407–431. http://dx.doi.org/10.1016/j.chemgeo.2004.06.053.

Han, C., & Young, S. L., 2014. Root growth of two perennial grass types and musk thistle (carduus nutans) in temperate grasslands of north america. Invasive Plant Science and Management, 7(3), 387-397. doi:10.1614/IPSM-D-13-00081.1

Hawkins, J. W. and W. W. Aljoe, 1991. Hydrologic characteristics of a surface mine spoil aquifer. In: Proceedings of the Second International Conference on the Abatement of Acid Drainage, Montreal, Quebec, Canada, Tome 1, pp. 47-68.

Hedin, R.S., Nairn, R.W., Kleinmann, R.L.P., 1994. Passive Treatment of Coal Mine Drainage, US Bur. Mines Info. Circ. No. 9389, US Dept. Interior: Washington, DC.

Hedin, R.S., 2004. The use of measured and calculated acidity values to improve the quality of AMD data sets. In: Proceedings of American Society for Mining & Reclamation conference, Morgantown, WV, April 18–24.

Heikkinen, P. M., Räisänen, M. L., & Johnson, R. H., 2009. Geochemical characterisation of seepage and drainage water quality from two sulphide mine tailings impoundments: Acid mine drainage versus neutral mine drainage. Mine Water and the Environment, 28(1), 30-49. doi:10.1007/s10230-008-0056-2.

Hengen, T.J., Squillace, M.K., O'Sullivan, A.D., Stone, J.J., 2014. Life cycle assessment analysis of active and passive acid mine drainage treatment technologies. Resour. Conserv. Recycl. 86, 160.

Herlihy, A.T., Kaufmann, P.R., Mitch, M.E., Brown, D.D., 1990. Regional estimates of acid mine drainage impact on streams in themid-Atlantic and southeastern United States. Water Air Soil Pollut. 50, 91–107.

Holdo, R. M., & Brocato, E. R., 2015. Tree–grass competition varies across select savanna tree species: A potential role for rooting depth. Plant Ecology, 216(4), 577-588. doi:10.1007/s11258-015-0460-1

Hook, J. E.; Hanna, W.; Maw, B. W., 1992. Quality and growth response of centipede grass to extended drought. Agron. J. 84: 606–612.

Huminicki, D.M.C., Rimstidt, J.D., 2009. Iron oxyhydroxide coating of pyrite for acid mine drainage control. Appl. Geochem. 24 (9):1626–1634. http://dx.doi.org/10.1016/j. apgeochem.2009.04.032.

Islam, A. M.; Hirata, M., 2005. Centipede grass (Eremochloa ophiuroides (Munro Hack.): Growth behaviour and multipurpose usages. Grassl. Sci 51: 183–190. doi:10.1111/j.1744-697X.2005.00014.x.

Jacques, D., J. Šimůnek, D. Mallants, and M. T. van Genuchten, 2006. Operator-splitting errors in coupled reactive transport codes for transient variably saturated flow and contaminant transport in layered soil profiles, J Contam Hydrol, 88(3), 197-218.

Jacques, D., J. Šimůnek, D. Mallants, and M. T. van Genuchten, 2008. Modeling coupled hydrologic and chemical processes: Long-term uranium transport following phosphorus fertilization, Vadose Zone J, 7(2), 698-711.

Jia, Y., Maurice, C., Öhlander, B., 2016. Mobility of As, Cu, Cr, and Zn from tailings covered with sealing materials using alkaline industrial residues: A comparison between two leaching methods. Environmental Science and Pollution Research, 23(1), 648-660. doi:10.1007/s11356-015-5300-2.

Johnson, D.B., Hallberg, K.B., 2005. Acid mine drainage remediation options: a review. Sci. Total Environ. 338 (1):3–14. http://dx.doi.org/10.1016/j.scitotenv.2004.09.002.

Jones, E.J.P., Nadeau, T., Voytek, M.A., Landa, E.R., 2006. Role ofmicrobial iron reduction in the dissolution of iron hydroxysulfate minerals. J. Geophys. Res. Biogeosci. 111 (G1), G01012. http://dx.doi.org/10.1029/2005JG000089.

Jurjovec, J., Ptacek, C. J., & Blowes, D. W., 2002. Acid neutralization mechanisms and metal release in mine tailings: A laboratory column experiment. Geochimica Et Cosmochimica Acta, 66(9), 1511-1523. doi:10.1016/S0016-7037(01)00874-2.

Kannan, R. S. S., Ziemkiewicz, P. F., & Siriwardane, H. J., 2003. Use of waste materials for control of acid mine drainage and subsidence. Journal of Environmental Engineering, 129(10), 910-915. doi:10.1061/(ASCE)0733-9372(2003)129:10(910).

Kimball, Briant A. and Broshears, Robert E. and Bencala, Kenneth E. and McKnight, Diane M., 1994. Coupling of Hydrologic Transport and Chemical Reactions in a Stream Affected by Acid Mine Drainage. Environmental Science & Technology 28 (12), 2065-2073 DOI: 10.1021/es00061a014.

Kirby, C.S., Cravotta, C.A., 2005a. Net alkalinity and net acidity 1: Theoretical considerations. Appl. Geochem. 20 (10), 1920–1940.

Kirby, C.S., Cravotta, C.A., 2005b. Net alkalinity and net acidity 2: Practical considerations. Appl. Geochem. 20 (10), 1941–1964.

Klaminder, J., Grip, H., Morth, C.-M., and Laudon, H., 2011. Carbon mineralization and pyrite oxidation in groundwater: Importance for silicate weathering in boreal forest soils and stream base-flow chemistry. Appl. Geochem., 26, 319–324, https://doi.org/10.1016/j.apgeochem.2010.12.005.

Kohfahl, C., Graupner, T., Fetzer, C., & Pekdeger, A., 2010. The impact of cemented layers and hardpans on oxygen diffusivity in mining waste heaps A field study of the halsbrücke lead–zinc mine tailings (germany). Science of the Total Environment, 408(23), 5932-5939. doi:10.1016/j.scitotenv.2010.08.034.

Kopittke, P. M., 2012. Interactions between ca, mg, na and K: Alleviation of toxicity in saline solutions. Plant and Soil, 352(1), 353-362. doi:10.1007/s11104-011-1001-x

Kumar, S., Udawatta, R. P., & Anderson, S. H., 2010. Root length density and carbon content of agroforestry and grass buffers under grazed pasture systems in a hapludalf. Agroforestry Systems, 80(1), 85-96. doi:10.1007/s10457-010-9312-0

Kuyukak, N., 2002. Role of microorganisms in mining: generation of acid rock drainage and its mitigation and treatment. Eur. J. Miner. Process. Environ. Prot. Vol. 2 (No. 3), 179–196 1303-0868.

Landry, G.; Murphy, T., 2002. Centipede lawns. Leaflet 313, cooperative extension service. The University of Georgia College of Agricultural and Environmental Sciences, Georgia, pp 1–4.

Lapointe, F., Fytas, K., & McConchie, D., 2006. Efficiency of bauxsol™ in permeable reactive barriers to treat acid rock drainage. Mine Water and the Environment, 25(1), 37-44. doi:10.1007/s10230-006-0106-6.

Lefebvre, R., 1994. Characterization and numerical modeling of acid mine drainage in waste rock dump.(In French.), Ph.D. thesis. Univ. Laval, Quebec, Canada.

Lidman, F., Boily, Å., Laudon, H., and Köhler, S. J., 2017. From soil water to surface water – how the riparian zone controls element transport from a boreal forest to a stream, Biogeosciences, 14, 3001-3014, https://doi.org/10.5194/bg-14-3001-2017.

Liu, M.; Yang, J.; Lu, S.; Guo, Z.; Lin, X.; Wu, H., 2008. Somatic embryogenesis and plant regeneration in centipede grass (Eremochloa ophiuroides [Munro] Hack.). In Vitro Cell. Dev. Biol. -Pl. 44: 100–104.

Lupton, M. K., Rojas, C., Drohan, P., & Bruns, M. A., 2013. Vegetation and soil development in Compost-amended iron oxide precipitates at a 50-year-old acid mine drainage barrens: Vegetating acid mine drainage barrens. Restoration Ecology, 21(3), 320-328. 10.1111/j.1526-100X.2012.00902.x

Ma, L., Rao, X., Lu, P., Huang, S., Chen, X., Xu, Z., Xie, J., 2015. Acid-tolerant plant species screened for rehabilitating acid mine drainage sites. J Soils Sediments 15(5):1104-1112.doi:10.1007/s11368-015-1128-0.

Madejon, P., Murillo, J.M., Maranon, T., Cabrera, F., Lopez, R., 2002. Bioaccumulation of As, Cd, Cu, Fe and Pb in wild grasses affected by the Aznalcóllar mine spill (SW Spain). Science of The Total Environment 290(1-3):105-20. DOI: 10.1016/S0048-9697(01)01070-1.

Madejon, P., Murillo, J.M., Maranon, T., Cabrera, F., 2006. Bioaccumulation of trace elements in wild grass three years after Aznalcóllar mine spill (South Spain). Environmental Monitoring and Assessment 114: 169–189. DOI: 10.1007/s10661-006-2523-1.

Masindi, V., Gitari, M. W., Tutu, H., De Beer, M., 2015. Passive remediation of acid mine drainage using cryptocrystalline magnesite: A batch experimental and geochemical modelling approach. Water SA. 41(5). http://dx.doi.org/10.4314/wsa.v41i5.10.

Mayer, K. U., E. O. Frind, and D. W. Blowes, 2002. Multicomponent reactive transport modeling in variably saturated porous media using a generalized formulation for kinetically controlled reactions, Water Resour Res, 38(9), 1174.

Mazzacavallo, M. G., & Kulmatiski, A., 2015. Modelling water uptake provides a new perspective on grass and tree coexistence. PloS One, 10(12), e0144300. doi:10.1371/journal.pone.0144300

McCarty, L. B., 1995. Centipede grass for Florida Lawns. Fact sheet ENH-8(a), Florida cooperative extension service. Institute of Food and Agric Sci, University Florida, Florida, pp 1–2.

McConchie D, Clark M, Maddocks G, Davies-McConchie F, Pope S, Caldicott W., 2003. The use of Bauxsol™ technology in mine site management and remediation. Proc, CIM Mining Industry Conf, Montreal, Canada.

Meers, E., Laing, G. Du, Unamuno, V. G., Lesage, E., Tack, F. M. G., Verloo, M. G., 2006. Water Extractability of Trace Metals from Soils: Some Pitfalls. Water Air Soil Pollut 176: 21. https://doi.org/10.1007/s11270-005-9070-1.

Mezga, L. J., 1973. Hydrology and water balance of a partially strip-mined watershed, WSD-19 of the Little Mill Creek Basin, Coshocton, Ohio, with emphasis on flow through spoil material. Unpublished Master's thesis, Kent State University, 82 p.

Molson, J., O. Fala, M. Aubertin, and B. Bussière, 2005. Numerical simulations of pyrite oxidation and acid mine drainage in unsaturated waste rock piles, J Contam Hydrol, 78(4), 343-371.

Morin, K. y Hutt, N. 2001. Relocation of net-acid-generating waste to improve post-mining water chemistry. Waste Management, 21 (2), 185-190.

Motalebi Damuchali, A., Asadollahfardi, G., Khodadadi, A., 2012. Effective parameter predictions in metals transport from the Zanjan zinc mine tailings using PHREEQC.Mine Water Environ. 31 (4):339–343. http://dx.doi.org/10.1007/s10230-012-0201-9.

Mueller, K. E., Tilman, D., Fornara, D. A., & Hobbie, S. E., 2013. Root depth distribution and the diversity-productivity relationship in a long-term grassland experiment. Ecology, 94(4), 787-793. doi:10.1890/12-1399.1

Murphy, S. R., Boschma, S. P. and Harden, S., 2017. Soil water dynamics and dry-matter production of old man saltbush-, native grass- and lucerne-based pastures in a variable summer-dominant rainfall environment, Australia. Grass Forage Sci, 72: 290–307. doi:10.1111/gfs.12239

Neitsch, S. L., J. G. Arnold, J. R. Kiniry, J. R. Williams, and K. W. King, 2002. Soil and Water Assessment Tool: Theoretical documentation, Version 2000, Temple, Tex.: Blackland

Research Center and USDA-ARS Grassland Soil and Water Research Laboratory Investigation.

Nippert, J. B., Wieme, R. A., Ocheltree, T. W., & Craine, J. M., 2012. Root characteristics of C4 grasses limit reliance on deep soil water in tallgrass prairie. Plant and Soil, 355(1), 385-394. doi:10.1007/s11104-011-1112-4

Nordstrom, D.K., 1982. Aqueous pyrite oxidation and the consequent formation of secondary iron minerals. In: Kittrick, J.A., Fanning, D.S., Hossner, L.R. (Eds.), Acid Sulfate Weathering. Soil Sci. Soc. Am. Publ., pp. 37–56.

Nordstrom, D. K., and Ball, J. W., 1986. The geochemical behavior of aluminum in acidified surface waters: Science, v. 232, p. 54-58. http://dx.doi.org/10.1126/science.232.4746.54.

Nordstrom, D.K., Alpers, C.N., 1999. Geochemistry of acid mine waters. In: ·Plumlee, G.S., Logsdon, M.J. (Eds.), Reviews in Economic Geology, vol. 6A, the Environmental Geochemistry of Mineral Deposits. Part A. Processes, Methods and Health Issues 133–160. Soc. Econ. Geol., Littleton, CO.

NRC - National Research Council (U.S.), Subcommittee on Mineral Toxicity in Animals, 1980. Mineral tolerance of domestic animals. Washington, D.C: National Academy of Sciences.

Ouangrawa, M., Molson, J., Aubertin, M., Bussière, B., Zagury, G.J., 2009. Reactive transport modelling of mine tailings columns with capillarity-induced high water saturation for preventing sulfide oxidation, Applied Geochemistry, Volume 24, Issue 7, Pages 1312-1323, ISSN 0883-2927, http://dx.doi.org/10.1016/j.apgeochem.2009.04.005.

Ouangrawa, M., Aubertin, M., Molson, J. W., Bussière, B., & Zagury, G. J., 2010. Preventing acid mine drainage with an elevated water table: Long-term column experiments and parameter analysis. Water, Air, & Soil Pollution, 213(1), 437-458. doi:10.1007/s11270-010-0397-x.

Pabst, T., Aubertin, M., Bussiere, B., & Molson, J., 2014. Column tests to characterise the hydrogeochemical response of pre-oxidised acid-generating tailings with a monolayer cover. Water, Air, & Soil Pollution, 225(2).

Padmavathiamma, P.K. & Li, L.Y., 2007. Phytoremediation Technology: Hyper-accumulation Metals in Plants. Water Air Soil Pollut. 184: 105. doi:10.1007/s11270-007-9401-5.

Paradis, M., Duchesne, J., Lamontagne, A., & Isabel, D., 2006. Using red mud bauxite for the neutralization of acid mine tailings: A column leaching test. Canadian Geotechnical Journal, 43(11), 1167-1167. doi:10.1139/T06-071.

Parkhurst, D. L., 1995. User's guide to PHREEQC: A computer program for speciation,reaction-path, advective transport, and inverse geochemical calculations.Rep., 95-4227 pp, USGS, Lakewood, Colorado.

Parkhurst, D.L., Appelo, C.A.J., Geological Survey (U.S.), 1999. User's Guide to PHREEQC (Version 2): A Computer Program for Speciation, Batch-reaction, One-dimensional Transport, and Inverse Geochemical Calculations. U.S. Geological Survey, Denver, Colo.

Parkhurst, D.L., Appelo, C.A.J., Geological Survey (U.S.), 2013. Description of Input and Examples for PHREEQC Version 3–A Computer Program for Speciation, Batch-reaction, One-dimensional Transport, and Inverse Geochemical Calculations. U.S. Department of the Interior, U.S. Geological Survey, Reston, Virginia.

Pennsylvania Department of Environmental Protection, & Pennsylvania. Bureau of Mining and Reclamation, 1998. Coal mine drainage prediction and pollution prevention in pennsylvania. (). Harrisburg, Pa.: Pennsylvania Dept. of Environmental Protection.

Pennsylvania Minefill Study, 2007. Impacts of Water Quality from Placement of Coal Combustion Waste in Pennsylvania Coal Mines. Clean Air Task Force.

Peppas, A., Komnitsas, K., Halikia, I., 2000. Use of organic covers for acid mine drainage control. Minerals Engineering, 13 (5), pp. 563–574.

Pérez-López, R., Cama, J., Nieto, J. M., & Ayora, C., 2007. The iron-coating role on the oxidation kinetics of a pyritic sludge doped with fly ash. Geochimica Et Cosmochimica Acta, 71(8), 1921-1934. doi:10.1016/j.gca.2007.01.019.

Pérez-López, R., Quispe, D., Castillo, J., Nieto, M., 2011. Acid neutralization by dissolution of alkaline paper millwastes and implications for treatment of sulfide-mine drainage. Am. Mineral. 96 (5):781–791. http://dx.doi.org/10.2138/am.2011.3685.

Petrilakova, A., Balintova, M., Holub, M., 2014. Precipitation of heavy metals from acid mine drainage and their geochemical modeling. SSP-Journal of Civil Engineering. 9(1), 79-86. DOI: 10.2478/sspjce-2014-0009.

Pitman MG, Läuchli A, 2002. Global impact of salinity and agricultural ecosystems. In: Läuchli A, Lüttge U (eds) Salinity: environment - plants - molecules. Kluwer Academic, Dordrecht, pp 3–20

Plaza, F., Wen, Y., Perone, H., Xu, Y., Liang, X., 2017. Acid rock drainage passive remediation: Potential use of alkaline clay, optimal mixing ratio and long-term impacts. Sci. Total Environ. 576: 572-585. http://dx.doi.org/10.1016/j.scitotenv.2016.10.076.

Plaza, F., Wen, Y., & Liang, X., 2018. Acid rock drainage passive remediation using alkaline clay: Hydro-geochemical study and impacts of vegetation and sand on remediation. Science of the Total Environment, 637-638, 1262-1278. doi:10.1016/j.scitotenv.2018.05.014.

PlumLee, G.S., Smith, K.S., Ficklin, W.H., Briggs, P.H., 1992. Geological and geochemical controls on the composition of mine drainages and natural drainages in mineralized areas. Proceedings, 7th International. Water-Rock Interaction Conference, Park City, Utah, July 1992, pp. 419–422.

PlumLee, G.S., Smith, K.S.,Montour,M.R., Ficklin,W.H., Mosier, E.L., 1999. Geologic controls on the composition of naturalwaters andmine waters draining diversemineral-deposit types. In: Filipek, L.H., Plumlee, G.S. (Eds.), The Environmental Geochemistry of Mineral Deposits, Part B: Case Studies and Research Topics, Rev Econ Geol. 6B, pp. 373–432.

Price, W.A., Errington, J., Koyanagi, V., 1997. Guidelines for the prediction of acid rock drainage andmetal leaching formines in British Columbia: part I. General procedures and information requirements: MEND, Natural Resources Canada, Ottawa. Proceedings of the 4th International Conference on Acid Rock Drainage. 1, pp. 1–14.

Pruess, K., 1991. TOUGH2: A general-purpose numerical simulator for multiphase fluid and heat transfer., LBL-29400. Lawrence Berkeley Laboratory,Berkeley, CA.

Qu, R. L., Li, D., Du, R., & Qu, R., 2003. Lead uptake by roots of four turfgrass species in hydroponic cultures. Hortscience, 38(4), 623-626.

Querol, X., Umana, J. C., Plana, F., Alastuey, A., Lopez-Solar, A., Medinaceli, A., et al., 2001. Synthesis of zeolites from fly ash at pilot scale. Examples of potential applications. Fuel, 80(60), 857–865.

Raffensperger, J. F., Milke, M. W., & SpringerLink (Online service), 2017. Smart markets for water resources: A manual for implementation. Cham: Springer International Publishing.

Reilly, A., & Reilly, C., 1973. Zinc, lead and copper tolerance in the grass stereochlaena cameronii (stapf) clayton. New Phytologist, 72(5), 1041-1046. doi:10.1111/j.1469-8137.1973.tb02080.x.

Rufaut, C. G., Craw, D., & Foley, A., 2015. Mitigation of acid mine drainage via a revegetation programme in a closed coal mine in southern new zealand. Mine Water and the Environment, 34(4), 464-477. 10.1007/s10230-014-0295-3

Runkel, R.L., Kimball, B.A.,Walton-Day, K., Verplanck, P.L., Broshears, R.E., 2012. Evaluating remedial alternatives for an acid mine drainage stream: a model post audit. Environ. Sci. Technol. 46 (1):340–347. http://dx.doi.org/10.1021/es2038504.

Saaltink, R., Dekker, S. C., Griffioen, J., Wassen, M.J., 2016. Wetland eco-engineering: measuring and modeling feedbacks of oxidation processes between plants and clay-rich material. Biogeosciences, 13(17), 4945-4957. doi:10.5194/bg-13-4945-2016.

Sahoo, P.K., Tripathy, S., Panigrahi, M.K., Equeenuddin, S.M., 2013. Inhibition of acid mine drainage from a pyrite-rich mining waste using industrial by-products: role of neoformed phases. Water Air Soil Pollut. 224 (11):1–11. http://dx.doi.org/10.1007/ s11270-013-1757-0.

Sams, J.I., Beer, K.M., 2000. Effects of coal-mine drainage on stream water quality in the Allegheny and Monongahela River basins: sulfate transport and trends. U.S. Geological Survey, Water-Resources Investigations Report 99–4208.

Sarmiento, A. M., Olías, M., Nieto, J. M., Cánovas, C. R., & Delgado, J., 2009. Natural attenuation processes in two water reservoirs receiving acid mine drainage. Science of the Total Environment, 407(6), 2051-2062. doi:10.1016/j.scitotenv.2008.11.011

Sheoran, V.; Sheoran, A. S.; and Poonia, P., 2010. Soil Reclamation of Abandoned Mine Land by Revegetation: A Review. International Journal of Soil, Sediment and Water: Vol. 3 : Iss. 2 Article 13.

Šimůnek, J., K. Huang, and M. T. Van Genuchten, 1998. The HYDRUS code for simulating the one-dimensional movement of water, heat, and multiple solutes in variably-saturated media,Version 6.0, Research Report No. 144, U.S. Salinity Laboratory, USDA, ARS,Rep., Riverside, California.

Šimůnek, J., M. Sejna, and M. T. van Genuchten, 1999. The Hydrus-2D software package for simulating two-dimensional movement of water, heat, and multiple solutes in variably saturated media. Version 2.0 /GWMC-TPS - 53Rep., 251 pp.

Šimůnek, J., M. T. van Genuchten, and M. Sejna, 2008. Development and applications of the HYDRUS and STANMOD software packages and related codes, Vadose Zone J, 7(2), 587-600.

Singer, P.C., Stumm, W., 1970. Acidic mine drainage: the rate-determining step. Science 167, 1121–1123.

Skousen, J., Simmons, J., McDonald, M. y Ziemkiewicz, P. 2002. Acid-base accounting to predict post-mining drainage quality on surface mines. Journal Environmental Quality, 31 (6), 2034-2044.

Sobek, A.A., Schuller,W.A., Freeman, J.R., Smith, R.M., 1978. Field and Laboratory Methods Applicable to Overburden and Mine Soils. EPA (600/2-78-054).

Sracek, O., Gzyl, G., Frolik, A., Kubica, J., Bzowski, Z., Gwodziewicz,M., Kura, K., 2010. Evaluation of the impacts of mine drainage from a coal waste pile on the surrounding environment at Smolnica, southern Poland. Environ.Monit. Assess. 165 (1–4):233–254. http://dx.doi.org/10.1007/s10661-009-0941-6.

Srinilta, 1967. flow of water through columns of layered soil. Doctoral Dissertation. Iowa State University.

Sun, J., Tang, C.,Wu, P., Strosnider,W.H.J., Han, Z., 2013. Hydrogeochemical characteristics of streams with and without acid mine drainage impacts: a paired catchment study in karst geology, SW China. J. Hydrol. 504:115–124. http://dx.doi.org/10.1016/j.jhydrol.2013.09.029.

Tack, F. M. G., Dezillie, N. and Verloo, M.G., 2002. Metal concentrations in soil paste extracts as affected by extraction ratio. The Scientific World Journal 2, 966–971.

Tavakkoli, E., Fatehi, F., Coventry, S., Rengasamy, P., & McDonald, G. K., 2011. Additive effects of Na+and Cl−ions on barley growth under salinity stress. Journal of Experimental Botany, 62(6), 2189-2203. doi:10.1093/jxb/erq422

Toffey W. E., Miller C. R., Saylor L. D., 1998. Two decades of mine reclamation: lessons learned from one of the Nation's largest biosolids beneficial use programs. http://www.dep.state.pa.us/dep/subject/advcoun/minrec/Reclamtn.pdf.

Toro, L., Pagnanelli, F., & Viggi, C., 2012. Acid mine drainage attenuation by inhibition of pyrite bioleaching using limestone and olive pomace. Chemistry and Ecology, 28(3), 293. doi:10.1080/02757540.2011.651128.

U.S. Environmental Protection Agency - EPA, 1994. Summary of EPA Finalized National Primary Drinking Water Regulations: U.S. Environmental Protection Agency Region VIII (7 p).

U.S. Environmental Protection Agency - EPA, 2002. Coal Mining Point Source Category: Effluent Limitations Guidelines and New Source Performance Standards (40 CFR Part 434).

Valente, T.M., Antunes, M., Sequeira Braga, M.A., Prudêncio, M.I., Marques, R., Pamplona, J., 2012. Mineralogical attenuation for metallic remediation in a passive system for mine water treatment. Environmental Earth Sciences, 66, Issue 1: 39-54.

Vandecasteele, B., De Vos, B. and Tack, F. M. G., 2002. Heavy metal contents in surface soils along the upper scheldt river (Belgium) affected by historical upland disposal of dredged materials. Sci. Total Environ. 290, 1–14.

Watzlaf, G., Kairies, C., Schroder, K., Danehy, T. y Beam, R. 2002. Quantitative results from the flushing of four reducing and alkalinity producing systems. 23rd Annual West Virginia Surface Mine Drainage Task Force Symposium. Morgantown, WV, USA. 11pp.

Watzlaf, G.R., Schroeder, K.T., Kleinmann, R.L.P., Caries, C.L., Nairn, R.W., 2004. The Passive Treatment of Coal Mine Drainage. US Department of Energy DOE/NETL-2004/1202, Available from: <ftp://ftp.netl.doe.gov/pub/Watzlaf/NETL-1202.pdf>, accessed October 2004.

Waybrant, K. R., Ptacek, C. J., Blowes, D. W., 2002. Treatment of Mine Drainage Using Permeable Reactive Barriers: Column Experiments. Environmental Science & Technology 2002 36 (6), 1349-1356. doi: 10.1021/es010751g.

Webster, J.G., Swedlund, P.J., Webster, K.S., 1998. Trace metal adsorption onto an acid mine drainage iron(III) oxy hydroxy sulfate. Environ. Sci. Technol. 32 (10): 1361–1368. http://dx.doi.org/10.1021/es9704390.

Wigmosta, M. S., L. W. Vail, and D. P. Lettenmaier, 1994. A distributed hydrology-vegetation model for complex terrain, Water Resour Res, 30(6), 1665-1679. doi: 10.1029/94WR00436.

Williams, D.R., Clark, M.E., Brown, J.B., 1990. StreamWater Quality in Coal Mined Areas of the Lower Cheat River Basin,West Virginia and Pennsylvania, During Low-Flow Conditions. U. S. Geological Survey, Water-Resources Investigations Report 98–4258.

Williamson, M.A., Rimstidt, J.D., 1994. The kinetics and electrochemical rate-determining step of aqueous pyrite oxidation. Geochim. Cosmochim. Acta 58, 5443–5454.

Williamson,M.A., Kirby, C.S., Rimstidt, J.D., 2006. Iron dynamics in acid mine drainage. In: Barnhisel, R.I. (Ed.), 7th Internat. Conf. Acid Rock Drainage. American Society of Mining and Reclamation, Lexington, KY 40502, St. Louis MO, pp. 2411–2423.

Wunderly, M. D., D. W. Blowes, E. O. Frind, and C. J. Ptacek, 1996. Sulfide mineral oxidation and subsequent reactive transport of oxidation products in mine tailings impoundments: A numerical model, Water Resour Res, 32(10), 3173-3187. doi: 10.1029/96WR02105.

Xu, Y., 2014. Investigation of Environmental Impacts of Beneficial Reuse of Bauxite Residue in Coal-Refuse Area Based on a Hydro-Thermal-Geochemical Model. Doctoral Dissertation, University of Pittsburgh.

Yan, X., Zhang, F., Zeng, C., Zhang, M., Devkota, L. P., & Yao, T., 2012. Relationship between heavy metal concentrations in soils and grasses of roadside farmland in Nepal. International Journal of Environmental Research and Public Health, 9(9), 3209-3226. doi:10.3390/ijerph9093209.

Yee, N., Shaw, S., Benning, L.G., Hien Nguyen, T., 2006. The rate of ferrihydrite transition to goethite via the Fe(II) pathway. Am. Mineral. 91, 92–96.

Yeheyis, M. B., Shang, J. Q., & Yanful, E. K. , 2009. Long-term evaluation of coal fly ash and mine tailings co-placement: A site-specific study. Journal of Environmental Management, 91(1), 237-244. doi:10.1016/j.jenvman.2009.08.010.

Younger, P.L., Banwart, S.A., Hedin, R.S., 2002. MineWater: Hydrology, Pollution, Remediation. Springer Publishing, New York, NY.

Ziemkiewicz, P., Donovan, J., Frazier, J., Daly, M., Black, C. y Wener, E. 2000. Experimental injection of alkaline lime slurry for in-situ remediation of an acidic surface-mine aquifer. West Virginia University. Morgantown, WV, USA. 26pp.